When a cut makes the difference

DNA damage incision from human cells to *C. elegans*

Mariangela Sabatella

ISBN/EAN: 978-94-6332-535-6

Cover design: Mariangela Sabatella & Ramon Mangold
Layout and design: Ferdinand van Nispen, *my*-thesis.nl
Printing: GVO drukkers & vormgevers B.V.

When a cut makes the difference

DNA damage incision from human cells to *C. elegans*

Als een knip het verschil maakt

DNA schade incisie van menselijke cellen tot *C. elegans*

Thesis

to obtain the degree of Doctor from the
Erasmus University Rotterdam
by command of the
rector magnificus

Prof.dr. R.C.M.E. Engels

and in accordance with the decision of the Doctorate Board.

The public defence shall be held on

Wednesday, 23rd of October 2019 at 13:30 hrs
by

Mariangela Sabatella

born in Potenza, Italy

Erasmus University Rotterdam

Doctoral Committee

Promotor:	Prof. dr. W. Vermeulen
Other members:	Prof. dr. R. Kanaar
	Dr. G. Jansen
	Dr. P. Knipscheer
Copromotor:	Dr. H. Lans

Table of contents

CHAPTER 1

Scope of the thesis and Introduction

Scope of the thesis

The DNA damage response (DDR) is a complex network of DNA repair processes and associated signaling mechanisms that maintains genome integrity by removing DNA lesions that are continuously induced by endogenous and exogenous sources. The presence of DNA damage in cells strongly affects DNA-dependent processes, such as transcription and replication, resulting in disturbed cellular homeostasis or mutations in genes, eventually leading to organismal aging or cancer. The intricate cooperation of all DNA repair and signaling mechanisms involved in the DDR determines how cells cope with DNA damage, i.e. whether lesions are bypassed or repaired and by which repair pathway lesions are removed, and whether cells stay functional and alive or are maintained in a dysfunctional state (senescence) or induced to cell death (apoptosis). The repair pathways involved in the DDR are summarized in **chapter 1**. Particular attention is given to nucleotide excision repair (NER) and interstrand crosslink repair (ICLR) pathways, which are the main DNA repair mechanisms investigated in this thesis. In addition, background is provided on the multiple functions of an essential player in these two repair pathways: the structure specific endonuclease complex ERCC1-XPF. Intriguingly, mutations in the *ERCC1* or *XPF* genes give rise to different hereditary DNA repair syndromes: Xeroderma pigmentosum (XP), Cockayne Syndrome (CS), Xeroderma pigmentosum-Cockayne Syndrome complex (XPCS) and Fanconi anemia (FA). The clinical characteristics of these syndromes are also summarized in chapter 1. Moreover, this chapter introduces the widely used model organism *C. elegans*, which is used in this thesis to investigate how DDR functions *in vivo* in intact multicellular organisms. Our lab and others have previously shown that *C. elegans* mutants of ERCC1-XPF display pleiotropic features, e.g. growth arrest, developmental failure and reduced replicative lifespan, strikingly similar to those observed in mammals.

Most of the XPF patients carry heterozygous mutations, which makes it difficult to dissect the link between each *XPF* allele and its phenotypic consequences. In **chapter 2**, we investigate how XPF mutations reported in XP and XPCS patients functionally affect XPF activity in NER. Our data indicate that XP-causative mutations in XPF reduce its recruitment efficiency to damaged DNA, albeit its repair capacity is only slightly affected. Conversely, XPCS-causative mutations strongly impair its repair capacity and lead to continuous recruitment of XPF and also of the core NER machinery.

Interstrand crosslinks (ICLs) are DNA lesions in which the two DNA strands are covalently linked, which fully block DNA replication and transcription and are thus extremely cytotoxic. Although the molecular mechanisms involved in repair of ICLs are still not fully understood, it is clear that multiple DNA repair pathways are involved. Intriguingly, the ERCC1-XPF complex functions in ICL repair (ICLR) both dependently and independently of the core-NER machinery, but it is not clear which factors regulate its recruitment to ICLs independently of the NER machinery. In **chapter 3** the recruitment of ERCC1-XPF to psoralen-DNA crosslinks repaired by ICLR or NER is investigated using imaging and dedicated laser micro-irradiation. We show that recruitment of ERCC1-XPF to ICLs is dependent on the ICLR-specific factor FANCD2. In addition, we show that specific ICLR-defective XPF mutants inefficiently associate with ICLs.

It is becoming increasingly clear that the cell type and its developmental and differentiation state within an organism determine - to a large extent - how lesions are dealt with. However, current knowledge about DDR is mostly based on *in vitro* and cell culture studies, making it difficult to use this knowledge for understanding how DDR is organized or changed in different cell types. In **chapter 4**, we present the development of *C. elegans* as new tool to allow *in vivo* imaging of repair factor kinetics in different cell types. By using this imaging platform, we were able to demonstrate that ERCC1-XPF exhibits tissue-specific activity in response to UV damage. In germ cells, XPF-1 (nematode ortholog of the human XPF) facilitates an unprecedented rapid removal of DNA-helix distorting lesions throughout the genome. In somatic cells, i.e. neurons, XPF-1 functions in NER of transcribed genes only while no XPF-1 activity was observed in muscle cells.

Trichothiodystrophy (TTD) is an autosomal recessive multisystem developmental disorder for which the molecular mechanisms contributing to the phenotype are partially unclear. In addition to the main clinical characteristics such as brittle hair and nails and ichthyosis, TTD patients display a heterogeneous set of other features, including intellectual impairment. Strikingly, about half of the patients display photosensitivity. This is caused by a defect in NER, associated with TTD-specific mutations in the *XPB, XPD* or *TTDA* genes, each coding for subunits of the TFIIH complex. As this complex is essential for both NER and transcription initiation, these mutations lead to DNA repair and gene expression defects. The other half of the patients is non-photosensitive (NPS-TTD). Recently, it was shown

that NPS-TTD is associated with impaired gene expression due to mutations in the beta subunit of the basal transcription factor TFIIE (*i.e. TFIIEβ*). NPS-TTD can furthermore be caused by mutations in *TTDN1*, but the function of this gene is not known and no link with gene expression regulation or DNA repair has been found so far. Our proteomics and live cell imaging studies, presented in **chapter 5**, suggest a possible functional link of TTDN1 in mRNA splicing and/or maturation as well as a possible involvement in DDR to ICLs and/or DNA strand breaks.

Finally, in **chapter 6**, the experimental data are summarized and discussed in terms of future perspectives.

Introduction

DNA damage, cause and consequences

DNA is irreplaceable and therefore the only biomolecule that is preserved by repair of existing molecules in order to ensure its proper function and the correct transmission of genetic information to the next generation. However, various endogenous and exogenous factors continuously damage DNA, which potentially interferes with replication, transcription and/or chromosomal segregation and causes mutagenesis, genomic instability, cell-cycle delay or arrest and cell death, ultimately leading to cancer and aging (1–3). Typically, DNA is damaged due to its inherent instability, e.g. by hydrolysis, or by noxious by-products of endogenous chemical reactions, such as reactive oxygen species (ROS), or by exogenous DNA damaging agents that are present in the environment. Well-known examples of environmental genotoxic agents are UV light, which induces cyclobutane-pyrimidine dimers (CPDs) and 6-4 pyrimidine-pyrimidone photoproducts (6-4PPs) (4), and ionizing radiation, which induces oxidative base damage, single strand breaks and double strand breaks (DSB) (5). Moreover, several antitumor agents and chemicals, such as cisplatin, psoralens and mitomycin C (MMC), can form interstrand crosslinks (ICLs), monoadducts or intrastrand crosslinks. Particularly ICLs are known to be highly cytotoxic as they can fully block DNA polymerase progression and RNA polymerase elongation (6–8).

The DNA damage response

To protect against the unfortunate consequences of DNA damage, organisms are equipped with a sophisticated network of DNA repair mechanisms, DNA damage signaling and tolerance processes and cell cycle checkpoint pathways, called the DNA damage response (DDR) (9). Recognition of damage is linked to an intricate signal cascade that halts the cell cycle to allow completion of repair prior to replication or cell division. Persisting DNA lesions that are not repaired, which block replication, can be temporarily ignored by activation of DNA damage tolerance pathways in which alternative DNA polymerases bypass the lesion, although at the expenses of fidelity, in a process called translesion synthesis (TLS). The type of DNA lesion, its genomic location and the cell cycle phase determine which DNA repair pathway removes DNA damage (9). Lesions in one strand of the DNA helix are usually repaired by pathways that excise and replace one or multiple bases. For instance, misincorporated DNA bases that are not corrected by proofreading during replication are replaced by DNA mismatch repair. Small chemical alterations to bases that mildly affect the DNA helix structure are removed and replaced by base excision repair (BER). Single strand breaks are repaired by part of the BER machinery in a process called single strand break repair. Finally, bulky lesions causing local DNA helix destabilization are repaired by nucleotide excision repair (NER; described below). More destructive lesions, such as DSBs that affect both strands of the DNA helix, are repaired by one of multiple DSB repair pathways, depending on the cell cycle phase and genomic location of the break. The best characterized and most used pathways are non-homologous end-joining (NHEJ) and homologous recombination (HR). NHEJ directly joins DNA ends and acts in any cell phase. Because DNA ends at most DSBs need to be processed before joining, which may lead to loss of or changes in a few nucleotides, this process is considered to be an error prone repair process. Alternatively, DSBs can be repaired during S/G2 phase by HR, an error free repair pathway that uses the sister chromatid as repair template. Other destructive lesions are those that do not form breaks but those that form covalent linkages between the two strands of the DNA helix, i.e. ICLs. These are repaired by complex, still not fully understood pathways collectively called interstrand crosslink repair (ICLR). Replication-dependent ICLR, which acts in S phase, is a collaborative repair pathway in which besides proteins from the Fanconi anemia (FA) repair pathway also HR, NER and TLS proteins are involved. As the focus of this thesis is on NER and ICLR, these two repair pathways will be discussed in more detail below.

Nucleotide excision repair

NER is one of the most peculiar DNA repair mechanisms due to its ability to resolve a large variety of structurally unrelated DNA lesions. These include DNA helix-distorting lesions induced by UV irradiation (i.e. CPDs and 6-4PPs), bulky lesions induced by covalent linkage of natural or synthetic aromatic compounds, chemotherapy drug-induced intrastrand crosslinks and ROS-generated cyclopurines (10, 11). NER can procede through by two sub-pathways: global genome NER (GG-NER), which removes lesions located everywhere in the genome, and transcription coupled NER (TC-NER), which specifically removes DNA damage from the transcribed strand of active genes (Figure 1). GG-NER is initiated by the heterotrimeric XPC complex consisting of XPC, RAD23 and CETN2. This complex continuously scans the DNA for helix-distorting lesions and binds the single stranded DNA (ssDNA) opposite to any lesion that causes DNA helix distortion (12–14). In order to efficiently recognize lesions that hardly induce DNA helix distortion, such as CPDs, damage detection by XPC is facilitated by the UV-DDB complex, consisting of DDB1 and DDB2. This complex directly recognizes photolesions and flips out the damaged nucleotides such that these lesions become accessible to XPC (15).TC-NER is initiated by the stalling of RNA polymerase II at DNA lesions and the subsequent recruitment of CSB, CSA and UVSSA (16, 17). Following DNA damage detection by either GG-NER or TC-NER, the damage is verified by the 10-subunit TFIIH complex, which is loaded on the damaged strand 5' to the lesion through a direct interaction with either XPC or UVSSA (18). TFIIH harbors two helicases needed to verify the damage: the 5'-3' helicase XPD translocates over the DNA until it encounters a DNA lesion which blocks its movement, and XPB, whose ATPase activity facilitates the recruitment of the TFIIH complex to DNA damage and which stimulates damage verification by XPD (19, 20). This unwinding and damage verification is thought to be stimulated by binding of XPA to the DNA damage, while the unwound status of the DNA is stabilized by RPA binding to the undamaged strand (21, 22). After damage verification, the pre-incision NER reaction intermediate consisting of TFIIH, XPA and RPA, recruits and properly orients the structure-specific endonucleases ERCC1-XPF and XPG to incise the damaged strand 5' and 3' to the lesion, respectively, creating a gap of 22-30 nucleotides (23). Finally, the gap is filled by DNA polymerase δ, ε or κ, PCNA and RFC and sealed by DNA ligase I or III (24–27).

Interstrand crosslink repair

The chemical conjugation of bi-functional agents, such as Cisplatin or MMC, to nucleotide bases on two opposing DNA strands creates ICLs. Multiple, but not mutually exclusive, models have been put forward to describe how cells deal with this kind of DNA damage. Despite intense research, many details about the molecular mechanism(s) of the ICLR process are still unclear, although it has become increasingly clear that cells can remove ICLs through multiple means depending on the cell cycle phase. Particularly, it is clear that a dedicated Fanconi anemia (FA) pathway, comprising the collaborative activity of multiple FA proteins, specifically targets ICLs (28, 29). In addition, several other DNA repair pathways are required for the removal of ICLs. Most ICLs are likely repaired in the S-phase of the cell cycle and ICLR is therefore also thought to be connected to and dependent on replication (30, 31). One model proposes that replication fork stalling by ICLs triggers the recruitment of the FANCM-FAAP24-MHF complex, which remodels the fork and recruits the ssDNA binding protein RPA (28) (Figure 2). Binding of RPA to ssDNA activates checkpoint signaling (32) and facilitates the recruitment of the FA-core complex (consisting of FANC-A, -B, -C, -E, -F, -G, -L) which recruits and monoubiquitylates the FANCD2-FANCI heterodimer by the FANCL ubiquitin ligase (33, 34). FANCD2-FANCI ubiquitylation is a key step in the ICLR pathway as it is essential for recruitment of the structure specific endonuclease ERCC1-XPF via interaction with the scaffold protein SLX4 (35, 36, chapter 3). This endonuclease unhooks the DNA crosslink from the lagging strand, possibly together with the activity of the 5' exonuclease SNM1A that digests the DNA past the ICL (37, 38), or by a still unresolved additional nuclease activity of the ERCC1-XPF complex (35, 36). This coordinate action creates a single stranded DNA gap in the leading strand, which is filled in by the TLS polymerases REV1 and pol ζ (31) and serves as template for homologous recombination-mediated repair of the resulting double strand break (DSB) in the lagging-strand (39). Next, NER probably completes a second step of unhooking by removing the remnant of the unhooked ICL from the leading strand.

Another model proposes that unhooking of certain ICLs is preferentially achieved by the DNA glycosylase NEIL3, which cleaves one of the two *N-glycosyl* bonds forming the crosslink. Contrarily to the model described above, this unhooking does not require the FANCI-FANCD2 heterodimer and nucleases-dependent

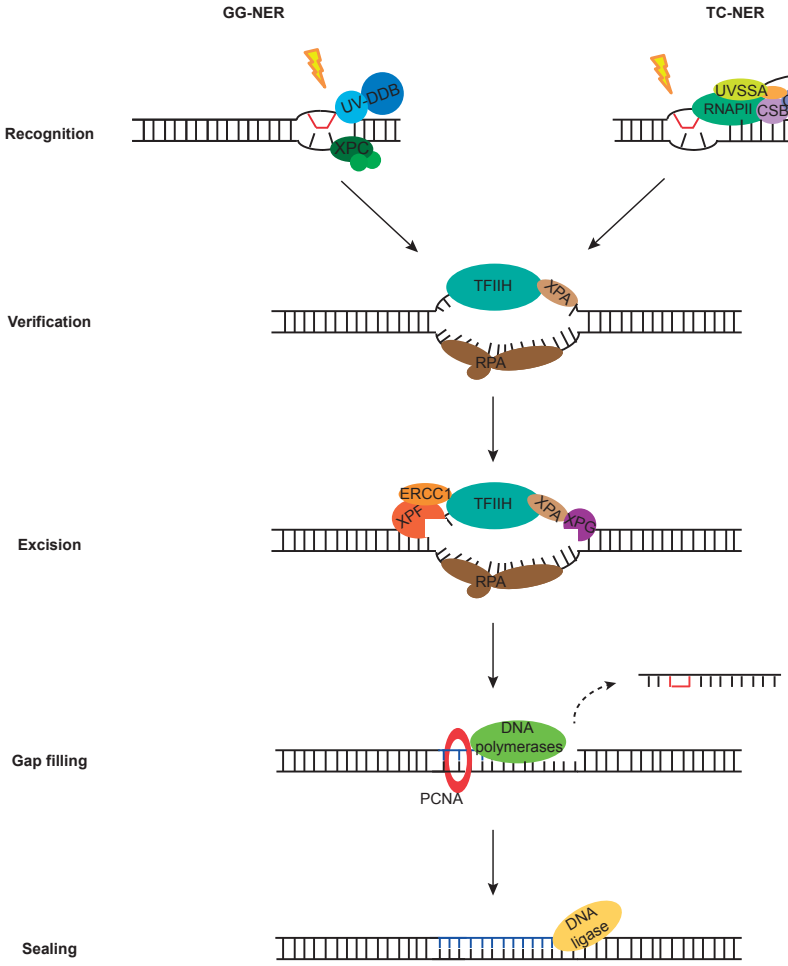

Figure 1. Simplified model of the nucleotide excision repair pathway. Nucleotide excision repair (NER) consists of five overall major steps: damage recognition, damage verification, damage excision, gap filling and sealing. It is initiated by either one of two damage recognition sub-pathways: global genome NER (GG-NER) or transcription-coupled NER (TC-NER). In GG-NER, DNA damage-induced helical distortion of the DNA duplex is recognized by the XPC complex, which, in case of UV photolesions such as CPDs, is aided by damage binding by the UV-DDB complex. TC-NER is initiated by DNA damage-stalling of RNA polymerase II (RNAPII) and subsequent recruitment of the CSB, CSA and UVSSA proteins. Next, in both pathways the DNA helix is unwound by TFIIH to verify the presence of the lesion with the help of the XPA protein that binds damaged DNA. Together with RPA, which binds and protects the unwound ssDNA opposite of the lesion, XPA and TFIIH position the structure specific endonucleases ERCC1-XPF and XPG that incise the DNA around the lesion. Finally, the PCNA protein loads DNA polymerases that fill the resulting gap, while DNA ligases seal the nick.

incisions. Consequently, formation of DSB intermediates is avoided, reducing the possibility of chromosomal rearrangements (40).

In addition to these replication-dependent ICLR, it has been suggested that in non-replicating cells ICLs are removed by NER and TLS. This replication-independent ICLR pathway is, however, very poorly understood. Probably, repair of ICLs, which form helix-distorting and transcription-blocking lesions, can be initiated by either GG-NER or TC-NER (41–43) (Figure 3) leading to recruitment of ERCC1-XPF that incises one DNA strand 5' to the ICL. It is not clear how the 3' side of the lesion is incised but it has been proposed that this could involve digestion past the ICL by the exonuclease SNM1A or flap nuclease FAN1 to accomplish unhooking, although currently clear evidence for their involvement is lacking. Next, TLS polymerases are thought to bypass the unhooked ICL and fill in the single stranded DNA gap. A second round of NER then removes the ICL remnant from the opposite strand (28, 44).

ERCC1-XPF

ERCC1 and XPF (also known as ERCC4) are the two subunits of a dimeric structure-specific endonuclease. During NER, ERCC1-XPF incises DNA at dsDNA/ssDNA junctions 5' with respect to the lesion (45). The complex also plays an important role in the replication-dependent and replication-independent ICLR by incising DNA to unhook an ICL. Furthermore, the complex is implicated in the removal of 3' overhangs in some branches of DSB repair and in regulating telomere length (35, 46–49). ERCC1 was the first mammalian DNA repair gene to be cloned after its isolation by complementation experiments in Chinese hamster ovary excision repair-deficient cell lines (50). ERCC1 consists of a central domain, which is critical for DNA and XPA binding (51, 52) (Figure 4), and a C-terminal helix-hairpin-helix (HhH) domain that is required for its interaction with XPF (53). XPF consists of an N-terminal helicase-like domain (HLD), a central domain that contains the nuclease activity and a C-terminal HhH domain that is required for its interaction with ERCC1 (54). The correct interaction of the two proteins is essential to stabilize the dimeric complex and to guarantee the proper translocation of both subunits to the cell nuclei by the XPF NLS signal (54–56, chapter 2). The HhH domains of both proteins further support the recognition of dsDNA/ssDNA junctions, where XPF incises damaged DNA (58). During NER, the ERCC1-XPF complex is recruited to the NER pre-incision complex by a direct interaction

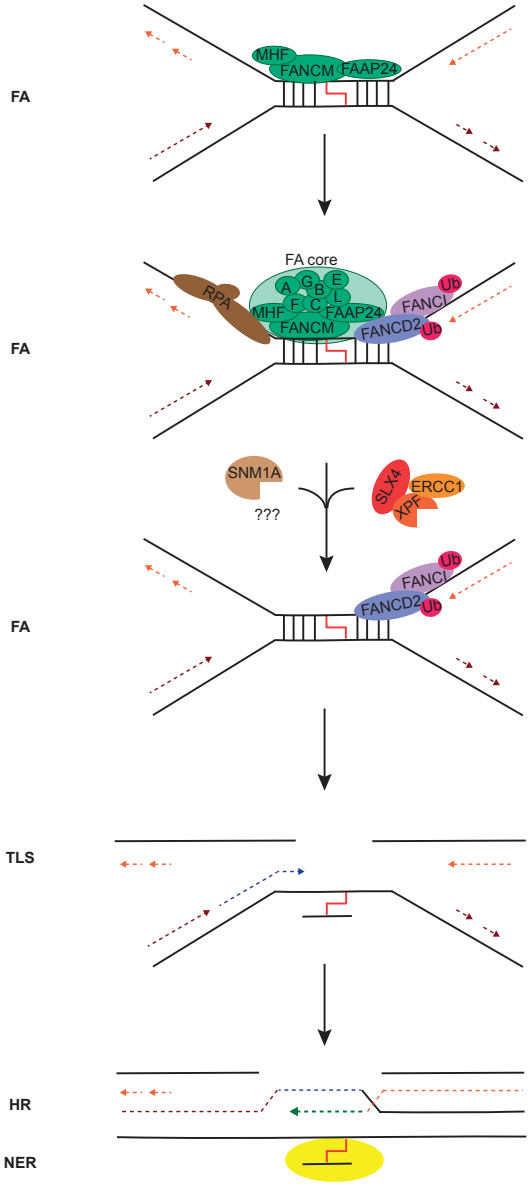

Figure 2. Simplified model of ICL repair during S phase. Interstrand crosslink repair (ICLR) during S phase is initiated when two replication forks converge on an interstrand crosslink (ICL) and stall before the lesion. Multiple DDR mechanisms, including the Fanconi anemia (FA) pathway, translesion synthesis (TLS) and homologous recombination (HR) and nucleotide excision repair (NER) consecutively act to remove the ICL. First, the stalled fork is recognized by the FANCM-FAAP24-MHF complex that recruits RPA and additional components of the FA core complex (consisting of FANC-A, -B, -C, -E, -F, -G, -L). Within the core complex, FANCL monoubiquitylates the FANCD2-FANCI complex. Next, the ERCC1-XPF endonuclease, via interaction with SLX4, and the 5' exonucleases SNM1A or possibly a second nuclease are recruited, to unhook the ICL from the lagging strand. TLS polymerases replicate over the unhooked ICL to fill the gap while NER is thought to perform a second step of unhooking to completely remove the ICL remnant. The remaining DSB is repaired by HR using the TLS-filled DNA strand as template.

of the central domain of ERCC1 with XPA (59). Interestingly, the XPF subunit provides specificity for participating in ICLR, as it was shown that its N-terminal HLD interacts with SLX4 (60). This HLD is also involved in the interaction with RPA, (52, 61), required for positioning the nuclease in NER (62) and activating the nuclease for ICLR (38).

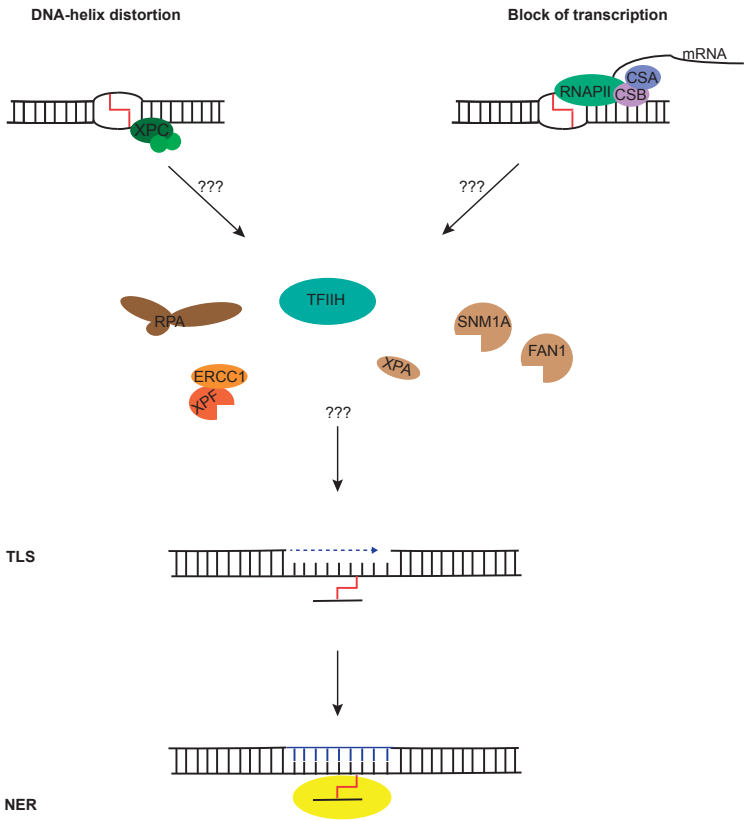

Figure 3. Proposed model of replication-independent ICLR. It was proposed that in non-replicating and postmitotic cells, the GG-NER protein XPC may recognize ICLs that induce DNA-helix distortions and that TC-NER proteins CSB and CSA may recognize ICL-blocked RNA polymerase II (RNAPII). This recognition may trigger the recruitment of downstream NER factors including RPA and ERCC1-XPF, which incises the DNA 5' to the lesion. It is, however, unclear whether this involves the complete core NER machinery and how this then may be accomplished as the crosslinked DNA would need to be unwound. Possibly, additional factors, such as the exonucleases SNM1A or FAN1 cooperate with ERCC1-XPF and RPA to complete the first step of unhooking. Next, the unhooked ICL is likely bypassed by translesion synthesis (TLS) polymerases such that the resulting gap is filled by newly synthetized DNA. NER probably removes the remainder of the unhooked ICL.

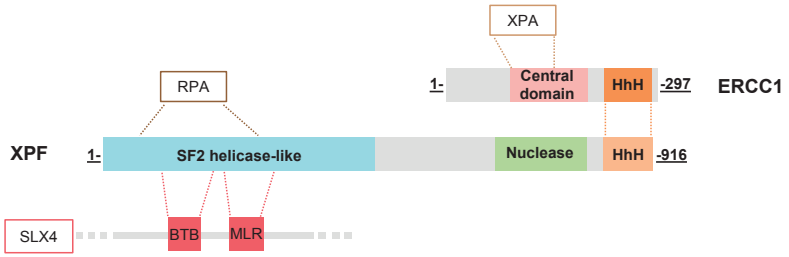

Figure 4. ERCC1-XPF domains and their interactors. Schematic representation of ERCC1 and XPF with protein domains and interacting proteins. XPF consist of an N-terminal helicase-like domain (HLD), a nuclease domain and C-terminal helix-hairpin-helix (HhH) domain. The HLD domain is necessary for XPF interaction with RPA and SLX4 (via the MUS312/MEI9 interaction-like (MLR) and the Bric-a-brac, Tramtrack and Broad complex (BTB) domains) and the HhH is necessary for interaction with the HhH domain of ERCC1. ERCC1 consist of a central domain, necessary for the interaction with XPA and an HhH. Both HhH domain of ERCC1 and XPF support dsDNA/ssDNA junctions recognition, where XPF incises damaged DNA via its nuclease domain. Interactions are represented by dashed lines.

Clinical consequences of ERCC1-XPF defects

The importance of efficient DNA maintenance is evident from the clinical phenotypes displayed by patients with inherited defects in specific DNA repair pathways (63). Curiously, mutations in the same pathway and even within the same gene can lead to diverse clinical outcomes. This is in particular exemplified by mutations in ERCC1-XPF, which, likely due to the multiple functions of the complex, give rise to different diseases with pleiotropic symptoms. These include xeroderma pigmentosum (XP), Cockayne syndrome (CS), xeroderma pigmentosum-Cockayne syndrome complex (XPCS), Fanconi anemia (FA), XPF-ERCC1 progeroid syndrome (XFE) and Cerebro-Oculo-Facio-Skeletal syndrome (COFS) (45, 55, 64–68). In chapters 2 and 3, the impact of patient-derived mutations associated with some of these diseases on ERCC1-XPF activity in NER and ICLR are studied in more detail.

Xeroderma pigmentosum

XP is an autosomal recessive disorder that results from defective repair of UV lesions by GG-NER, due to mutations in genes *XPA* to *XPG* (69), or from defective TLS due to mutations in the *POLH* gene (70, 71). XP patients are characterized by extreme photosensitivity, about 10,000 fold increased risk of non-melanoma cancer and a 2,000 fold increased risk of melanoma within the first 20 years of life (72). About 50-60% of patients show severe sunburn reaction upon short sun exposure and 20-30% of patients develop neurological deficiencies as a result of progressive

neurological degeneration. This more severe form of XP is also often referred to as De Sanctis-Cacchione syndrome. As a consequence of neuronal degeneration, these patients show deafness, impaired eyesight, ataxia and microcephaly. The XP-related cutaneous features are easily explained, since the skin is the sole organ to be potentially harmed by UV-light. However, the cause for the neurodegeneration in XP is still unclear. It has been hypothesized that sporadic DNA lesions induced by the cell's metabolic by-products, such as cyclopurines, accumulate as the NER defect precludes their removal (73). As a consequence of accumulating DNA lesions, the cellular homeostasis will be disturbed. The spectrum of clinical features and severity of the disease depends on the affected gene and the type of mutation. The molecular mechanism and differential consequences associated with specific XPF mutations were further investigated in chapter 2. XP due to NER deficiency is diagnosed by measuring UV-induced unscheduled DNA synthesis, which is low in case of impaired NER.

Cockayne syndrome

CS is an autosomal recessive disorder associated with defects in TC-NER, due to mutations in genes *CSA* and *CSB* (74, 75). Typically, CS is characterized by a wide spectrum of features that can vary strongly in severity, including growth retardation, cachetic dwarfism, photosensitivity, pigmentary retinopathy, progeria, progressive hearing loss, impairment of the neuronal system and early death (69, 76). Remarkably, CS patients do not develop skin cancer and their neuronal impairment is characterized by neuron demyelination rather than degeneration, which is different from that in XP patients with neurodegeneration (75). CS diagnosis is confirmed by impaired RNA transcription recovery after UV-induced DNA damage.

Xeroderma pigmentosum-Cockayne syndrome complex

In some cases clinical features of both XP and CS are displayed and represent the group of the rare neurodegenerative disease XPCS complex, which is associated with defects in either the *XPB*, *XPD*, *XPF* or *XPG* gene (69, 76). XPCS patients are characterized by progressive cognitive, hearing and motor skills loss, short stature, progeria and neurological problems. Like CS patients, they show neurodemyelination rather than primary neurodegeneration, and skin features typical of XP, but a low rate of skin cancer development. As for CS, also for XPCS, a variation in severity of the symptoms has been described. Moreover, other more

severe diseases have been described in patients carrying defects in *ERCC1-XPF*, which could be considered extreme forms of XPCS, i.e. XFE (68), characterized by more severe liver and kidney dysfunction and hypertension (76), or COFS (67), characterized by typical dysmorphic features, bilateral congenital hip dislocation, mild hypoplasia of the kidneys and cerebellar hypoplasia.

Additional NER-related syndromes

In addition to the above mentioned diseases, NER deficiency can give rise to two additional syndromes: UV-sensitive syndrome ($UV^{S}S$) and the photosensitive form of trichothiodystrophy (TTD). $UV^{S}S$ is associated with defects in TC-NER, similarly to CS, due to mutations in *UVSSA* or specific mutations in *CSA* or *CSB* (77, 78). $UV^{S}S$ patients are characterized by hypersensitivity to sunlight with acute sunburns and mild cutaneous pigmentation abnormalities but lack the severe symptoms typical of CS (79). The reason for this remarkable difference between the $UV^{S}S$ and CS clinical features is currently unknown (10).

TTD is thought to be caused by defects leading to impairment of gene expression. It is associated with a broad spectrum of phenotypes, including brittle hair and nails, mental and growth retardation, severe neurological development, ichthyosis, proneness to infections, osteopenia and osteosclerosis and premature ageing (69, 80). Half of the patients displays photosensitivity caused by specific mutations in TFIIH subunits *XPB, XPD* or *TTDA,* impairing NER and transcription initiation (80–83). The other half of the patients displays non-photosensitive TTD (NPS-TTD) and carries mutations in the subunit *TFIIEβ* of the transcription factor TFIIE (84, 85) or *RNF113A*, associated with spliceosomal protein complexes (86, 87), also impairing transcription. A subgroup of NPS-TTD patients carries mutations in *TTDN1* (88), for which no function is known and no clear link to transcription, gene expression or DNA repair has been identified. TTDN1 function in genome maintenance and transcription is investigated in chapter 5.

Fanconi anemia

FA is an autosomal recessive disorder affecting multiple organs. FA patients typically display bone marrow failure, somatic malformations (e.g. dysplastic thumbs and radii often visible in neonates or early infancy), high susceptibility to develop cancer, primarily acute myeloid leukemia and epithelial cancers of the head and neck, chromosome fragility and extreme sensitivity to DNA crosslinking

agents (89, 90). In some cases, absence of these symptoms in early infancy as well as absence of a family history make FA diagnosis extremely difficult. As a consequence, in one-third of FA patients the disease is only recognized in adulthood, when patients display high sensitivity to cytotoxic chemotherapeutics (90). Up to date, 22 FA genes with a role in ICLR have been identified. Therefore, FA is typically diagnosed by assessment of chromosomal aberrations after ICL induction and hypersensitivity to ICL-inducing agents such as MMC.

C. elegans as model organism to study DDR

The various symptoms associated with the above-described syndromes suggest that DNA damage affects tissues differently and that DDR might act and/or be organized differently according to the function and differentiation stage of each tissue (91). To explore this hypothesis, in chapter 4 we used the model organism *C. elegans*, which in the last years has emerged as an ideal system to study *in vivo* cell-type specific differences in DDR organization (92).

C. elegans (Figure 5A) is a tiny nematode (adults are 1 mm long) first used by Sydney Brenner to study the genetics underlying development and behavior (93). Since then, *C. elegans* has extensively been used to study the genetics of many biological processes thanks to advantageous characteristics that make this organism practical and easy to work with. These include a short life cycle (3 days at 25°C from egg to egg-laying adult) (Figure 5B), a small size, easy and cost-effective culturing on Petri dishes containing buffered agar and uracil biosynthesis defective *E. coli* as food, suitability for microscopy because of its transparency and a well-annotated genome sequence (94). Moreover, *C. elegans* is relatively easy to genetically manipulate, allowing straightforward forward and reverse genetic screening, as well as germline manipulation to generate new transgenic strains in only a few days. *C. elegans* is mostly hermaphrodite (only 0.05% of wild type animals is male) and develops through four larval stages (L1-L4). Under adverse environmental conditions, nematodes molt from L2 into an alternative L3 stage called "dauer", in which the animals are more resistant to environmental stresses and caustic agents and have, consequently, an increased lifespan. *C. elegans* has a very well characterized cell lineage, making it excellently suited to study cellular processes, including DDR, *in vivo* throughout development and in different cell types. Each adult hermaphrodite contains 959 postmitotic somatic cells that form different tissues and organs, such as muscles, hypodermis, intestine, reproductive

system and neurons (Figure 5B). The exact position, developmental timing and lineage of all somatic cells is known and mostly invariant. Adults contain two U-shaped gonad arms connected by a spermatheca to the uterus. Distally in each of the arms mitotic germ cells proliferate until they enter meiotic prophase and move more proximally. The first approximately 40 germ cells initiating meiotic development undergo spermatogenesis in the proximal region of each gonad arm and complete meiosis I and II to form spermatids capable of fertilizing oocytes that subsequently enter the spermatheca. Female germ cell nuclei proceed through pachytene stage of meiotic prophase in the distal arm, diplotene in the loop of the arm and diakinesis in the proximal arm. In the latter stage, oocytes are enclosed by a membrane and become bigger. The most proximal oocyte (also called -1 oocyte) undergoes maturation and ovulates into the spermatheca where it is fertilized prior to moving into the uterus to continue and complete the divisions of meiosis I and II and development as embryo (95). Each hermaphrodite *C. elegans* produces up to 300 self-progeny, fertilized by sperm stored in the spermatheca, or up to 1000 non-self-progeny when crossed with a male. Both *C. elegans* sexes are diploid with 5 autosomal chromosomes and two X chromosomes for hermaphrodites and one X chromosome for males.

Most major mammalian DDR pathways, including NER, are highly conserved in *C. elegans*. Interestingly, their activity was found to differ depending on the type of tissue and developmental stage of cell (92, 96, 97). Most DDR pathways appear to be active in proliferating germ cells, but this changes as cells enter meiosis. For instance, in meiotic germ cells HR is the preferred pathway to repair DSBs while NHEJ is actively suppressed. Also GG-NER is an essential DDR pathway in germ cells to remove helix-distorting DNA damage, but this is different in somatic cells, in which TC-NER and not GG-NER becomes essential (97, chapter 4). Furthermore, in early embryogenesis, DDR and DNA damage signaling appear to be actively suppressed while TLS is active to permit rapid cell divisions even when DNA is damaged (99, 100).

Our lab has particularly investigated the ERCC-1/XPF-1 complex in *C. elegans*, which has conserved roles in NER, ICLR, meiotic recombination and DSB repair (47, 98, 101, 102). Mutations that impair the activity of the complex give rise to a remarkable pleiotropic phenotype and features that are strikingly reminiscent of those observed in mammals with ERCC1-XPF defects, which include:

growth arrest, developmental failure, reduced replicative lifespan and increased accumulation of spontaneous oxidative DNA lesions (cyclopurines) compared to wild-type worms (47, 101–104). These observations provide further support to the choice of *C. elegans* as model organism to investigate the link between tissue-specific activities of ERCC1-XPF and tissue-specific symptoms displayed in patients carrying defect in this complex.

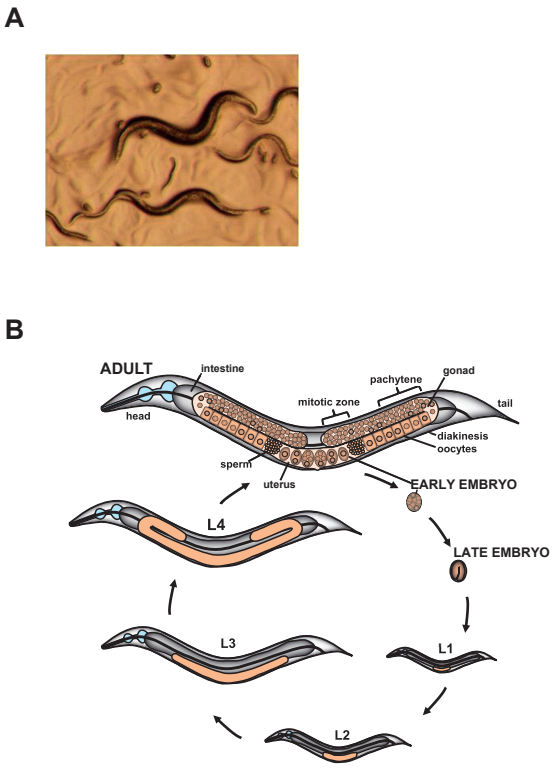

Figure 5. Model organism *C. elegans*. (**A**) Depicted are several *C. elegans* in different stages of development, including embryos, crawling on a lawn of bacteria on an agar plate, as viewed through a dissection microscope. (**B**) *C. elegans* anatomy and life cycle. *C. elegans* hermaphrodites develop from egg (embryo) through four larval stages (L1-L4) to adulthood within 3 days at 25°C. Depicted are the intestine and gonad within the adult animal. In the gonad, female germ cells proliferate in the mitotic zone and enter meiosis, maturing through different stages (as depicted, e.g. pachytene and diakinesis) to form oocytes that are fertilized by sperm, producing early embryos in the uterus. As a result, adult worms can produce up to 300 progeny over their life span. The figure was adapted from Lans & Vermeulen (92).

References

1. Hoeijmakers JHJ (2009) DNA Damage, Aging, and Cancer. *N Engl J Med* 361(15):1475–1485.
2. Garinis GA, van der Horst GTJ, Vijg J, Hoeijmakers JHJ (2008) DNA damage and ageing: New-age ideas for an age-old problem. *Nat Cell Biol* 10(11):1241–1247.
3. Vermeij WP, Hoeijmakers JHJ, Pothof J (2014) Aging: Not all DNA damage is equal. *Curr Opin Genet Dev* 26:124–130.
4. Pattison DI, Davies MJ (2006) Actions of ultraviolet light on cellular structures. *Cancer: Cell Structures, Carcinogens and Genomic Instability*, pp 131–157.
5. Lomax ME, Folkes LK, O'Neill P (2013) Biological consequences of radiation-induced DNA damage: Relevance to radiotherapy. *Clin Oncol* 25(10):578–585.
6. Riddell IA, Lippard SJ (2018) Cisplatin and Oxaliplatin: Our Current Understanding of Their Actions. *Metal Ions in Life Sciences*, eds Sigel A, Sigel H, Freisinger E, Sigel RKO (De Gruyter, Berlin, Boston), pp 1–42.
7. Cimino GD, Gamper HB, Isaacs ST, Hearst JE (1985) Psoralens as Photoactive Probes of Nucleic Acid Structure and Function: Organic Chemistry, Photochemistry, and Biochemistry. *Annu Rev Biochem* 54(1):1151–1193.
8. Tomasz M (1995) Mitomycin C: small, fast and deadly (but very selective). *Chem Biol* 2(9):575–579.
9. Giglia-Mari G, Zotter A, Vermeulen W (2011) DNA damage response. *Cold Spring Harb Perspect Biol* 3(1):1–19.
10. Marteijn JA, Lans H, Vermeulen W, Hoeijmakers JHJ (2014) Understanding nucleotide excision repair and its roles in cancer and ageing. *Nat Rev Mol Cell Biol* 15(7):465–481.
11. Schärer OD (2013) Nucleotide excision repair in Eukaryotes. *Cold Spring Harb Perspect Biol* 5(10):a012609–a012609.
12. Sugasawa K, Shimizu Y, Iwai S, Hanaoka F (2002) A molecular mechanism for DNA damage recognition by the xeroderma pigmentosum group C protein complex. *DNA Repair (Amst)* 1(1):95–107.
13. Hoogstraten D, et al. (2008) Versatile DNA damage detection by the global genome nucleotide excision repair protein XPC. *J Cell Sci* 121(23):3991–3991.
14. Min JH, Pavletich NP (2007) Recognition of DNA damage by the Rad4 nucleotide excision repair protein. *Nature* 449(7162):570–575.
15. Sugasawa K (2016) Molecular mechanisms of DNA damage recognition for mammalian nucleotide excision repair. *DNA Repair (Amst)* 44:110–117.
16. Vermeulen W, Fousteri M (2013) Mammalian transcription-coupled excision repair. *Cold Spring Harb Perspect Biol* 5(8):a012625.
17. Geijer ME, Marteijn JA (2018) What happens at the lesion does not stay at the lesion: Transcription-coupled nucleotide excision repair and the effects of DNA damage on transcription in cis and trans. *DNA Repair (Amst)* 71:56–68.
18. Okuda M, Nakazawa Y, Guo C, Ogi T, Nishimura Y (2017) Common TFIIH recruitment mechanism in global genome and transcription-coupled repair subpathways. *Nucleic Acids Res* 45(22):13043–13055.
19. Coin F, Oksenych V, Egly J-M (2007) Distinct roles for the XPB/p52 and XPD/p44 subcomplexes of TFIIH in damaged DNA opening during nucleotide excision repair. *Mol Cell* 26(2):245–56.
20. Sugasawa K, et al. (2009) Two-step recognition of DNA damage for mammalian nucleotide excision repair: Directional binding of the XPC complex and DNA strand scanning. *Mol Cell* 36(4):642–53.
21. Li CL, et al. (2015) Tripartite DNA Lesion Recognition and Verification by XPC, TFIIH, and XPA in Nucleotide Excision Repair. *Mol Cell* 59(6):1025–1034.
22. Sugitani N, Sivley RM, Perry KE, Capra JA, Chazin WJ (2016) XPA: A key scaffold for human nucleotide excision repair. *DNA Repair (Amst)* 44:123–135.
23. Fagbemi AF, Orelli B, Schärer OD (2011) Regulation of endonuclease activity in human nucleotide excision repair. *DNA Repair (Amst)* 10(7):722–729.
24. Ogi T, et al. (2010) Three DNA Polymerases, Recruited by Different Mechanisms, Carry Out NER Repair Synthesis in Human Cells. *Mol Cell* 37(5):714–727.
25. Lehmann AR (2011) DNA polymerases and repair synthesis in NER in human cells. *DNA Repair (Amst)* 10(7):730–733.
26. Shivji MK, Podust VN, Hübscher U, Wood RD (1995) Nucleotide excision repair DNA synthesis by DNA polymerase epsilon in the presence of PCNA, RFC, and RPA. *Biochemistry*, pp 5011–7.

27. Moser J, et al. (2007) Sealing of Chromosomal DNA Nicks during Nucleotide Excision Repair Requires XRCC1 and DNA Ligase IIIα in a Cell-Cycle-Specific Manner. *Mol Cell* 27(2):311–323.
28. Clauson C, Scharer OD, Niedernhofer L (2013) Advances in Understanding the Complex Mechanisms of DNA Interstrand Cross-Link Repair. *Cold Spring Harb Perspect Biol* 5(10):a012732–a012732.
29. Ceccaldi R, Sarangi P, D'Andrea AD (2016) The Fanconi anaemia pathway: new players and new functions. *Nat Rev Mol Cell Biol* 17(6):337–349.
30. Knipscheer P, et al. (2009) The fanconi anemia pathway promotes replication-dependent DNA interstrand cross-link repair. *Science (80-)* 326(5960):1698–1701.
31. Räschle M, et al. (2008) Mechanism of Replication-Coupled DNA Interstrand Crosslink Repair. *Cell* 134(6):969–980.
32. Huang M, et al. (2010) The FANCM/FAAP24 complex is required for the DNA interstrand crosslink-induced checkpoint response. *Mol Cell* 39(2):259–68.
33. Andreassen PR, D'Andrea AD, Taniguchi T (2004) ATR couples FANCD2 monoubiquitination to the DNA-damage response. *Genes Dev* 18(16):1958–63.
34. Smogorzewska A, et al. (2007) Identification of the FANCI Protein, a Monoubiquitinated FANCD2 Paralog Required for DNA Repair. *Cell* 129(2):289–301.
35. Klein Douwel D, et al. (2014) XPF-ERCC1 Acts in Unhooking DNA Interstrand Crosslinks in Cooperation with FANCD2 and FANCP/SLX4. *Mol Cell* 54(3):460–471.
36. Hoogenboom WS, Boonen RACM, Knipscheer P (2019) The role of SLX4 and its associated nucleases in DNA interstrand crosslink repair. *Nucleic Acids Res* 47(5):2377–2388.
37. Wang AT, et al. (2011) Human SNM1a and XPF-ERCC1 collaborate to initiate DNA interstrand cross-link repair. *Genes Dev* 25(17):1859–1870.
38. Abdullah UB, et al. (2017) RPA activates the XPF-ERCC1 endonuclease to initiate processing of DNA interstrand crosslinks. *EMBO J* 36(14):2047–2060.
39. Long DT, Räschle M, Joukov V, Walter JC (2011) Mechanism of RAD51-dependent DNA interstrand cross-link repair. *Science (80-)* 333(6038):84–87.
40. Semlow DR, Zhang J, Budzowska M, Drohat AC, Walter JC (2016) Replication-Dependent Unhooking of DNA Interstrand Cross-Links by the NEIL3 Glycosylase. *Cell* 167(2):498-511.e14.
41. Enoiu M, Jiricny J, Schärer OD (2012) Repair of cisplatin-induced DNA interstrand crosslinks by a replication-independent pathway involving transcription-coupled repair and translesion synthesis. *Nucleic Acids Res* 40(18):8953–64.
42. Wang X, et al. (2001) Involvement of nucleotide excision repair in a recombination-independent and error-prone pathway of DNA interstrand cross-link repair. *Mol Cell Biol* 21(3):713–20.
43. Sarkar S, Davies AA, Ulrich HD, McHugh PJ (2006) DNA interstrand crosslink repair during G1 involves nucleotide excision repair and DNA polymerase zeta. *EMBO J* 25(6):1285–94.
44. Roy U, Schärer OD (2016) Involvement of translesion synthesis DNA polymerases in DNA interstrand crosslink repair. *DNA Repair (Amst)* 44:33–41.
45. Sijbers AM, et al. (1996) Xeroderma pigmentosum group F caused by a defect in a structure-specific DNA repair endonuclease. *Cell* 86(5):811–822.
46. Bhagwat N, et al. (2009) XPF-ERCC1 Participates in the Fanconi Anemia Pathway of Cross-Link Repair. *Mol Cell Biol* 29(24):6427–6437.
47. Pontier DB, Tijsterman M (2009) A Robust Network of Double-Strand Break Repair Pathways Governs Genome Integrity during C. elegans Development. *Curr Biol* 19(16):1384–1388.
48. Zhu XD, et al. (2003) ERCC1/XPF Removes the 3' Overhang from Uncapped Telomeres and Represses Formation of Telomeric DNA-Containing Double Minute Chromosomes. *Mol Cell* 12(6):1489–1498.
49. Muñoz P, Blanco R, Flores JM, Blasco MA (2005) XPF nuclease-dependent telomere loss and increased DNA damage in mice overexpressing TRF2 result in premature aging and cancer. *Nat Genet* 37(10):1063–1071.
50. Westerveld A, et al. (1984) Molecular cloning of a human DNA repair gene. *Nature* 310(5976):425–429.
51. Tsodikov O V., Enzlin JH, Scharer OD, Ellenberger T (2005) Crystal structure and DNA binding functions of ERCC1, a subunit of the DNA structure-specific endonuclease XPF-ERCC1. *Proc Natl Acad Sci* 102(32):11236–11241.
52. Li L, Elledge SJ, Peterson CA, Bales ES, Legerski RJ (1994) Specific association between the human DNA repair proteins XPA and ERCC1. *Proc Natl Acad Sci U S A* 91(11):5012–6.

53. De Laat WL, Sijbers AM, Odijk H, Jaspers NGJ, Hoeijmakers JHJ (1998) Mapping of interaction domains between human repair proteins ERCC1 and XPF. *Nucleic Acids Res* 26(18):4146–4152.
54. Schärer OD (2017) ERCC1-XPF endonuclease—positioned to cut. *EMBO J* 36(14):1993–1995.
55. Ahmad A, et al. (2010) Mislocalization of XPF-ERCC1 nuclease contributes to reduced DNA repair in XP-F patients. *PLoS Genet* 6(3):e1000871.
56. Biggerstaff M, Szymkowski DE, Wood RD (1993) Co-correction of the ERCC1, ERCC4 and xeroderma pigmentosum group F DNA repair defects in vitro. *EMBO J* 12(9):3685–92.
57. Boulikas T (1997) Nuclear import of DNA repair proteins. *Anticancer Res* 17(2A):843–63.
58. Das D, et al. (2012) The structure of the XPF-ssDNA complex underscores the distinct roles of the XPF and ERCC1 helix-hairpin-helix domains in ss/ds DNA recognition. *Structure* 20(4):667–675.
59. Orelli B, et al. (2010) The XPA-binding domain of ERCC1 is required for nucleotide excision repair but not other DNA repair pathways. *J Biol Chem* 285(6):3705–3712.
60. Klein Douwel D, Hoogenboom WS, Boonen RA, Knipscheer P (2017) Recruitment and positioning determine the specific role of the XPF-ERCC1 endonuclease in interstrand crosslink repair. *EMBO J* 36(14):2034–2046.
61. Park CH, Sancar A (1994) Formation of a ternary complex by human XPA, ERCC1, and ERCC4(XPF) excision repair proteins. *Proc Natl Acad Sci U S A* 91(11):5017–5021.
62. de Laat WL, et al. (1998) DNA-binding polarity of human replication protein A positions nucleases in nucleotide excision repair. *Genes Dev* 12(16):2598–609.
63. Keijzers G, Bakula D, Scheibye-Knudsen M (2017) Monogenic Diseases of DNA Repair. *N Engl J Med* 377(19):1868–1876.
64. Fassihi H, et al. (2016) Deep phenotyping of 89 xeroderma pigmentosum patients reveals unexpected heterogeneity dependent on the precise molecular defect. *Proc Natl Acad Sci* 113(9):E1236–E1245.
65. Kashiyama K, et al. (2013) Malfunction of nuclease ERCC1-XPF results in diverse clinical manifestations and causes Cockayne syndrome, xeroderma pigmentosum, and Fanconi anemia. *Am J Hum Genet* 92(5):807–819.
66. Bogliolo M, et al. (2013) Mutations in ERCC4, encoding the DNA-repair endonuclease XPF, cause Fanconi anemia. *Am J Hum Genet* 92(5):800–806.
67. Jaspers NGJ, et al. (2007) First Reported Patient with Human ERCC1 Deficiency Has Cerebro-Oculo-Facio-Skeletal Syndrome with a Mild Defect in Nucleotide Excision Repair and Severe Developmental Failure. *Am J Hum Genet* 80(3):457–466.
68. Niedernhofer LJ, et al. (2006) A new progeroid syndrome reveals that genotoxic stress suppresses the somatotroph axis. *Nature* 444(7122):1038–1043.
69. Kraemer KH, et al. (2007) Xeroderma pigmentosum, trichothiodystrophy and Cockayne syndrome: A complex genotype-phenotype relationship. *Neuroscience* 145(4):1388–1396.
70. Lehman AR, et al. (1975) Xeroderma pigmentosum cells with normal levels of excision repair have a defect in DNA synthesis after UV-irradiation. *Proc Natl Acad Sci* 72(1):219–223.
71. Masutani C, et al. (1999) The XPV (xeroderma pigmentosum variant) gene encodes human DNA polymerase η. *Nature* 399(6737):700–704.
72. Lehmann AR, McGibbon D SM (2011) Xeroderma pigmentosum. *Orphanet J Rare Dis* 6(70):1–6.
73. Brooks PJ (2008) The 8,5'-cyclopurine-2'-deoxynucleosides: Candidate neurodegenerative DNA lesions in xeroderma pigmentosum, and unique probes of transcription and nucleotide excision repair. *DNA Repair (Amst)* 7(7):1168–1179.
74. Natale V (2011) A comprehensive description of the severity groups in Cockayne syndrome. *Am J Med Genet Part A* 155(5):1081–1095.
75. Karikkineth AC, Scheibye-Knudsen M, Fivenson E, Croteau DL, Bohr VA (2017) Cockayne syndrome: Clinical features, model systems and pathways. *Ageing Res Rev* 33:3–17.
76. Natale V, Raquer H (2017) Xeroderma pigmentosum-Cockayne syndrome complex. *Orphanet J Rare Dis* 12(1):65.
77. Nakazawa Y, et al. (2012) Mutations in UVSSA cause UV-sensitive syndrome and impair RNA polymerase IIo processing in transcription-coupled nucleotide-excision repair. *Nat Genet* 44(5):586–592.
78. Zhang X, et al. (2012) Mutations in UVSSA cause UV-sensitive syndrome and destabilize ERCC6 in transcription-coupled DNA repair. *Nat Genet* 44(5):593–597.
79. Spivak G (2005) UV-sensitive syndrome. *Mutat Res - Fundam Mol Mech Mutagen* 577(1-2 SPEC. ISS.):162–169.

80. Stefanini M, Botta E, Lanzafame M, Orioli D (2010) Trichothiodystrophy: From basic mechanisms to clinical implications. *DNA Repair (Amst)* 9(1):2–10.
81. Theil AF, Hoeijmakers JHJ, Vermeulen W (2014) TTDA: Big impact of a small protein. *Exp Cell Res* 329(1):61–68.
82. De Boer J, et al. (1998) A mouse model for the basal transcription/DNA repair syndrome trichothiodystrophy. *Mol Cell* 1(7):981–990.
83. Theil AF, et al. (2013) Disruption of TTDA Results in Complete Nucleotide Excision Repair Deficiency and Embryonic Lethality. *PLoS Genet* 9(4):e1003431.
84. Kuschal C, et al. (2016) GTF2E2 Mutations Destabilize the General Transcription Factor Complex TFIIE in Individuals with DNA Repair-Proficient Trichothiodystrophy. *Am J Hum Genet* 98(4):627–642.
85. Theil AF, et al. (2017) Trichothiodystrophy causative TFIIEβ mutation affects transcription in highly differentiated tissue. *Hum Mol Genet* 26(23):4689–4698.
86. Bessonov S, et al. (2010) Characterization of purified human Bact spliceosomal complexes reveals compositional and morphological changes during spliceosome activation and first step catalysis. *RNA* 16(12):2384–2403.
87. Hegele A, et al. (2012) Dynamic Protein-Protein Interaction Wiring of the Human Spliceosome. *Mol Cell* 45(4):567–580.
88. Heller ER, et al. (2015) Mutations in the TTDN1 gene are associated with a distinct trichothiodystrophy phenotype. *J Invest Dermatol* 135(3):734–741.
89. Dufour C (2017) How I manage patients with Fanconi anaemia. *Br J Haematol* 178(1):32–47.
90. Nalepa G, Clapp DW (2018) Fanconi anaemia and cancer: An intricate relationship. *Nat Rev Cancer* 18(3):168–185.
91. Niedernhofer LJ (2008) Tissue-specific accelerated aging in nucleotide excision repair deficiency. *Mech Ageing Dev* 129(7–8):408–15.
92. Lans H, Vermeulen W (2015) Tissue specific response to DNA damage: C. elegans as role model. *DNA Repair (Amst)* 32:141–148.
93. Brenner S (1974) The genetics of Caenorhabditis elegans. *Genetics* 77(1):71–94.
94. Corsi AK, Wightman B, Chalfie M (2015) A transparent window into biology: A primer on Caenorhabditis elegans. *Genetics* 200(2):387–407.
95. McCarter J, Bartlett B, Dang T, Schedl T (1999) On the Control of Oocyte Meiotic Maturation and Ovulation inCaenorhabditis elegans. *Dev Biol* 205(1):111–128.
96. Rieckher M, Bujarrabal A, Doll MA, Soltanmohammadi N, Schumacher B (2017) A simple answer to complex questions: Caenorhabditis elegans as an experimental model for examining the DNA damage response and disease genes. *J Cell Physiol* 233(4):2781–2790.
97. Boulton SJ, et al. (2002) Combined functional genomic maps of the C. elegans DNA damage response. *Science* 295(5552):127–31.
98. Lans H, et al. (2010) Involvement of global genome repair, transcription coupled repair, and chromatin remodeling in UV DNA damage response changes during developm. *PLoS Genet* 6(5):e1000941.
99. Holway AH, Kim S-H, La Volpe A, Michael WM (2006) Checkpoint silencing during the DNA damage response in Caenorhabditis elegans embryos. *J Cell Biol* 172(7):999–1008.
100. Roerink SF, Koole W, Stapel LC, Romeijn RJ, Tijsterman M (2012) A broad requirement for TLS polymerases η and κ, and interacting sumoylation and nuclear pore proteins, in lesion bypass during C. elegans embryogenesis. *PLoS Genet* 8(6):e1002800.
101. Ward JD, Barber LJ, Petalcorin MIR, Yanowitz J, Boulton SJ (2007) Replication blocking lesions present a unique substrate for homologous recombination. *EMBO J* 26(14):3384–3396.
102. Saito TT, Youds JL, Boulton SJ, Colaiácovo MP (2009) Caenorhabditis elegans HIM-18/SLX-4 interacts with SLX-1 and XPF-1 and maintains genomic integrity in the germline by processing recombination intermediates. *PLoS Genet* 5(11):e1000735.
103. Lans H, et al. (2013) DNA damage leads to progressive replicative decline but extends the life span of long-lived mutant animals. *Cell Death Differ* 20(12):1709–1718.
104. Gurkar AU, et al. (2018) Dysregulation of DAF-16/FOXO3A-mediated stress responses accelerates oxidative DNA damage induced aging. *Redox Biol* 18:191–199.

CHAPTER 2

Repair protein persistence at DNA lesions characterizes XPF defect with Cockayne syndrome features

Mariangela Sabatella[1,2], Arjan F. Theil[1,2], Cristina Ribeiro-Silva[1,2], Jana Slyskova[1,2], Karen Thijssen[1,2], Chantal Voskamp[1], Hannes Lans[1,2], Wim Vermeulen[1,2]

[1]. Department of Molecular Genetics, Erasmus MC, University Erasmus Medical Center Rotterdam, 3015 GD, The Netherlands
[2]. Oncode Institute, Erasmus MC, Rotterdam, 3015 GD, The Netherlands

Nucleic Acids Research, 2018

Abstract

The structure-specific ERCC1-XPF endonuclease plays a key role in DNA damage excision by nucleotide excision repair (NER) and interstrand crosslink repair. Mutations in this complex can either cause xeroderma pigmentosum (XP) or XP combined with Cockayne syndrome (XPCS-complex) or Fanconi anemia. However, most patients carry compound heterozygous mutations, which confounds the dissection of the phenotypic consequences for each of the identified *XPF* alleles. Here, we analyzed the functional impact of individual pathogenic *XPF* alleles on NER. We show that XP-causing mutations diminish XPF recruitment to DNA damage and only mildly affect global genome NER. In contrast, an XPCS-complex-specific mutation causes persistent recruitment of XPF and the upstream core NER machinery to DNA damage and severely impairs both global genome and transcription-coupled NER. Remarkably, persistence of NER factors at DNA damage appears to be a common feature of XPCS-complex cells, suggesting that this could be a determining factor contributing to the development of additional developmental and/or neurodegenerative features in XP patients.

Introduction

Xeroderma pigmentosum (XP) and Cockayne syndrome (CS) are rare autosomal recessive photosensitive disorders caused by mutations in genes that encode factors involved in nucleotide excision repair (NER). XP patients display pigmentation abnormalities, a greater than a 2000-fold increased risk of skin cancer and over 20% of the patients develop progressive neurodegeneration (1). CS patients display severe growth failure, progressive neurodegeneration and segmental progeria but do not develop cancer (2). XP patients are classified in complementation groups XP-A to XP-G and the variant XP-V, according to the mutated gene, while CS is caused by mutations in the *CSA* and *CSB* genes. Intriguingly, some patients from complementation groups XP-B, XP-D, XP-G and XP-F combine dermatological features of XP with developmental and progressive neurodegenerative features of CS, representing the rare xeroderma pigmentosum-Cockayne syndrome (XPCS) complex (3, 4). Also, patients from complementation group XP-A can exhibit XP combined with severe growth failure and progressive neurodegeneration, which is often referred to as De Sanctis Cacchione (DSC) syndrome (5). The type of disease and severity of symptoms are thought to depend on which gene is mutated and to which extent NER is affected, but it is not properly understood how mutations in the same genes can cause different diseases.

NER is a major DNA repair pathway responsible for removing UV light-induced cyclobutane-pyrimidine dimers (CPDs) and 6-4 pyrimidine-pyrimidone photoproducts (6-4PPs) and other bulky lesions such as intrastrand crosslinks and ROS-induced cyclopurines (6, 7). DNA damage is detected by two sub-pathways: global genome-NER (GG-NER), which detects damage located anywhere in the genome by the concerted action of the UV-DDB/XPE and XPC-RAD23B-CETN2 complex, and transcription coupled-NER (TC-NER), which detects damage in the template strand of transcribed genes through stalling of RNA polymerase II and subsequent recruitment of the CSA (ERCC8), CSB (ERCC6) and UVSSA proteins. Damage detection by either sub-pathway leads to recruitment of the basal transcription factor complex IIH (TFIIH). TFIIH opens the DNA helix and verifies the presence of DNA lesions using its XPB (ERCC3) ATPase and the 5′–3′ helicase activity of its XPD (ERCC2) subunit, which is stimulated by the single strand DNA damage binding protein XPA. XPA binds damaged DNA and interacts with multiple NER factors and is therefore considered a central NER organizer.

Together with RPA, XPA facilitates the recruitment and correct positioning of the two structure-specific endonucleases, ERCC1-XPF (XPF is also known as ERCC4) and XPG (ERCC5), that incise the damaged strand respectively 5' and 3' to the lesion. The resulting 22-30 nt gap is then repaired by DNA synthesis and sealed by ligation.

ERCC1-XPF is an obligate dimer that binds to XPA via its ERCC1 subunit and incises double stranded DNA 5' to a stretch of single stranded DNA using the catalytic activity of the highly conserved nuclease domain in XPF (8–11). Besides NER, ERCC1-XPF nuclease activity is also implicated in removing 3' overhangs during some forms of double strand break repair and is critical in unhooking interstrand crosslinks (ICLs) as part of the Fanconi anemia (FA) repair pathway (12, 13). Defects in this latter repair pathway lead to the rare disease FA, which is characterized by congenital growth abnormalities, bone marrow failure and increased susceptibility to cancer (14). Mutations in *ERCC1-XPF* have been found in patients exhibiting a range of phenotypically pleiotropic diseases including XP, CS, XPCS and FA, but also the more severe cerebro-oculo-facio-skeletal syndrome and XPF–ERCC1 progeroid syndrome (11, 15–18).

The difference in severity of symptoms associated with ERCC1-XPF defects have been attributed to differences is mislocalization of the complex to the cytoplasm, which is observed in many XP-F group patient fibroblasts (19). There exists wide consensus that XP symptoms are specifically caused by defects in GG-NER (1) and FA symptoms by defects in ICL repair (ICLR) (14, 20). Thus, mutations that impair the activity of ERCC1-XPF in either GG-NER or ICLR will give rise to XP or FA, respectively. The exact etiology of CS is, however, debated and opinions vary as to whether CS symptoms are primarily caused by defects in TC-NER or whether defects in other DNA repair pathways, transcription, stress responses and/or mitochondria may play a role as well (6, 21–23). It is therefore not understood why certain mutations in ERCC1-XPF only give rise to XP or FA whereas others in addition cause CS features. Moreover, in most patients, mutations are present as compound heterozygous and different mutation combinations are associated with different diseases (Table 1), convoluting a clear understanding of the contribution of each mutation to the disease phenotype.

Table 1: Features of studied XPF mutations

Amino acid change	Nucleotide change	Compound heterozygous with	Cell line	Disease[1]	UV sensitivity[2]	MMC sensitivity[2]	UDS[3]	RRS[3]	Reference
C236R	706T>C	R589W	XPCS1CD	XPCS + FA features	+	+	8%	24%	(15)
		Y577*	CS1USAU	XPCS	+	-	10%	16%	(15)
P379S	1135C>T	R589W	XP32BR	mild XP	+	ND	10-16%	ND	(19, 39)
			XP72BR	mild XP		ND	36%	ND	(39)
		silent allele	XP7NE	mild XP	+	ND	30%	ND	(19)
R589W	1765C>T	P379S	XP32BR	mild XP	+	ND	10-16%	ND	(15, 39)
		R799W	XP24BR	severe XP, neurodegeneration	+	ND	4-5%	ND	(15, 19, 39)
		del exon 3	AS871	severe XP, neurodegeneration	+	ND	15%	ND	(15, 19)
		C236R	XPCS1CD	XPCS + FA features	+	+	8%	24%	(15)
R689S	2065C>A	T495Nfs*6	FA104	FA	-	+	ND	ND	(16)
D715A	2144A>C				ND	ND	ND	ND	(8)
S786F	2357C>T				-	+	ND	ND	(40)

[1] XP: xeroderma pigmentosum; CS: Cockayne syndrome; XPCS: xeroderma pigmentosum-Cockayne syndrome; FA: Fanconi anemia.
[2] + hypersensitive to either UV or MMC; - not hypersensitive; ND, not determined
[3] RRS and UDS levels in XPCS1CD and CS1USAU were estimated based on graphs in Figure 1C and D of (15)

To clarify the molecular mechanism that gives rise to XPCS, we investigated how specific XPF mutations found in patients affected with XP, XPCS or FA impair the activity of the ERCC1-XPF complex in response to DNA damage induction by UV irradiation. We show that XPF with an XP mutation is inefficiently recruited into the NER machinery but retains repair activity. Conversely, XPCS mutant XPF persists at sites of DNA damage and hardly displays repair activity, leading to continuous recruitment of the core NER machinery.

Material and methods

Cell culture, generation of cell lines and cloning of XPF-GFP constructs

U2OS cell lines were cultured in a 1:1 mixture of DMEM and F10 supplemented with 10% fetal calf serum (FCS) and 1% penicillin-streptomycin (PS) at 37°C and 5% CO_2. Wild type hTERT immortalized C5RO and patient fibroblasts XPCS1CD, CS1USAU (15), hTERT immortalized XP42RO (24), XP32BR (19), XP6BE (25), hTERT immortalized XPCS1RO (26), XPCS2 (27), XPCS1BA (28) and XP25RO (29) were cultured in F10 supplemented with 15% FCS and 1% PS at 37°C and 5% CO_2. To generate U2OS XPF KO cells, U2OS cells were simultaneously transfected with pLentiCRISPR-V2 plasmids (30) containing an sgRNA targeting exon 1 (TGGAACTGCTCGACACTGAC) and an sgRNA targeting exon 2 (CGCTATGAAGTTTACACACA) of XPF. Following selection with puromycin, single XPF KO clones were analyzed by immunoblot and sequencing. Tracking Indels by Decomposition analysis was performed as described in Brinkman *et al* (31). To generate GFP-tagged wild type XPF (XPF-wt), full length XPF cDNA, kindly provided by Orlando D. Schärer, was fused to GFP at its C-terminus and cloned into pLenti-CMV-Blast-DEST (32). GFP-tagged XPF mutants were generated by site directed mutagenesis using primers listed in Supplementary Table S1 and cloned into pLenti-CMV-Blast-DEST or pLenti-CMV-Puro-DEST. GFP-tagged wild type and mutant XPF were introduced in U2OS XPF KO cells by lentiviral transduction and cells were selected using blasticidin or puromycin. Cloning details are available upon request.

Clonogenic survival assays

To determine UV and mitomycin C (MMC) sensitivity, 500 cells were seeded in triplicate in 6-well plates. 24 h after seeding, cells were irradiated with UV (0, 0.5,

1, 2, 4 J/m^2; 254 nm UVmp, Philips) or treated with MMC (0, 0.3, 0.6, 0.9, 1.2, 1.5 μg/ml; Sigma). After 5 to 7 days, cells were fixed and stained with 50% Methanol, 7% Acetic Acid, 0.1 % Brilliant Blue R (Sigma) and counted using the integrated colony counter GelCount (Oxford Optronix). The number of colonies after treatment was normalized to the number in non-treated conditions and plotted as average survival percentage of three independent experiments. Statistical difference was calculated using a one-way ANOVA followed by post-hoc analysis by Bonferroni's test.

Live cell imaging and fluorescence recovery after photobleaching (FRAP)

For live cell imaging, cells were seeded on coverslips and imaged with a Leica TCS SP5 confocal microscope using a 63x/1.4 NA HCX PL APO CS oil immersion lens (Leica Microsystems) at 37°C and 5% CO_2. FRAP was performed as previously described (33). Briefly, fluorescence was imaged within a strip of 512 x 16 pixels stretched over the width of the nucleus (zoom 9x) at 1400 Hz every 22 ms using 488 nm laser at low power until steady-state levels were reached. Next, fluorescence signal was bleached using high laser power (100%) and recovery of the signal was measured at low laser power every 22 ms until steady-state levels were reached. To perform FRAP on local UV damaged areas (Figure 3D), the entire nucleus of each cell was imaged at 400 Hz every 648 ms using low laser power. Fluorescence signal within a small region (1.5 μm x 1.5 μm) stretched over the local damage area was bleached with high laser power and recovery of the fluorescence in time was measured at low laser power every 648 ms. Fluorescence signals were normalized to the average fluorescence intensity before bleaching and bleach depth. The immobile fraction (F_{imm}) (Figure 3C) was determined using the fluorescence intensity measured immediately after bleaching (I_0), and the average steady-state fluorescence level once recovery was complete, from untreated cells ($I_{final,\ unt}$) and UV- treated cells ($I_{final,\ UV}$) and applying the formula: $F_{imm} = 1-(I_{final,\ UV} - I_{0,\ UV}) / (I_{final,\ unt} - I_{0,\ uv})$ (34). Statistical difference was calculated using a one-way ANOVA followed by post-hoc analysis by Bonferroni's test. LAS AF software (Leica) was used for imaging and quantification.

Immunofluorescence

To perform immunofluorescence experiments, cells were seeded on coverslips and, when indicated, irradiated with 60 J/m^2 (254 nm UVC lamp, Philips) through an 8 μm microporous filter (Millipore) to inflict local DNA damage. To determine

CPD removal, cells were globally irradiated with 10 J/m^2. Cells were fixed at the indicated time points with 2% paraformaldehyde and 0.1 %Triton X-100 and permeabilized for 20 min using 0.1 % Triton X-100 in PBS. To visualize CPDs, cells were incubated with 0.07 M NaOH in PBS for 5 min to denature DNA. Cells were then washed with PBS containing 0.15% glycine and 0.5% BSA and incubated with primary antibodies for 2 h. After thorough washing with PBS containing 0.1% Triton X-100, cells were incubated with Alexa Fluor conjugated secondary antibodies (488, 555 and 633; Invitrogen) for 1 h. Coverslips were mounted using DAPI Vectashield (Vector Laboratories) and imaged using an LSM700 microscope equipped with a 40x Plan-apochromat 1.3 NA oil immersion lens (Carl Zeiss). Quantification of repair protein recruitment or CPD signal was performed using FIJI image analysis software. Statistical difference was calculated using an unpaired two-tailed Student's t-test for two groups comparisons (Figure 6C) or an one-way ANOVA followed by Bonferroni post hoc test for more than two groups comparisons. Primary antibodies used were against XPF (sc-136153, Santa Cruz Biotechnology), XPC (home-made fraction 5 or A301-121A, Bethyl), ERCC1 (ab129267, Abcam), GFP (ab290, Abcam), CPD (TDM-2; Cosmobio), XPB (sc-293, Santa Cruz), XPD (ab54676, Abcam), XPG (A301-484A, Bethyl) and XPA (sc-853, Santa Cruz Biotechnology).

Cell fractionation

For cell fractionation, cells were irradiated with 5 J/m^2 UVC (254 nm lamp, Philips) or left untreated. Cells were collected by trypsinization, washed and incubated in HEPES Buffer (30 mM HEPES pH 7.5, 130 mM NaCl, 1mM $MgCl_2$, 0.5% triton X-100 and protease inhibitors) on ice for 30 min. Samples were centrifuged at 15000g for 20 min and separated into supernatant (soluble fraction) and pellet (chromatin fraction), which was solubilized by treatment with 250U of benzonase (Merck Millipore). Both fractions were analyzed by immunoblot. Statistical difference was calculated using a one-way ANOVA followed by Bonferroni post hoc test.

Immunoblot

For immunoblot analysis, cells or samples were collected in 2x sample buffer (125 mM Tris-HCl pH 6.8, 20% Glycerol, 10% 2-β-Mercaptoethanol, 4% SDS, 0.01% Bromophenol Blue) and boiled at 98°C for 5 min. Protein lysate was separated by SDS-PAGE and transferred to a PVDF membrane (0.45 µm, Merck Millipore).

Membranes were blocked in 2% BSA and incubated with primary and secondary antibodies for 2 h or overnight. Antibodies used were against XPF (sc-136153, Santa Cruz), ERCC1 (sc-17809, Santa Cruz), CSB (sc-10459, Santa Cruz), H2B (sc-8650, Santa Cruz) and Ku-70 (sc-17789, Santa Cruz Biotechnology). Secondary antibodies were conjugated with CF IRDye 680 or 770 (Sigma) and visualized using the Odyssey CLx Infrared Imaging System (LI-COR Biosciences).

Recovery of RNA synthesis

RRS was performed as described (35). Briefly, cells were mock treated or irradiated with 6 J/m^2 UVC (254 nm lamp, Philips) and RNA was labeled 24 h later by incubation with EU for 1 h. Cells were fixed in 4% paraformaldehyde and permeabilized with 0.1% Triton X-100 in PBS. To visualize EU incorporation, cells were incubated in Click-it buffer containing Atto 594 Azide (60 μM, Atto Tec.), Tris-HCl (50 mM, pH 7.6), CuSO4*5H2O (4 mM, Sigma) and ascorbic acid (10 mM, Sigma) for 1 h and then washed with PBS containing 0.1% Triton X-100. DAPI (Sigma) was used to stain DNA and slides were mounted using Aqua-Poly/Mount (Polysciences, Inc.). Images were acquired using an LSM700 confocal microscope equipped with a 40x Plan-apochromat 1.3 NA oil immersion lens (Carl Zeiss Micro Imaging Inc.). RRS levels were quantified by averaging the total nuclear fluorescence intensities of at least 100 cells per experiment with FIJI image analysis software and normalization to fluorescence levels in control conditions.

Unscheduled DNA synthesis

UDS was measured in local UV damaged areas within cells after irradiation with 60 J/m^2 (254 nm UVC lamp, Philips) through an 8 μm microporous filter (Millipore). Cells were incubated with EdU for 30 min or 1 h, pre-extracted with PBS containing 0.1% Triton X-100 and fixed with 2% paraformaldehyde in PBS. Next, cells were permeabilized using PBS containing 0.1% Triton X-100 for 10 min and blocked in PBS containing 1.5% BSA for 10 min. To visualize CPDs, DNA was denatured with 0.07 M NaOH for 5 min. To visualize EdU incorporation, cells were incubated in Click-it buffer containing Atto 594 Azide (60 μM, Atto Tec.), Tris-HCl (50 mM, pH 7.6), CuSO4*5H2O (4 mM, Sigma) and ascorbic acid (10 mM, Sigma) for 1 h and then washed with PBS containing 0.1% Triton X-100. Subsequently, cells were washed with PBS containing 0.15% glycine and 0.5% BSA and incubated with GFP (ab290, Abcam) and CPD (TDM-2; Cosmobio) antibodies for 2 h. After washing with PBS containing 0.1% Triton X-100 and

PBS, cells were incubated with Alexa Fluor conjugated secondary antibodies (488 and 633; Invitrogen) for 1 h. Coverslips were mounted using DAPI Vectashield (Vector Laboratories) and imaged using an LSM700 microscope and 40x Plan-apochromat 1.3 NA oil immersion lens (Carl Zeiss). The fluorescent EdU signal at local sites of damage from at least 60 cells per condition was quantified using FIJI image analysis and averaged. Statistical difference was calculated using an one-way ANOVA followed by Bonferroni post hoc test.

Results

Generation of *XPF* knockout and XPF-GFP expressing cells

To study how *XPF* deficiency can lead to different diseases, we determined how XPF mutations found in XP, XPCS and FA patients affect the spatio-temporal response of the ERCC1-XPF complex to DNA damage. To this end, we first generated an XPF knockout (KO) cell line, to be able to compare different mutant XPF proteins, which in patients most often occur as compound heterozygous, in the same genetic background. Following transfection of U2OS cells with plasmids expressing Cas9 and sgRNAs targeting exon 1 and exon 2 of *XPF*, we selected an *XPF* KO clone carrying multiple indel mutations in both exons predicted to lead to early truncation of the protein, as revealed by sequencing and tracking indels by decomposition analysis (31) (Supplementary Figure S1). In this clone, XPF was not detectable by immunoblot nor by immunofluorescence (Figure 1A, B). To functionally confirm the absence of XPF, we determined protein levels of ERCC1, whose stability depends on the presence of XPF (36, 37), and found these to be strongly reduced in the XPF KO cells (Figure 1A). Moreover, extreme hypersensitivity to UV (Figure 1C), which generates lesions that are substrates for NER, and to Mitomycin C (MMC; Figure 1D), which in addition induces ICLs, confirmed that these KO cells lack XPF activity and are therefore completely NER and ICLR-deficient. Next, we stably expressed GFP-tagged wild type XPF (XPF-wt) in the XPF KO cells, which rescued UV and MMC hypersensitivity and stabilized protein levels of ERCC1 (Figure 1A, C and D). To further validate the functionality of XPF-wt, we applied UVC irradiation through a microporous filter to inflict local DNA damage within the nuclei of the cells (38). XPF-wt clearly accumulated at sites of local UV damage (LUD) marked by XPC, in cells fixed 30 min after irradiation, similarly to endogenous XPF in control U2OS cells (Figure

1B). Together, these data indicate that repair deficient XPF KO cells can be fully complemented by GFP-tagged wild type XPF.

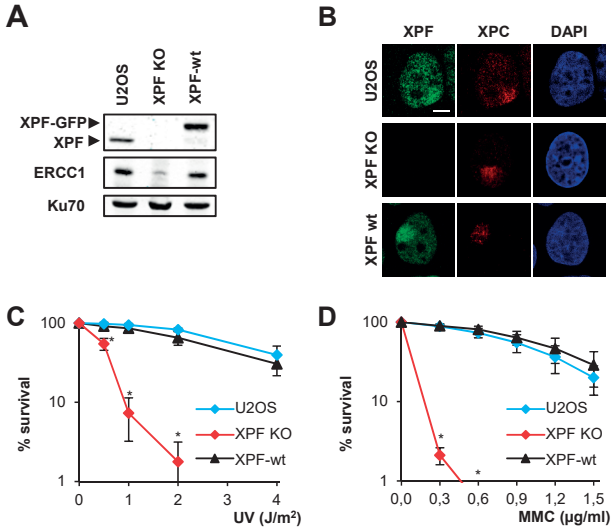

Figure 1. Generation of *XPF* knockout and XPF-GFP expressing cells. (**A**) Immunoblot showing XPF and ERCC1 expression in U2OS, XPF knockout (KO) and XPF-GFP (XPF-wt) expressing XPF KO cells. Ku70 staining is shown as loading control. (**B**) Immunofluorescence pictures showing localization of endogenous XPF in U2OS (top panel) and XPF-wt in XPF KO cells (bottom panel) to LUD induced by 60 J/m^2 UVC irradiation through an 8 µm microporous filter. Cells were fixed 30 minutes after UV and stained against XPF and XPC, to mark sites of local damage. Scale bar: 5 µm. (**C**) Clonogenic UV survival assays of U2OS, XPF KO and XPF-wt expressing XPF KO cells. (**D**) Clonogenic MMC survival assays of U2OS, XPF KO and XPF-wt expressing XPF KO cells. Survival assays are plotted as average of three independent experiments, each performed in triplicate. Error bars represent the SEM. Statistical significant difference ($p<0.05$) compared to U2OS for each dose is indicated by *.

XP, XPCS and FA mutations differently affect UV and MMC sensitivity

Next, we stably expressed GFP-tagged XPF mutants mimicking alleles previously reported in patients affected with XP, XPCS and FA in the XPF KO cells (Table 1 and Figure 2A). We introduced two amino acid substitutions in the helicase-like domain of XPF: P379S (XPF-P379S), found in patients affected with mild XP (39) and C236R (XPF-C236R), found in XPCS patients (15). We also introduced the R589W substitution (XPF-R589W), found as compound heterozygous together with P379S in mild XP but together with C236R in XPCS with FA features (15, 19, 39). Furthermore, we generated nuclease domain substitution mutants R689S (XPF-R689S), found in an XPF FA patient (16) and S786F (XPF-S786F), which was

reported to disrupt ICLR but not NER (40). As control, we generated a nuclease-dead mutant unable to cleave DNA, by introducing the D715A substitution (XPF-D715A) (8).

Live cell imaging and immunofluorescence showed that all XPF mutants, except XPF-R589W, localized exclusively in the nucleus (Figure 2B, C). ERCC1 is stabilized by its interaction with XPF and translocates to the nucleus only when in complex with nuclear XPF (19, 36, 37, 41). Noticeably, in all cell lines expressing XPF mutants, except in the cell line expressing the R589W mutant, ERCC1 protein levels were increased (Supplementary Figure 1B; compare with XPF KO in Figure 1A) and ERCC1 was clearly localized in the nucleus compared to XPF KO (Figure 2C). These results indicate that these XPF mutants interact normally with ERCC1, which was previously also shown for C236R, R689S and D715A XPF mutants (8, 15, 16). The only exception was XPF-R589W, which showed predominant or exclusive localization in the cytoplasm in ~54% of cells and equal localization in cytoplasm and nucleus in ~44% of cells (Figure 2B). Although this mutant appeared to stabilize ERCC1 levels on immunoblot (Supplementary Figure 1B), in immunofluorescence no clearly increased ERCC1 levels were observed, not even when XPF was also partially localized in the nucleus (Figure 2C). To determine the impact of each separate mutation on the different functions of XPF in NER and ICLR, we measured sensitivity of each cell line to UV irradiation and MMC. This showed that cells expressing the C236R, R589W and D715A XPF mutants were strongly hypersensitive to UV (Figure 2D), but cells expressing the P379S, R689S and S786F XPF mutants only showed mild to hardly any UV sensitivity. Cells expressing the C236R, R589W and D715A XPF mutants were also strongly hypersensitive to MMC, while cells expressing XPF-P379S were not sensitive to MMC (Figure 2E). However, contrarily to their mild UV survival, cells expressing XPF-R689S and XPF-S786F were hypersensitive to MMC. These data indicate that XPF mutations found in mild XP and FA patients, i.e. P379S and R689S, and the ICLR-defective S786F mutation, do not fully compromise the ability of XPF to function in NER. R689S and S786F nonetheless do impair XPF function in

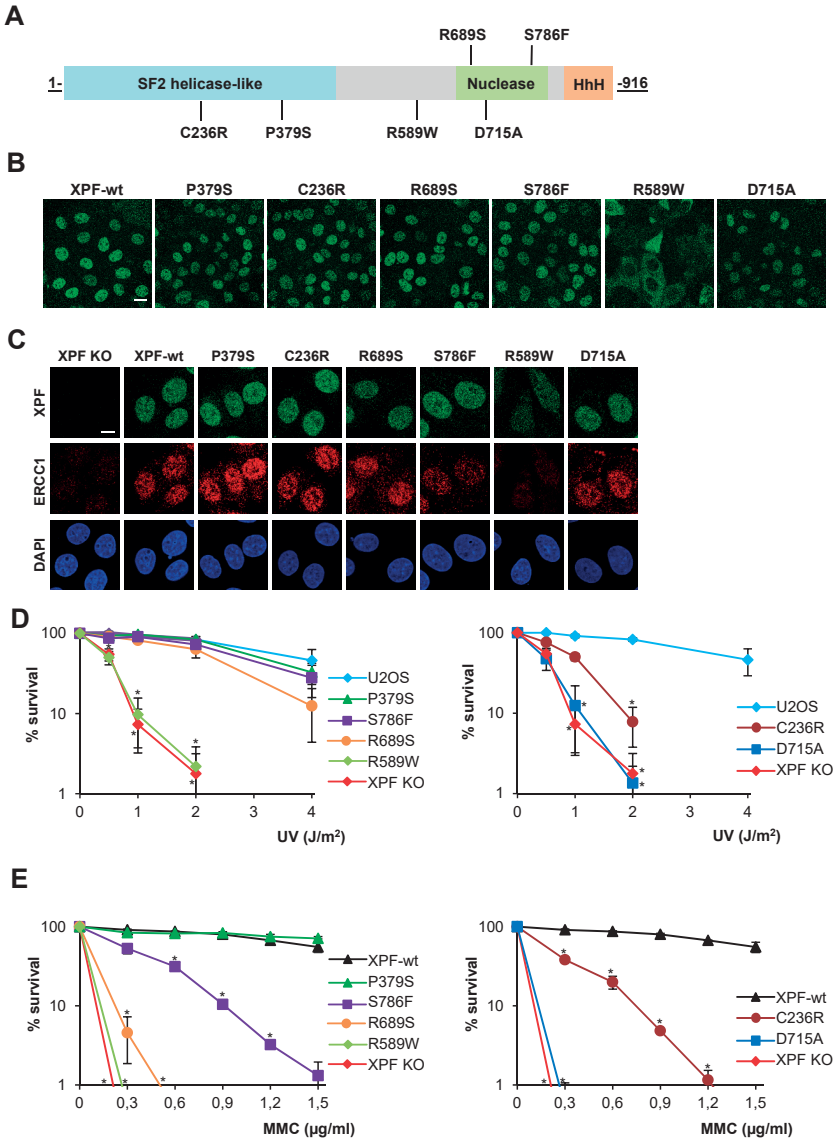

Figure 2. Expression of XPF mutants and sensitivity to UV and MMC. (**A**) Schematic representation of the XPF protein and annotation of the amino acid substitutions studied in this paper. (**B**) Live cell images showing the subcellular distribution of GFP-tagged XPF-wt and XPF mutants stably expressed in U2OS XPF KO cells. Scale bar: 20 µm. (**C**) Immunofluorescence images showing the subcellular distribution of GFP-tagged XPF-wt and XPF mutants stably expressed in XPF KO cells, together with ERCC1 expression visualized by staining with an antibody against ERCC1. Scale bar: 10 µm. (**D,E**) Clonogenic survival assays showing the sensitivity to UV (D) and MMC (E) treatment of XPF KO cells expressing XPF mutants compared to U2OS, XPF KO only and XPF-wt expressing cells. Results are plotted as average of three independent experiments, each performed in triplicate. Error bars represent the SEM. Statistical significant difference ($p<0.05$) compared to U2OS or XPF-wt for each dose is indicated by *.

ICLR. The C236R mutation found in XPCS patients, of which one has features of FA, impedes XPF function in NER and possibly also in ICLR, but this latter is difficult to judge because mild MMC sensitivity can also be caused by a NER defect (17, 42). Strikingly, XPF-R589W was unable to complement both NER and ICLR, similar as nuclease-dead XPF-D715A. We therefore conclude that R589W, which causes XPF to localize in the cytoplasm and is only found in compound heterozygous combinations in patients (Table 1) (15, 19, 39), is a functional null mutation.

Impaired recruitment of XPF-P379S contrasts persistent recruitment of XPF-C236R

To better understand the activity of each XPF mutant in NER, we determined LUD recruitment of the mutants at multiple time points after UV irradiation through a microporous filter using immunofluorescence. LUD was visualized using CPD staining, which is commonly used as a marker for sites of UV damage because CPDs are only very slowly repaired in human cells (43) and still visible up to 24 h after DNA damage induction. XPF-wt clearly accumulated at 1 h and 2 h after UV and showed gradual diminished recruitment at later time points (Figure 3A, B and Supplementary Figure S2A). XPF-R689S and XPF-S786F showed similar recruitment kinetics, albeit XPF-R689S showed slightly delayed release from sites of damage. In contrast, XPF-P379S was inefficiently recruited to LUD at early time points whereas its recruitment also gradually diminished at later time points. Strikingly, XPF-C236R, as well as the nuclease dead XPF-D715A, were strongly recruited at all time points and, remarkably, still persisted at LUD at 24 h. XPF-R589W did not accumulate at all to LUD, even in cells that showed some nuclear localization of the mutant protein, confirming that this is a null mutation.

To further study the dynamic interaction of each of the XPF mutants with UV-irradiated, damaged chromatin, we performed fluorescence recovery after photobleaching (FRAP) in untreated and UV treated cells immediately after irradiation. In untreated cells, all tested XPF mutants showed comparable mobility to XPF-wt, indicating that the mutations do not interfere with XPF's ability to freely move through the nucleus (Supplementary Figure S2B). XPF-R589W could not be tested because its nuclear expression was too low to perform FRAP. Upon UV treatment, incomplete fluorescence recovery of XPF-wt was observed due to XPF immobilization on UV-damaged chromatin, reflecting active participation in NER (33). The fraction of immobilized wild type XPF after 5 J/m^2 UVC was calculated

to be around 12% (Figure 3C). Similar UV-induced immobilization was observed for XPF-S786F while XPF-R689S showed increased immobilization compared to wild type, in accord with its slightly delayed release from LUD observed with immunofluorescence (Figure 3C and Supplementary Figure S2B). Also in line with the immunofluorescence, we observed diminished UV-induced immobilization for XPF-P379S, suggesting that this XP mutant is not efficiently recruited or less stably bound to UV damage. In contrast, XPF-C236R and XPF-D715A showed much stronger UV-induced immobilization than XPF-wt. These data, together with the prolonged LUD accumulation observed in immunofluorescence, indicate that although both mutants are efficiently recruited by the NER machinery, their release from UV damage sites is impaired. This prolonged retention at UV damage sites is likely because both mutants cannot efficiently incise damaged DNA during NER, as it was found that the C236R and D715A mutations respectively reduce (15) and disrupt (8) XPF endonuclease activity *in vitro*.

Because of the strong and prolonged accumulation of XPF-C236R at LUD sites, we investigated if in time this mutant becomes permanently bound to sites of damage or if it is still dynamically binding and dissociating. To this aim, we performed FRAP on LUD inflicted through a microporous filter to measure the mobility (association/dissociation) of XPF-C236R at sites of DNA damage 1 and 6 h after irradiation. As comparison, we measured the mobility of XPF-wt and XPF-P379S on LUD 1 h after UV. Although mutant XPF-P379S was capable of accumulating at LUD (in reduced amounts), its faster recovery of fluorescence after bleaching as compared to XPF-wt (Figure 3D) suggests that this mutant is swiftly exchanged with non-bound XPF. Recruitment and binding of ERCC1-XPF to damaged DNA is thought to be mediated by an interaction of ERCC1 with XPA (9, 10, 44, 45), while XPF activity may be stimulated by an interaction with RPA (46). Thus, it may be that a mutated ERCC1-XPF-P379S complex has reduced affinity for one of these proteins or is less well able to bind to DNA. Interestingly, XPF-C236R at both the 1 h and 6 h time points after UV showed increased initial immobilization but its fluorescence slowly recovered in time (the ascending slope of the FRAP curve in Figure 3D), reflecting delayed but still continuous dissociation. These data confirm that XPF-P379S is inefficiently incorporated into the NER incision complex. Conversely, XPF-C236R is not released as efficiently as XPF-wt, i.e. as when damage is excised, but it likely associates and dissociates continuously to deal with persistent NER substrates.

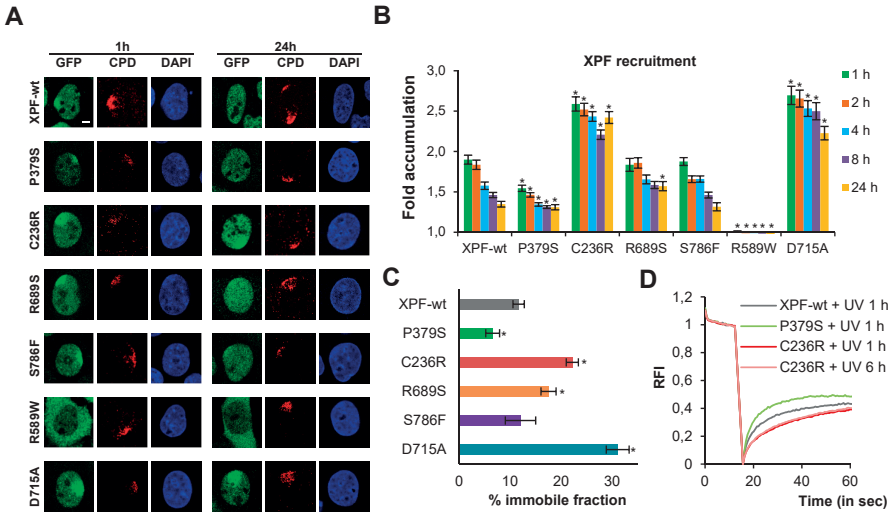

Figure 3. XPF-P379S shows diminished and XPF-C236R persistent DNA damage recruitment. (**A**) Representative immunofluorescence pictures of LUD recruitment of XPF-wt and XPF mutants 1 h and 24 h after local UV irradiation (60 J/m^2) through an 8 μm microporous filter. Cells were stained with antibodies against GFP and CPD, as damage marker. Cells showing clear and comparable local CPD staining are depicted. Scale bar: 5 μm. (**B**) Quantification of LUD recruitment of XPF-wt and XPF mutants, at 1, 2, 4, 8 and 24 h after UV irradiation (60 J/m^2) through a microporous filter, determined by immunofluorescence as shown in (A) and in Supplementary Figure S2A. The fold accumulation was calculated by normalizing fluorescence intensity at sites of local damage to the nuclear background and plotted as average of at least 60 cells per condition from two independent experiments. Statistical significant difference ($p<0.05$) compared to wt for each time point is indicated by *. (**C**) Percentage immobile fraction of XPF-wt and XPF mutants following UV irradiation (5 J/m^2), as determined by FRAP analysis, shown in Supplementary Figure S2B, of at least 20 cells per condition from at least two independent experiments. Statistical significant difference ($p<0.05$) compared to wt is indicated by *. In (B) and (C), error bars represent the SEM. (**D**) FRAP analysis of XPF-wt, XPF-P379S (1 h after UV) and XPF-C236R (1 and 6 h after UV) accumulated at LUD, inflicted by 60 J/m^2 UVC through an 8 μm microporous filter. Each curve represents the average of 30 cells per condition from at least three different experiments. RFI indicates relative fluorescence intensity.

The NER machinery is continuously recruited to DNA damage in the absence of XPF incision

Next, we investigated how the different recruitment behavior of XPF-P379S and XPF-C236R affects the DNA damage recruitment of upstream NER factors, using immunofluorescence. In cells expressing XPF-wt and XPF-P379S, XPC, XPB, XPG and XPA (Figure 4) clearly accumulated at sites of local damage, marked by CPD staining, 1 h after UV and had disappeared after 8 h. In contrast, in XPF KO cells and cells expressing XPF-C236R, as well as in cells expressing catalytically inactive XPF-D715A, accumulation of these NER factors was still clearly visible 8 h after UV. Moreover, also in cells expressing the XPF-R589W null mutant in the nucleus, XPB localization at LUD persisted up to 8 h after UV (Figure 4C).

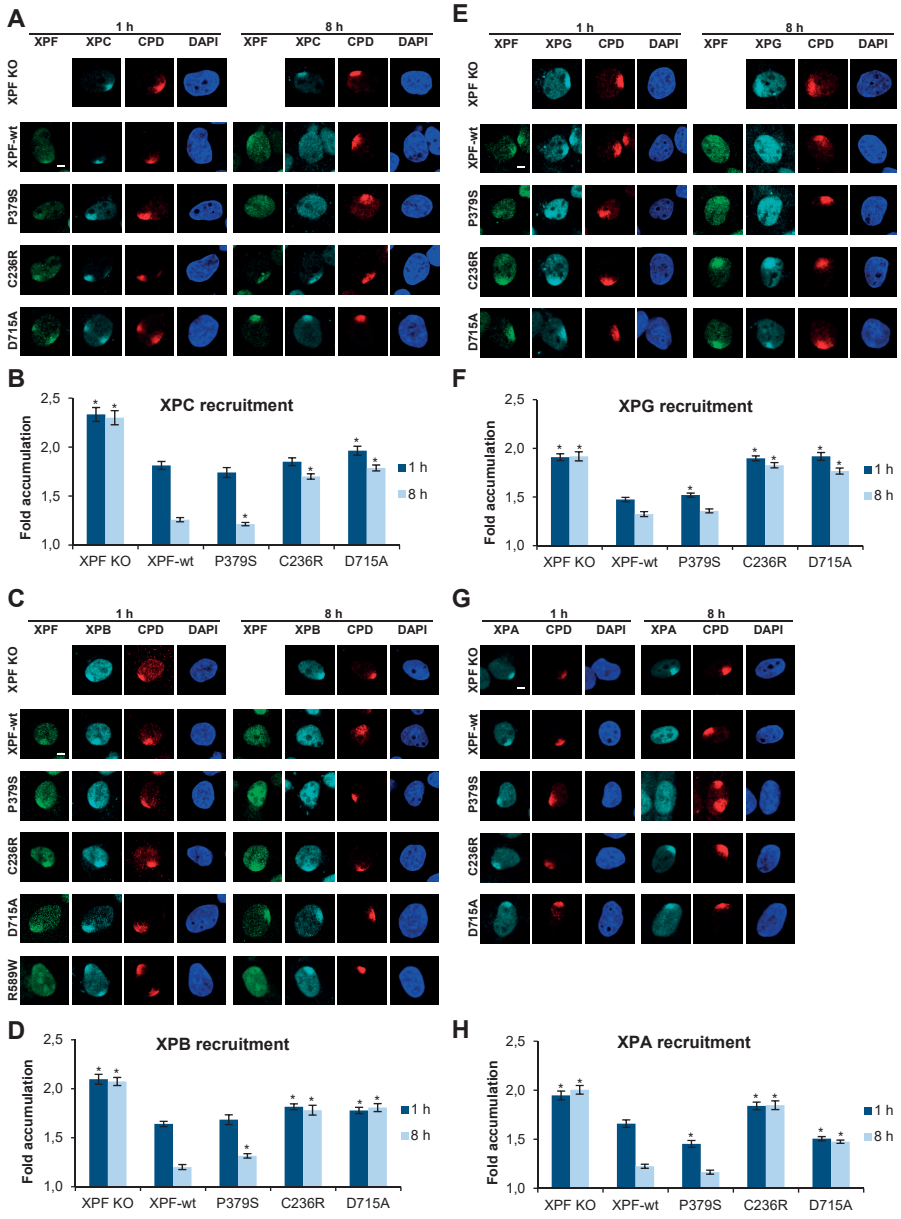

Figure 4. The NER machinery is continuously recruited at sites of DNA damage in XPF KO and XPF-C236R expressing cells. Representative immunofluorescence pictures and quantification of LUD recruitment of XPC (**A** and **B**), XPB (**C** and **D**), XPG (**E** and **F**) and XPA (**G** and **H**) 1 h and 8 h after 60 J/m^2 UVC irradiation through an 8 µm microporous filter in XPF KO cells and cells expressing XPF-wt, XPF-P379S, XPF-C236R, XPF-D715A and (only in C) XPF-R589W. UV damage was visualized by CPD staining. Scale bar: 5 µm. Fold accumulation was calculated by normalizing fluorescence at sites of local damage to the nuclear background and plotted as average of at least 111 (XPC), 85 (XPB), 137 (XPG) and 105 (XPA) cells per condition from at least two independent experiments. Statistical significant difference ($p<0.05$) compared to wt for each time point is indicated by *.

As LUD recruitment of TC-NER factors, such as CSB, is difficult to visualize using immunofluorescence, we measured chromatin binding of CSB after UV using cellular fractionation. CSB was strongly enriched in chromatin of all cells 1 h after irradiation but showed delayed release from chromatin in XPF-P379S and XPF-C236R expressing cells, which was strongest for XPF-C236R (Figure 5). Taken together, these data indicate that in the absence of XPF-mediated incision, also upstream NER factors XPC, TFIIH, XPA, XPG and CSB are continuously recruited to sites of damage and/or less efficiently dissociated, likely in a vain attempt to repair persisting lesions.

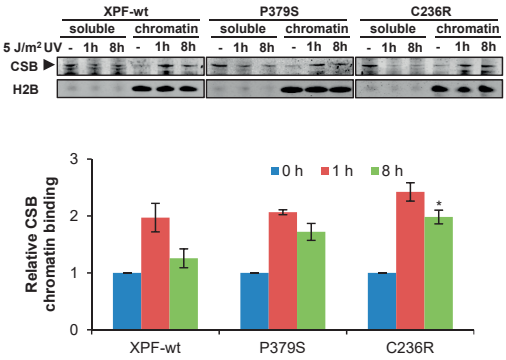

Figure 5. Delayed CSB release from chromatin in XPF-P379S and XPF-C236R cells. Representative cell fractionation of XPF-wt, XPF-P379S and XPF-C236R cells analyzed by immunoblot against CSB and H2B (as loading control; upper panel). Cells were mock treated (-) or irradiated with 5 J/m^2 UVC, lysed after 1 h and 8 h and fractionated into non-chromatin bound (soluble) and chromatin-bound proteins. Lower panel shows quantified levels of CSB bound to the chromatin relative to H2B averaged from four independent experiments. Error bars indicate SEM. Statistical significant difference ($p<0.05$) compared to wt for each time point is indicated by *.

XPF-P379S still allows slow repair while XPF-C236R blocks repair

To explore how NER activity itself is affected by XPF-P379S and XPF-C236R, we determined TC- and GG-NER capacity by measuring respectively recovery of RNA synthesis (RRS) after UV-induced transcription inhibition and unscheduled DNA synthesis (UDS) after UV in XPF KO cells expressing both mutant proteins. RRS, quantified by measuring 5-ethynyluridine (EU) incorporation into RNA 24 h after UV, showed that TC-NER was severely affected in XPF KO and XPF-C236R cells but not in cells expressing XPF-wt or XPF-P379S (Figure 6A). UDS was determined by quantifying incorporation of 5-ethynyl-2-deoxiuridine (EdU) for 30 and 60 min. We measured EdU levels at LUD sites, to be sure that UDS measurements were not obscured by EdU incorporated during replication in the

rapidly proliferating U2OS cells. UDS levels in XPF-P379S cells increased from 30 min to 60 min but were lower than in XPF-wt cells, indicating that repair took place but less efficiently. However, strikingly, XPF-C236R cells only showed baseline UDS levels that did not increase in time, suggesting that these cells are severely deficient in GG-NER (Figure 6B). To confirm this, we measured clearance of CPD lesions in 24 h by immunofluorescence after global UV irradiation of cells. This showed that CPDs are indeed repaired in XPF-P379S cells, although with slight delay as compared to U2OS and XPF-wt cells (Figure 6C). Both XPF KO and XPF-C236R cells did not repair CPDs. These results indicate that the C236R mutation leads to a much stronger NER defect than the P379S mutation, causing impaired transcription after DNA damage, which may very well explain the more severe and CS-like features in patients carrying this mutation.

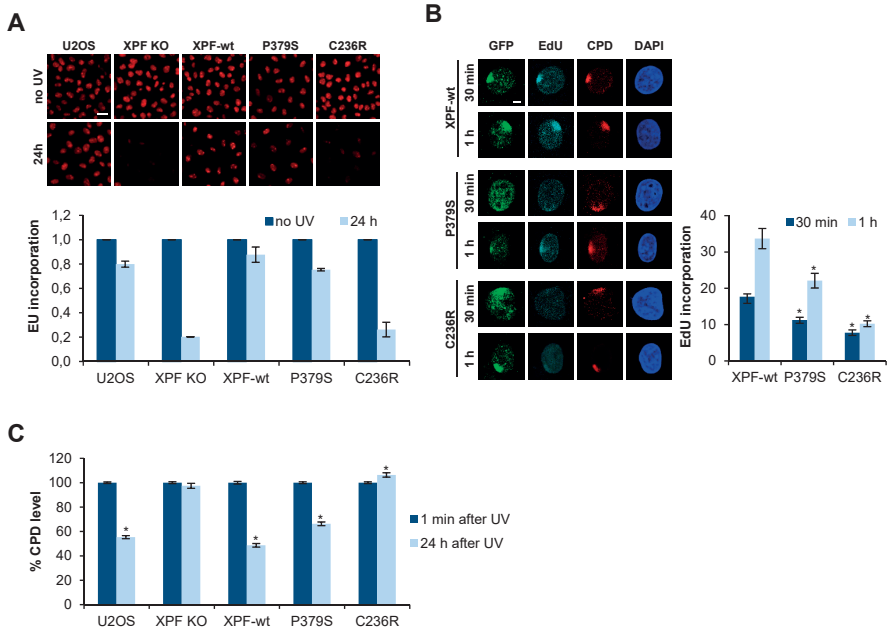

Figure 6. NER is delayed by XPF-P379S and strongly inhibited by XPF-C236R. (**A**) RRS measured by EU incorporation 24 h after mock-treatment (no UV) or 6 J/m^2 UVC in U2OS, XPF KO and XPF-wt, XPF-P379S and XPF-C236R expressing cells. Upper panel shows representative images of red nuclear EU staining. Lower panel shows quantified EU incorporation levels averaged from at least 100 cells in two independent experiments. Scale bar: 25 µm. (**B**) UDS determined by measuring EdU incorporation at LUD sites for 30 min and for 1 h after UV irradiation (60 J/m2) inflicted through an 8 µm microporous filter. Left panel shows representative images of cells stained for EdU (cyan) and CPD (red). Right panel shows quantified EdU incorporation levels averaged from at least 60 cells from two independent experiments. Scale bar: 5 µm. (**C**) CPD removal, as determined by immunofluorescence in U2OS, XPF KO cells and cells expressing XPF-wt, XPF-P379S and XPF-C236R 1 min and 24 h after irradiation with 10 J/m^2 UVC. CPD levels were measured from at least 277 cells from two independent experiments, averaged and normalized to levels 1 min after UV irradiation. Statistical significant difference ($p<0.05$) compared to wt for each time point (B) or compared to 1 min after UV (C) is indicated by *.

Continuous recruitment of the NER machinery is a common feature of XPCS cells

To verify that also in XPCS complex patient cells the NER machinery persistently binds to DNA damage, we tested the DNA damage recruitment of XPF and XPB in CS1USAU and XPCS1CD fibroblasts that carry the C236R mutation in XPF (Table 1) (15). XPF and XPB clearly co-localized in nuclear LUD foci in wild type C5RO fibroblasts as well as in the XPCS fibroblasts 1 h after UV (Figure 7A). No co-localization was observed 8 h after UV in wild type fibroblasts, due to removal of lesions, but intriguingly the co-localization did not disappear in XPCS cells.

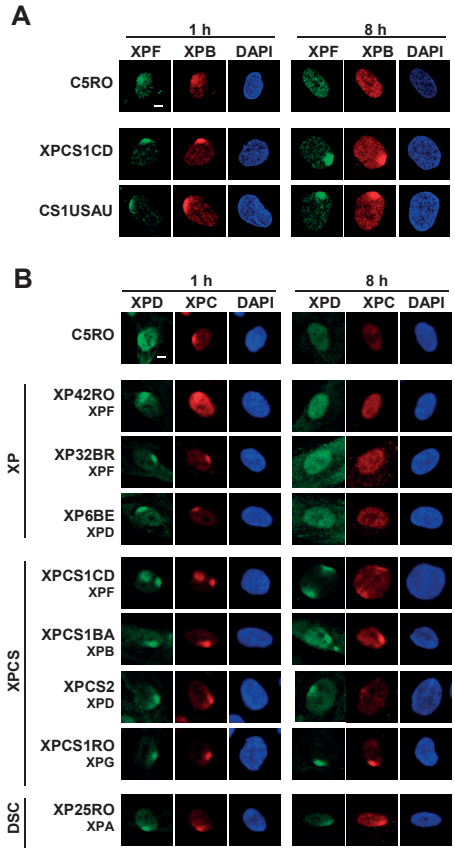

Figure 7. XPC and TFIIH are continuously recruited to UV damage in XPCS patient fibroblasts. (**A**) Representative immunofluorescence pictures showing the co-localization of XPF and XPB at LUD in patient fibroblasts XPCS1CD and CS1USAU, compared to wild type C5RO fibroblasts. Cells were stained 1 h and 8 h after local UV irradiation (60 J/m^2) through an 8 μm microporous filter with antibodies against XPF and XPB. (**B**) Representative immunofluorescence pictures showing the LUD recruitment of XPD and XPC in fibroblasts derived from patients carrying mutations in XPB, XPD, XPG, XPF and XPA, affected by mild XP (XP42RO, XP32BR, XP6BE), XPCS (XPCS1CD, XPCS1BA, XPCS2, XPCS1RO) or DSC (XP25RO) compared to wild type C5RO fibroblasts. Cells were locally UV irradiated with 60 J/m^2 UVC through an 8 μm microporous filter and stained 1 h and 8 h after irradiation with antibodies against XPD and XPC. Scale bar: 5 μm.

Next, we investigated whether persistent recruitment of NER proteins is a specific feature also of other XPCS complex patient fibroblasts, which is not observed in cells from patients affected by XP only, and whether similar persistent recruitment can be observed in cells from severe DSC syndrome. Therefore, we tested the LUD recruitment of XPC, TFIIH subunits XPB and XPD, XPA, XPG and XPF in XP patient fibroblasts carrying mutations in *XPD* or *XPF*, in XPCS complex patient fibroblasts carrying mutations in *XPB*, *XPD*, *XPG* or *XPF* and in DSC patient fibroblasts carrying a mutation in *XPA*. In wild type and XP fibroblasts, XPC, XPB, XPD, and XPG localized to sites of damage 1 h after UV and had (mostly) disappeared at 8 h (Figure 7B and Supplementary Figures S3-S4; Table 2). Similar transient recruitment was observed for XPA in wild type and XPF-deficient XP cells, but XPA recruitment was not observed in XPD-deficient XP cells (Supplementary Figure S5), likely because XPA acts downstream of TFIIH. XPF LUD recruitment was not clearly visible in the XPF-deficient XP-patient cells XP32BR, expressing R589W and P379S mutant XPF, and XP42RO, expressing XPF with a R799W mutation. This result is in line with the diminished recruitment we had observed for XPF-P379S and may indicate that, similarly, XPF carrying a R799W mutation is less efficiently recruited. In contrast, in XPCS cells, we observed persistent DNA damage recruitment of XPC, XPB and XPD at 8 h after UV. Persistent XPA and XPF recruitment was only clearly observed in XPF- and XPG-deficient XPCS cells, but not in XPB- and XPD-deficient cells. XPG also persisted at LUD in XPF-deficient XPCS cells but its recruitment, even at 1 h, could hardly be discerned in XPB- and XPD-deficient XPCS cells. Intriguingly, DSC patient fibroblasts also showed persistent recruitment of XPC, XPB and XPD. These data indicate that continuous DNA damage recruitment of part of the core NER machinery, i.e. XPC and TFIIH, is a general feature of cells derived from XP patients showing additional CS features and/or severe growth and progressive neurological defects.

Table 2: Localization of NER factors to LUD in XP, XPCS and DSC patient fibroblasts

disease	cell line	gene affected	1 hr	8 hr	1 hr	8 hr	1 hr	8 hr	1 hr	8 hr	1 hr	8 hr	1 hr	8 hr
			XPC	XPC	XPB	XPB	XPD	XPD	XPA	XPA	XPG	XPG	XPF	XPF
	C5RO		+	-	+	-	+	-	+	-	+-	-	+	-
XP	XP42RO	XPF (R799W)	+	-	+	-	+	+-	+	-	+	-	-	-
XP	XP32BR	XPF (R589W P379S)	+	-	+	-	+	-	+	-	+	-	-	-
XP	XP6BE	XPD (R683W)	+	-	+-	+-	+	-	-	-	+-	+-	+-	-
XPCS	XPCS1CD	XPF (C236R R589W)	+	+	+	+	+	+	+	+	+	+	+	+
XPCS	XPCS1BA	XPB (F99S)	+	+	+-	+-	+	+	-	-	-	-	+-	-
XPCS	XPCS2	XPD (G602D)	+	+-	+	+-	+	+	+	+-	+-	+-	+	-
XPCS	XPCS1RO	XPG (926fs)	+	+	+	+	+	+	+	+	-	-	+	+
DSC	XP25RO	XPA (R207X)	+	+	+	+	+	+	-	-	+	-	-	-

+ (almost) always visible
+- intermediate visible
- not or hardly visible
XP: xeroderma pigmentosum
XPCS: xeroderma pigmentosum-Cockayne syndrome;
DSC: De Sanctis Cacchione

Discussion

As most ERCC1-XPF patient mutations manifest as compound heterozygous, obscuring a clear understanding of their individual pathogenic impact, we individually expressed XPF mutants in XPF KO cells to study how each mutation affects ERCC1-XPF activity in NER. XP-associated P379S mutant XPF, which in patients is found homozygous or heterozygous with a silent allele or the null allele R589W (Table 1) (19, 39), was inefficiently recruited to DNA damage. Still, this mutant conserved significant residual repair capacity, as shown by increasing UDS levels and repair of CPDs in time. Thus, P379S does not fully abolish but only slows down NER, explaining the almost complete transcription recovery after UV and very mild UV sensitivity observed with this mutant. This is in agreement with significant UDS levels reported for XP72BR, XP7NE and XP32BR patient fibroblasts carrying this mutation (19, 39) (Table 1). Intriguingly, Fassihi and coworkers noticed that P379S occurs with a high allele frequency of 0.3% in the SNP database which would predict more homozygous P379S individuals than patients currently diagnosed with XP (39). Our results, showing that this mutation only mildly impairs ERCC1-XPF activity in NER, might explain this disparity. Residual GG-NER activity has also been reported in cells expressing another XP-associated XPF mutant, i.e. R799W (16, 19, 24). In XP42RO fibroblasts expressing this mutant, we hardly observed DNA damage XPF recruitment but also did not notice persistent recruitment of the upstream NER machinery (Figure 7B and Supplementary Figures S3-S5) as in XPF KO and nuclease-dead XPF-D715A cells, suggesting that NER is not completely impaired. Similarly, residual but slower NER activity was reported for mild XP patient cells from XP complementation groups other than *XP-F* (47–52). Our data therefore support the idea that mild XP symptoms result from mutations in NER genes that reduce, but do not abolish, GG-NER activity (Figure 8).

XPF mutation C236R was identified in two XPCS patients, either as compound heterozygous with R589W or with an allele encoding a barely expressed truncated XPF lacking its nuclease domain (Table 1) (15). Strikingly, this mutation affected XPF activity in NER much more severely than P379S. Similarly to nuclease-dead XPF-D715A, XPF-C236R was persistently recruited to DNA damage (up to 24 h). This was confirmed by FRAP analyses, which, however, indicated that XPF-C236R is not statically bound to damaged DNA. If a fraction of XPF-C236R was statically

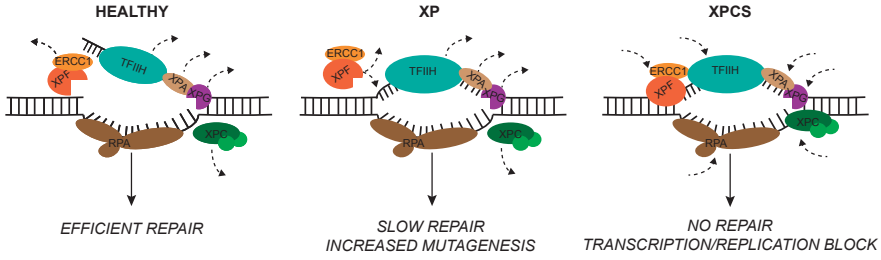

Figure 8. Model showing the difference in NER between XPF-deficient XP and XPCS cells. Left: Wild-type XPF allows efficient recruitment, endonucleolytic function and subsequent release (symbolized by the dashed arrows) of ERCC1-XPF and other NER factors, resulting in efficient repair. Middle: In XP cells with mutated XPF, such as in cells expressing the P379S mutant, XPF is less efficiently recruited to DNA damage. Repair still takes place but at a lower rate and the NER machinery is able to dissociate normally from sites of DNA damage. As a consequence, lesions are less efficiently removed, leading to increased mutagenesis and symptoms associated with XP. Right: In contrast, in XPCS cells with mutated XPF, such as in cells expressing the C236R mutant, the repair reaction is severely blocked. As a consequence, the core NER machinery persistently binds to lesions, likely in a futile attempt to build up a functional NER complex. Impaired repair and persistence of the NER machinery at DNA lesions may enhance transcription impairment due to stalled RNA polymerase II and lead to replication defects, triggering senescence and apoptosis rather than cancer, causing the additional and severe symptoms found in XPCS patients. The same persistent recruitment of part of the core NER machinery is observed in XPCS patient fibroblasts from different XP complementation groups as well as in DSC XPA-deficient cells.

bound, its fluorescence recovery in LUD (as measured in Figure 3D) would be expected to reach a steady-state plateau below the level of XPF-wt, whereas instead we observed continued recovery (i.e. an ascending slope), albeit delayed, of the fluorescence signal in time. Thus, considering also the reduced nuclease activity *in vitro* and the low UDS, RRS and CPD repair levels associated with this mutation, as observed in our cells and previously in patient fibroblasts (15) (Table 1), we speculate that C236R mutant XPF likely continuously binds and dissociates from sites of damage because it is incapable of efficiently incising DNA. In XPF-C236R as well as in XPF-D715A and XPF KO cells, in which obviously no incision is made, the core NER factors XPC, CSB, TFIIH, XPA and XPG were also persistently recruited to sites of damage. It is therefore likely that in XPF-C236R cells the repair reaction is severely blocked (Figure 8). The continuous presence of the core NER machinery probably reflects a futile attempt to build up a functional NER complex, which is also continuously aborted because of the absence of functional XPF. Strikingly, we observed the same persistent recruitment of part of the core NER machinery in XPCS patient fibroblasts from different XP complementation groups as well as in DSC XPA-deficient cells, likely because in these cells NER is strongly blocked as well. Thus, a major difference between mutations that cause

only mild XP and mutations that cause additional developmental and progressive neurodegenerative symptoms might be that these latter mutations much more strongly reduce, or even abolish, NER. Such strongly or completely impaired NER may elicit more untoward events than simply failure to prevent mutagenesis, thus contributing to the more severe phenotype observed in XPCS and DSC.

In the absence of NER, recovery of lesion-stalled transcription is impeded. This could possibly be exacerbated because the NER machinery is continuously binding the same lesion in a vain attempt of repair. As a side consequence, lesions may become less accessible to other repair mechanisms, leading to permanent transcription and possibly also replication defects. This is in line with a model previously proposed for CS in which RNA polymerase II stuck on lesions renders lesions inaccessible to any repair mechanism (6). Unrepaired lesions interfering with transcription and replication will cause a persistent DNA damage response and may induce specific cell fate decisions, leading to senescence or cell death, which might contribute to the more severe phenotypes observed in XPCS while reducing cancer incidence as compared to XP (3, 6). Also, continuous recruitment and activation of the NER machinery may hyperactivate PARP, causing continuous PAR recycling and thus higher ATP consumption, which might ultimately contribute to defective mitophagy often connected to neurodegeneration observed in CS or DSC (53). Additionally, prolonged binding of DNA damage by TFIIH was previously proposed to lead to extensive ssDNA formation contributing to DNA break formation and genomic instability, as observed in mouse and human XPD-XPCS cells (54, 55). Based on structural analysis of a distantly related XPD ortholog from *Sulfolobus acidocaldarius* (56), it was hypothesized that XPD-XPCS mutations may reduce the flexibility of XPD and force the protein in an abnormal conformation that compromises TFIIH function in TC-NER, leading to CS features (57). XP mutations in XPD, on the other hand, may only reduce helicase activity and DNA binding, making NER less efficient, leading to XP and cancer. Mutational analysis in *S. cerevisiae* furthermore suggested that XPD-XPCS mutations still allow partial DNA unwinding by TFIIH, increasing its affinity towards DNA and leading to its permanent recruitment at sites of damage, leaving TFIIH unavailable for transcription resumption (58). Our results also resemble those observed in mouse models with different XPG mutations. Mice carrying a point mutation in XPG that is predicted to affect its endonuclease activity (D811A) show severe, but not completely impaired 6-4PP lesion removal and

UV survival and no CS features (59). In contrast, mice which XPCS mimicking truncating XPG mutations or lacking XPG show stronger defects in lesion removal and UV survival and display a CS phenotype. Such severe truncating mutations in XPG have, however, also been noted to affect other processes besides NER, which may be causative for (part of) the CS phenotype. For instance, severe C-terminal truncation of XPG was suggested to affect its stabilization of TFIIH, leading to dysregulation of gene expression (60), and its non-enzymatic role in regulating homologous recombination and BRCA1 function (61). Similarly, it could be that severe mutations in XPF affect other processes besides NER. For instance, besides its role in DNA repair, ERCC1-XPF has been implicated in control of gene expression by chromatin looping (together with XPG) (62) and transcription initiation during postnatal development (63), in which the DNA substrate on which ERCC1-XPF acts may be similar as in NER. Thus, the inability of XPF-C236R to incise DNA or its persistence at DNA damage sites may impair these processes as well and lead to (some of the) CS features. All of the different, not mutually exclusive, models proposed to explain the severe XPCS phenotype suggest severe disturbance of the normal activity of multifunctional NER factors that eventually compromises chromatin-associated processes. Our data further expand these models by showing that persistent assembly of advanced but non-functional NER pre-incision complexes may strongly interfere with chromatin-associated processes, including transcription which is severely impaired after UV damage in XPF-C236R and XPF KO cells.

The advantage of our XPF KO system for studying functionality of single XPF mutants is clearly illustrated by analysis of the R589W mutation, which is found in both mild and severe XP and XPCS patients as heterozygous combination with P379S, R799W, C236R or an exon 3 deletion (Table 1) (15, 19, 39). XPF with this mutation localized predominantly in the cytoplasm and was unable to bind DNA damage or rescue UV and MMC sensitivity of XPF KO cells, clearly indicating that R589W can be considered as a functional null mutation. Its cytoplasmic localization is in line with the previously observed cytoplasmic XPF localization in patient fibroblasts expressing this mutant (19). It is thus likely that differences in symptoms observed in patients carrying this mutation are mainly derived from differences in the capacity of the other affected *XPF* allele to function in NER. Thus, patients carrying P379S besides R589W (e.g. XP32BR; Table 1) will have residual repair and exhibit mild XP symptoms, whereas patients carrying C236R

besides R589W (e.g. XPCS1CD; Table 1) will hardly have repair and therefore exhibit additional CS symptoms.

Finally, we analyzed two nuclease domain mutations not implicated in XP or XPCS but associated with defects in ICLR and FA. S786F, identified in a breast cancer, was shown to sensitize cells to MMC, but not to UV (40), and to lead to defective ICL unhooking in *Xenopus laevis* egg extracts (20), which was confirmed by our damage recruitment and UV and MMC survival analyses. R689S was found in an FA patient together with an allele encoding a non-expressed frameshift XPF mutant. Both the absence of typical XP features as well as analysis of patient fibroblasts suggested that R689S renders XPF fully defective in ICLR but only partially defective in NER (16) (Table 1). This was confirmed by mild UV but strong MMC hypersensitivity we observed for XPF-R689S expressing cells. Previously, mutation of R689 in human and its equivalent residue in *Xenopus laevis* XPF was shown to reduce XPF nuclease activity *in vitro* and to diminish UV lesion removal (8, 20, 64). In accordance, we noticed slightly increased UV-induced immobilization and delayed damage dissociation of XPF-R689S. These results might therefore indicate that NER is mildly retarded by this mutation because XPF is slightly less able to perform DNA incision, possibly because of defects in positioning of active site residues that carry out this incision (64).

In summary, our analysis indicates that impaired repair and persistence of the NER machinery at DNA lesions characterizes cells from XP patients exhibiting additional developmental and neurodegenerative symptoms (Figure 8). Possibly, the continuous targeting of the core NER machinery to lesions further enhances transcription impairment due to stalled RNA polymerase II, resulting in additional CS-like features. It has always been difficult to grasp how mutations within the same repair pathway and even within the same gene lead to the complex and pleiotropic features associated with hereditary defects in NER, especially since many mutations occur in varying compound heterozygous combinations. Our functional analysis of single XPF mutants exemplifies the advantage of separately studying the impact of each individual allele. The current advance of precise genome editing techniques will likely ease and speed up similar approaches to scrutinize mutations in other NER genes, leading to improved understanding of the molecular mechanisms that underlie different DNA repair disorders.

Funding

This work was supported by the Marie Curie Initial Training Network 'aDDRess' funded by the European Commission 7th Framework Programme [316390], a European Research Council Advanced Grant [340988-ERC-ID to W.V.], an EMBO long-term fellowship [ALTF 663-2014 to J.S.], and the Dutch Cancer Society [10506]. This work is part of the Oncode Institute which is partly financed by the Dutch Cancer Society and was funded by the gravitation program CancerGenomiCs.nl from the Netherlands Organization for Scientific Research (NWO).

Acknowledgement

the authors would like to thank Dr. Gijsbert J. van Belle for advice, Ciske Bertens for technical assistance, Dr. Orlando D. Schärer for providing XPF cDNA, Dr. Tomoo Ogi for cell lines XPCS1CD and CS1USAU. We are also thankful to the Erasmus MC Optical Imaging Center for support with microscopes.

Conflict of interest

None declared.

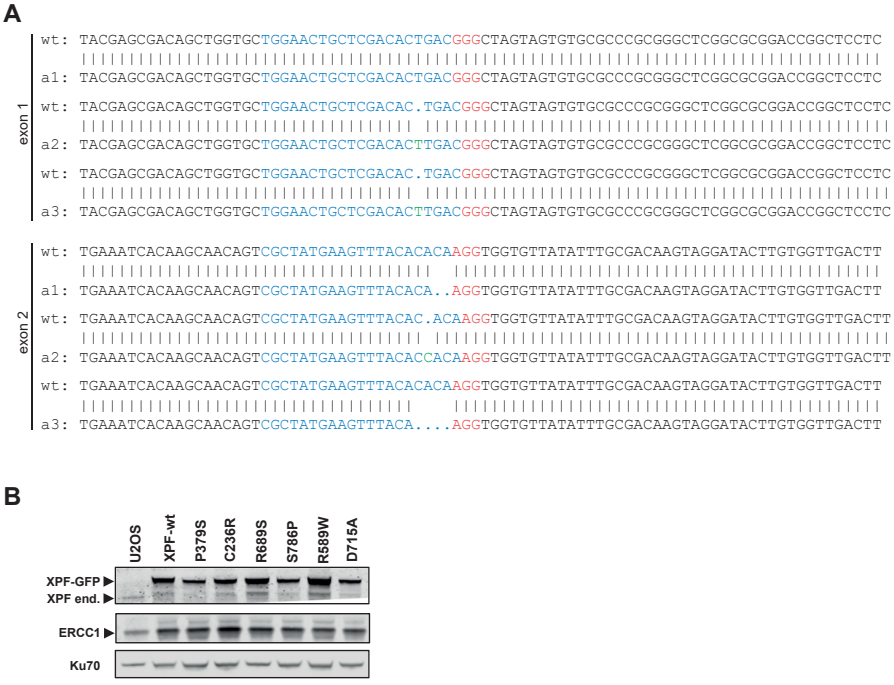

Supplementary Figure S1. Generation of *XPF* knockout and XPF-GFP expressing cells. (**A**) Sequence details of the mutations in the three XPF alleles in U2OS XPF KO cells, induced by XPF sgRNAs targeting exon 1 and exon 2. sgRNA target sequence is indicated in blue, PAM sequence in red and insertions in green. (**B**) Immunoblot showing XPF-GFP, endogenous XPF (XPF end.) and ERCC1 expression in U2OS and XPF KO cells expressing XPF-wt, XPF-P379S, XPF-C236R, XPF-R689S, XPF-S786P, XPF-R589W and XPF-D715A. Ku70 staining is shown as loading control.

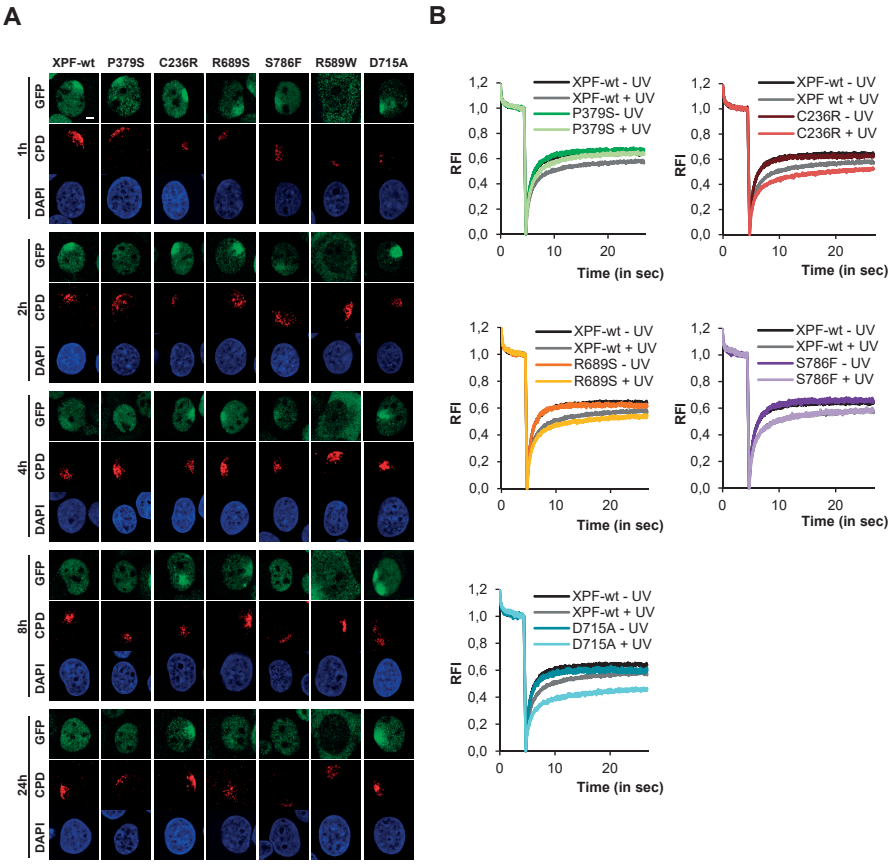

Supplementary Figure S2. XPCS and nuclease-dead XPF mutants are persistently recruited to sites of UV damage. (**A**) Representative immunofluorescence pictures of the LUD recruitment of XPF-wt and XPF mutants 1, 2, 4, 8 and 24 h after UV irradiation (60 J/m^2) through an 8 μm microporous filter. Cells were stained with antibodies against GFP and CPD, as damage marker. Cells showing clear and comparable local CPD staining are depicted. Scale bar: 5 μm. (**B**) FRAP analysis of XPF-wt and XPF mutants in unperturbed (-UV) and UV irradiated cells (+UV; 5 J/m^2). Each curve depicts the average of at least 20 cells per condition from at least two independent experiments. RFI indicates relative fluorescence intensity.

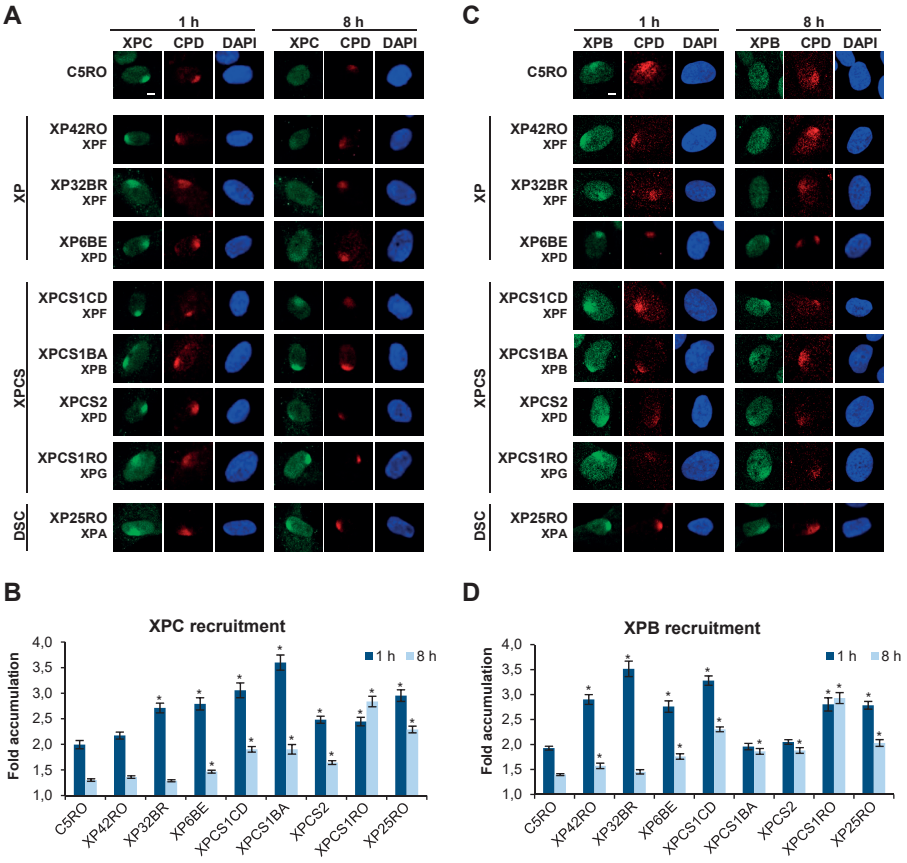

Supplementary Figure S3. DNA damage recruitment of XPC and XPB in XP, XPCS and DSC patient fibroblasts. Representative immunofluorescence pictures and quantification of LUD recruitment of XPC (**A** and **B**) and XPB (**C** and **D**) in fibroblasts derived from patients carrying mutations in XPB, XPD, XPG, XPF and XPA, affected with mild XP (XP42RO, XP32BR, XP6BE), XPCS (XPCS1CD, XPCS1BA, XPCS2, XPCS1RO) or DSC (XP25RO) compared to wild type C5RO fibroblasts. Cells were locally UV irradiated with 60 J/m2 UVC through an 8 μm microporous filter and stained 1 h and 8 h after irradiation with antibodies against XPC or XPB and CPD, to visualize UV damage. Scale bar: 5 μm. Fold accumulation was calculated by normalizing fluorescence at sites of local damage to the nuclear background and plotted as average of at least 46 (XPC) and 41 (XPB) cells per condition from at least two independent experiments. Statistical significant difference ($p<0.05$) compared to C5RO for each time point is indicated by *.

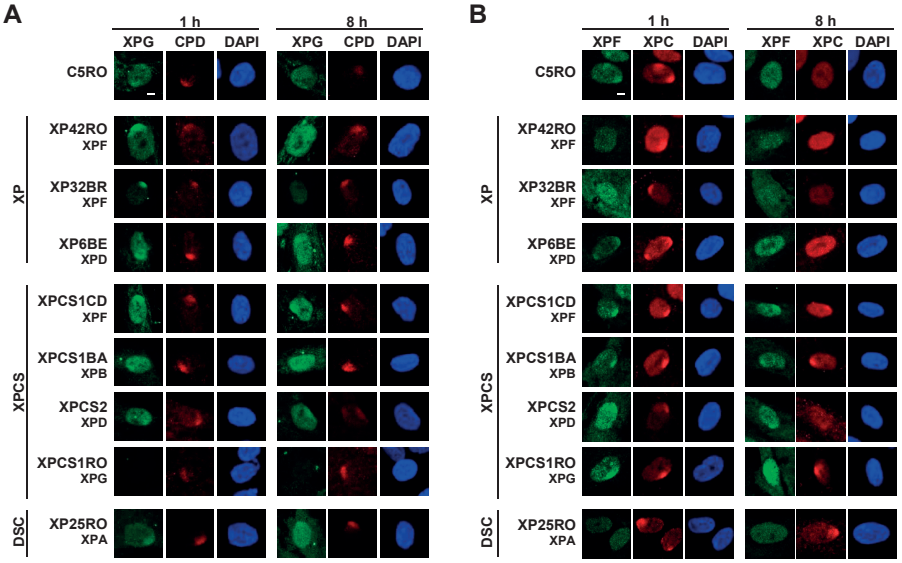

Supplementary Figure S4. DNA damage recruitment of XPG and XPF in XP, XPCS and DSC patient fibroblasts. (**A**-**B**) Representative immunofluorescence pictures showing the LUD recruitment of XPG (A) and XPF (B) in fibroblasts derived from patients carrying mutations in XPB, XPD, XPG, XPF and XPA, affected with mild XP (XP42RO, XP32BR, XP6BE), XPCS (XPCS1CD, XPCS1BA, XPCS2, XPCS1RO) or DSC (XP25RO) compared to wild type C5RO fibroblasts. Cells were locally UV irradiated with 60 J/m^2 UVC through an 8 μm microporous filter and stained 1 h and 8 h after irradiation with antibodies against XPG or XPF and CPD or XPC, to visualize UV damage. Scale bar: 5 μm.

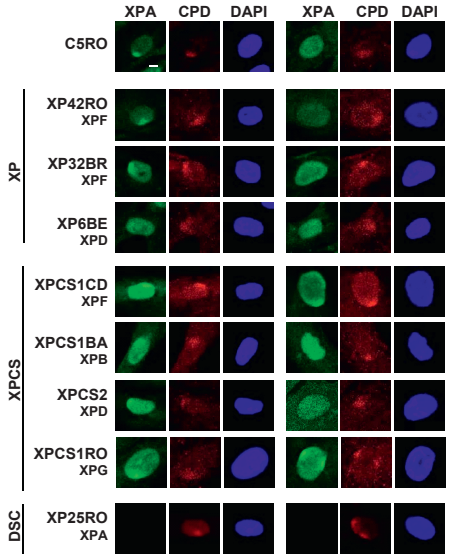

Supplementary Figure S5. DNA damage recruitment of XPA in XP, XPCS and DSC patient fibroblasts. Representative immunofluorescence pictures showing the LUD recruitment of XPA in fibroblasts derived from patients carrying mutations in XPB, XPD, XPG, XPF and XPA, affected with mild XP (XP42RO, XP32BR, XP6BE), XPCS (XPCS1CD, XPCS1BA, XPCS2, XPCS1RO) or DSC (XP25RO) compared to wild type C5RO fibroblasts. Cells were locally UV irradiated with 60 J/m^2 UVC through an 8 μm microporous filter and stained 1 h and 8 h after irradiation with antibodies against XPA and CPD, to visualize UV damage. Scale bar: 5 μm.

Supplementary Table S1: Primers used for site directed mutagenesis

Mutation	Forward primer	Reverse primer
P379S	CTGGTCCTAGAAAGCAACTCAAAGTGGGAGGCACTGACTG	CAGTCAGTGCCTCCCACTTTGAGTTGCTTTCTAGGACCAG
C236R	CTATACTGGACATTTTAAATGCACGTCTAAAGGAACTAAAATGCC	GGCATTTTAGTTCCTTTAGACGTGCATTTAAAATGTCCAGTATAG
R689S	CAAAGCATAGTTGTGGATATGAGTGAATTTCGAAGTGAGC	GCTCACTTCGAAATTCACTCATATCCACAACTATGCTTTG
S786F	CTCCAGCAATGACATTAGTTTCAAACTCACTCTTCTTACAC	GTGTAAGAAGAGTGAGTTTGAAACTAATGTCATTGCTGGAG
R589W	GCAGAGCTAACCTTTGTTTGGCAGCTTGAAATTTACAG	CTGTAAATTTCAAGCTGCCAAACAAAGGTTAGCTCTGC
D715A	GACTTTAGAGGTTGGAGCTTACATCCTCACTCCA	TGGAGTGAGGATGTAAGCTCCAACCTCTAAAGTC

References

1. Lehmann AR, McGibbon D SM (2011) Xeroderma pigmentosum. *Orphanet J Rare Dis* 6(70):1–6.
2. Natale V (2011) A comprehensive description of the severity groups in Cockayne syndrome. *Am J Med Genet Part A* 155(5):1081–1095.
3. Natale V, Raquer H (2017) Xeroderma pigmentosum-Cockayne syndrome complex. *Orphanet J Rare Dis* 12(1):65.
4. Kraemer KH, et al. (2007) Xeroderma pigmentosum, trichothiodystrophy and Cockayne syndrome: A complex genotype-phenotype relationship. *Neuroscience* 145(4):1388–1396.
5. Rahbar Z, Naraghi M (2015) De Sanctis–Cacchione syndrome: A case report and literature review. *Int J Women's Dermatology* 1(3):136–139.
6. Marteijn JA, Lans H, Vermeulen W, Hoeijmakers JHJ (2014) Understanding nucleotide excision repair and its roles in cancer and ageing. *Nat Rev Mol Cell Biol* 15(7):465–481.
7. Schärer OD (2013) Nucleotide excision repair in Eukaryotes. *Cold Spring Harb Perspect Biol* 5(10):a012609–a012609.
8. Enzlin JH, Schärer OD (2002) The active site of the DNA repair endonuclease XPF-ERCC1 forms a highly conserved nuclease motif. *EMBO J* 21(8):2045–2053.
9. Manandhar M, Boulware KS, Wood RD (2015) The ERCC1 and ERCC4 (XPF) genes and gene products. *Gene* 569(2):153–161.
10. Tsodikov O V, et al. (2007) Structural basis for the recruitment of ERCC1-XPF to nucleotide excision repair complexes by XPA. *EMBO J* 26(22):4768–4776.
11. Sijbers AM, et al. (1996) Xeroderma pigmentosum group F caused by a defect in a structure-specific DNA repair endonuclease. *Cell* 86(5):811–822.
12. Bhagwat N, et al. (2009) XPF-ERCC1 Participates in the Fanconi Anemia Pathway of Cross-Link Repair. *Mol Cell Biol* 29(24):6427–6437.
13. Klein Douwel D, et al. (2014) XPF-ERCC1 Acts in Unhooking DNA Interstrand Crosslinks in Cooperation with FANCD2 and FANCP/SLX4. *Mol Cell* 54(3):460–471.
14. Kee Y, D'Andrea A (2012) Molecular pathogenesis and clinical management of Fanconi anemia. *J Clin Invest* 122(11):3799–3806.
15. Kashiyama K, et al. (2013) Malfunction of nuclease ERCC1-XPF results in diverse clinical manifestations and causes Cockayne syndrome, xeroderma pigmentosum, and Fanconi anemia. *Am J Hum Genet* 92(5):807–819.
16. Bogliolo M, et al. (2013) Mutations in ERCC4, encoding the DNA-repair endonuclease XPF, cause Fanconi anemia. *Am J Hum Genet* 92(5):800–806.
17. Niedernhofer LJ, et al. (2006) A new progeroid syndrome reveals that genotoxic stress suppresses the somatotroph axis. *Nature* 444(7122):1038–1043.
18. Jaspers NGJ, et al. (2007) First Reported Patient with Human ERCC1 Deficiency Has Cerebro-Oculo-Facio-Skeletal Syndrome with a Mild Defect in Nucleotide Excision Repair and Severe Developmental Failure. *Am J Hum Genet* 80(3):457–466.
19. Ahmad A, et al. (2010) Mislocalization of XPF-ERCC1 nuclease contributes to reduced DNA repair in XP-F patients. *PLoS Genet* 6(3):e1000871.
20. Klein Douwel D, Hoogenboom WS, Boonen RA, Knipscheer P (2017) Recruitment and positioning determine the specific role of the XPF-ERCC1 endonuclease in interstrand crosslink repair. *EMBO J* 36(14):2034–2046.
21. Vélez-Cruz R, Egly JM (2013) Cockayne syndrome group B (CSB) protein: At the crossroads of transcriptional networks. *Mech Ageing Dev* 134(5–6):234–242.
22. Karikkineth AC, Scheibye-Knudsen M, Fivenson E, Croteau DL, Bohr VA (2017) Cockayne syndrome: Clinical features, model systems and pathways. *Ageing Res Rev* 33:3–17.
23. Wang Y, et al. (2014) Dysregulation of gene expression as a cause of Cockayne syndrome neurological disease. *Proc Natl Acad Sci* 111(40):14454–14459.

24. Sijbers AM, et al. (1998) Homozygous R788W point mutation in the XPF gene of a patient with xeroderma pigmentosum and late-onset neurologic disease. *J Invest Dermatol* 110(5):832–836.
25. Robbins JH, Kraemer KH, Lutzner MA, Festoff BW, Coon HG (1974) Xeroderma pigmentosum: an inherited disease with sun sensitivity, multiple cutaneous neoplasms, and abnormal DNA repair. *Ann Intern Med* 80(2):221–248.
26. Ellison AR, Nouspikel T, Jaspers NG, Clarkson SG, Gruenert DC (1998) Complementation of transformed fibroblasts from patients with combined xeroderma pigmentosum-Cockayne syndrome. *Exp Cell Res* 243(1):22–8.
27. Vermeulen W, Stefanini M, Giliani S, Hoeijmakers JHJ, Bootsma D (1991) Xeroderma pigmentosum complementation group H falls into cornplementation group D. *Mutat Res DNA Repair* 255:201–208.
28. Scott RJ, et al. (1993) Xeroderma pigmentosum-Cockayne syndrome complex in two patients: Absence of slun tumors despite severe deficiency of DNA excision repair. *J Am Acad Dermatol* 29(5):883–889.
29. Kaloustian VM Der, de Weerd-Kastelein EA, Kleijer WJ, Keijzer W, Bootsma D (1974) The Genetic Defect in the De Sanctis-Cacchione Syndrome. *J Invest Dermatol* 63(5):392–396.
30. Sanjana NE, Shalem O, Zhang F (2014) Improved vectors and genome-wide libraries for CRISPR screening. *Nat Methods* 11(8):783–784.
31. Brinkman EK, Chen T, Amendola M, Van Steensel B (2014) Easy quantitative assessment of genome editing by sequence trace decomposition. *Nucleic Acids Res* 42(22):e168.
32. Campeau E, et al. (2009) A versatile viral system for expression and depletion of proteins in mammalian cells. *PLoS One* 4(8):e6529.
33. Houtsmuller AB (1999) Action of DNA Repair Endonuclease ERCC1/XPF in Living Cells. *Science (80-)* 284(5416):958–961.
34. Van Cuijk L, et al. (2015) SUMO and ubiquitin-dependent XPC exchange drives nucleotide excision repair. *Nat Commun* 6(1):7499.
35. Aydin ÖZ, et al. (2014) Human ISWI complexes are targeted by SMARCA5 ATPase and SLIDE domains to help resolve lesion-stalled transcription. *Nucleic Acids Res* 42(13):8473–85.
36. van Vuuren AJ, et al. (1993) Evidence for a repair enzyme complex involving ERCC1 and complementing activities of ERCC4, ERCC11 and xeroderma pigmentosum group F. *EMBO J* 12(9):3693–701.
37. Biggerstaff M, Szymkowski DE, Wood RD (1993) Co-correction of the ERCC1, ERCC4 and xeroderma pigmentosum group F DNA repair defects in vitro. *EMBO J* 12(9):3685–92.
38. Volker M, et al. (2001) Sequential assembly of the nucleotide excision repair factors in vivo. *Mol Cell* 8(1):213–224.
39. Fassihi H, et al. (2016) Deep phenotyping of 89 xeroderma pigmentosum patients reveals unexpected heterogeneity dependent on the precise molecular defect. *Proc Natl Acad Sci* 113(9):E1236–E1245.
40. Osorio A, et al. (2013) Evaluation of Rare Variants in the New Fanconi Anemia Gene ERCC4 (FANCQ) as Familial Breast/Ovarian Cancer Susceptibility Alleles. *Hum Mutat* 34(12):1615–1618.
41. Lehmann J, Seebode C, Smolorz S, Schubert S, Emmert S (2017) XPF knockout via CRISPR/Cas9 reveals that ERCC1 is retained in the cytoplasm without its heterodimer partner XPF. *Cell Mol Life Sci* 74(11):1–14.
42. Zheng H, et al. (2003) Nucleotide Excision Repair- and Polymerase -Mediated Error-Prone Removal of Mitomycin C Interstrand Cross-Links. *Mol Cell Biol* 23(2):754–761.
43. Mitchell DL, Haipek CA, Clarkson JM (1985) (6–4)Photoproducts are removed from the DNA of UV-irradiated mammalian cells more efficiently than cyclobutane pyrimidine dimers. *Mutat Res - Mutat Res Lett* 143(3):109–112.
44. Li L, Elledge SJ, Peterson CA, Bales ES, Legerski RJ (1994) Specific association between the human DNA repair proteins XPA and ERCC1. *Proc Natl Acad Sci U S A* 91(11):5012–6.
45. Park CH, Sancar A (1994) Formation of a ternary complex by human XPA, ERCC1, and ERCC4(XPF) excision repair proteins. *Proc Natl Acad Sci U S A* 91(11):5017–5021.
46. Bessho T, Sancar A, Thompson LH, Thelen MP (1997) Reconstitution of human excision nuclease with recombinant XPF-ERCC1 complex. *J Biol Chem* 272(6):3833–3837.
47. Ichihashi M, Fujiwara Y, Uehara Y, Matsumoto A (1985) A Mild Form of Xeroderma Pigmentosum Assigned to Complementation Group G and Its Repair Heterogeneity. *J Invest Dermatol* 85(3):284–287.

48. Nakano E, et al. (2014) Differences in clinical phenotype among patients with XP complementation group D: 3D structure and ATP-docking of XPD in silico. *J Invest Dermatol* 134(6):1775–1778.
49. de Weerd-Kastelein EA, Keijzer W, Bootsma D (1974) A third complementation group in xeroderma pigmentosum. *Mutat Res - Fundam Mol Mech Mutagen* 22(1):87–91.
50. Chavanne F, et al. (2000) Mutations in the XPC gene in families with xeroderma pigmentosum and consequences at the cell, protein, and transcript levels. *Cancer Res* 60(7):1974–1982.
51. Sethi M, et al. (2016) A Distinct Genotype of XP Complementation Group A: Surprisingly Mild Phenotype Highly Prevalent in Northern India/Pakistan/Afghanistan. *J Invest Dermatol* 136(4):869–872.
52. Sidwell RU, et al. (2006) A novel mutation in the XPA gene associated with unusually mild clinical features in a patient who developed a spindle cell melanoma. *Br J Dermatol* 155(1):81–88.
53. Fang EF, et al. (2014) Defective mitophagy in XPA via PARP-1 hyperactivation and NAD+/SIRT1 reduction. *Cell* 157(4):882–896.
54. Godon C, et al. (2012) Generation of DNA single-strand displacement by compromised nucleotide excision repair. *EMBO J* 31(17):3550–3563.
55. Andressoo J-O, et al. (2006) An Xpd mouse model for the combined xeroderma pigmentosum/Cockayne syndrome exhibiting both cancer predisposition and segmental progeria. *Cancer Cell* 10(2):121–132.
56. Fan L, et al. (2008) XPD helicase structures and activities: insights into the cancer and aging phenotypes from XPD mutations. *Cell* 133(5):789–800.
57. Fuss JO, Tainer JA (2011) XPB and XPD helicases in TFIIH orchestrate DNA duplex opening and damage verification to coordinate repair with transcription and cell cycle via CAK kinase. *DNA Repair (Amst)* 10(7):697–713.
58. Moriel-Carretero M, Herrera-Moyano E, Aguilera A (2015) A unified model for the molecular basis of Xeroderma pigmentosum -Cockayne Syndrome. *Rare Dis* 3(1):e1079362.
59. Shiomi N, et al. (2004) Identification of the XPG region that causes the onset of Cockayne syndrome by using Xpg mutant mice generated by the cDNA-mediated knock-in method. *Mol Cell Biol* 24(9):3712–3719.
60. Ito S, et al. (2007) XPG stabilizes TFIIH, allowing transactivation of nuclear receptors: implications for Cockayne syndrome in XP-G/CS patients. *Mol Cell* 26(2):231–43.
61. Trego KS, et al. (2016) Non-catalytic Roles for XPG with BRCA1 and BRCA2 in Homologous Recombination and Genome Stability. *Mol Cell* 61(4):535–546.
62. Le May N, Fradin D, Iltis I, Bougnères P, Egly JM (2012) XPG and XPF Endonucleases Trigger Chromatin Looping and DNA Demethylation for Accurate Expression of Activated Genes. *Mol Cell* 47(4):622–632.
63. Kamileri I, et al. (2012) Defective transcription initiation causes postnatal growth failure in a mouse model of nucleotide excision repair (NER) progeria. *Proc Natl Acad Sci* 109(8):2995–3000.
64. Su Y, Orelli B, Madireddy A, Niedernhofer LJ, Schärer OD (2012) Multiple DNA binding domains mediate the function of the ERCC1-XPF protein in nucleotide excision repair. *J Biol Chem* 287(26):21846–21855.

CHAPTER 3

ERCC1-XPF targeting to psoralen-DNA crosslinks depends on XPA and FANCD2

Mariangela Sabatella[1,2], Alex Pines[1,2], Jana Slyskova[1,2], Wim Vermeulen[1,2], Hannes Lans[1,2]

1. Department of Molecular Genetics, Erasmus MC, 3015 GE, Rotterdam, The Netherlands
2. Oncode Institute, Erasmus MC, 3015 GE, Rotterdam, The Netherlands

Cellular and Molecular Life Sciences, 2019

Abstract

The effectiveness of many DNA damaging chemotherapeutic drugs depends on their ability to form monoadducts, intrastrand crosslinks and/or interstrand crosslinks (ICLs) that interfere with transcription and replication. The ERCC1-XPF endonuclease plays a critical role in removal of these lesions by incising DNA either as part of nucleotide excision repair (NER) or interstrand crosslink repair (ICLR). Engagement of ERCC1-XPF in NER is well characterized and is facilitated by binding to the XPA protein. However, ERCC1-XPF recruitment to ICLs is less well understood. Moreover, specific mutations in XPF have been found to disrupt its function in ICLR but not in NER, but whether this involves differences in lesion targeting is unknown. Here, we imaged GFP-tagged ERCC1, XPF and ICLR-defective XPF mutants to investigate how in human cells ERCC1-XPF is localized to different types of psoralen-induced DNA lesions, repaired by either NER or ICLR. Our results confirm its dependence on XPA in NER and furthermore show that its engagement in ICLR is dependent on FANCD2. Interestingly, we find that two ICLR-defective XPF mutants (R689S and S786F) are less well recruited to ICLs. These studies highlight the differential mechanisms that regulate ERCC1-XPF activity in DNA repair.

Introduction

The heterodimeric ERCC1-XPF complex (also called ERCC1-ERCC4) is a structure-specific endonuclease that plays an essential role in multiple DNA repair pathways by incising DNA repair intermediate fork-structures at the junction between single stranded and double stranded DNA. ERCC1-XPF excises bulky DNA lesions in nucleotide excision repair (NER) (1), unhooks interstrand crosslinks (ICLs), i.e. covalent linkages between two bases on opposite DNA strands, in interstrand crosslink repair (ICLR) (2–4), removes 3' flaps of DNA intermediate structures in specific double strand break (DBS) repair pathways (5) and cleaves 3' overhangs from uncapped telomeres to shorten them (6). Hereditary mutations in ERCC1-XPF cause several distinct human syndromes characterized by either (skin) cancer-proneness, i.e. xeroderma pigmentosum (XP), developmental abnormalities and accelerated aging, i.e. XP combined with Cockayne syndrome (XPCS complex), or bone marrow failure and chromosome fragility, i.e. Fanconi anemia (FA) (1, 7–10). The severe and pleiotropic symptoms associated with these syndromes highlight the fundamental role of the complex in promoting health by its essential role in different DNA repair processes.

The ERCC1-XPF complex was initially identified as an essential endonuclease in NER (1). This DNA repair pathway removes many different types of DNA lesions that disrupt base-pairing, including photolesions induced by UV light and monoadducts and intrastrand crosslinks induced by widely used chemotherapeutic drugs such as mitomycin C (MMC), cisplatin and psoralens (11, 12). NER is a multistep process consisting of the coordinated, sequential assembly of multiple repair enzymes guided by direct protein-protein and protein-DNA interactions. NER is initiated by two different damage sensing mechanisms. In global genome NER (GG-NER), lesions located anywhere in the genome are recognized by the UV-DDB and XPC-RAD23B-CETN2 complexes. In transcription-coupled NER, lesions located in the transcribed strand are sensed by stalling of elongating RNA polymerase II, which leads to the recruitment of the CSA, CSB and UVSSA proteins. Lesion recognition in both sub-pathways is followed by recruitment of the transcription factor TFIIH, which unwinds the DNA and verifies the presence of damage. TFIIH function is stimulated by the DNA damage binding protein XPA (13), which together with the single stranded DNA binding protein RPA coordinates the positioning of the endonucleases ERCC1-XPF and XPG. XPG

is first recruited through an interaction with TFIIH (14). Next, ERCC1-XPF is recruited through a direct interaction between XPA and an XPA-binding region located within the central domain of ERCC1 (15–19). XPF is the actual nuclease of this complex and incises the DNA 5' to the lesion (20), after which XPG incises the DNA 3' of the lesion. Following excision, the resulting 22-30 nt gap is filled by DNA synthesis and ligation.

In addition to NER, ERCC1-XPF is essential for the removal of ICLs. These are rare DNA modifications induced by either endogenous aldehydes (21) or by chemotherapeutic drugs such as MMC, cisplatin and psoralens (22). ICLs are highly cytotoxic as they obstruct DNA strand separation, required for both replication and transcription. However, despite many studies focused on understanding how ICLs are removed from the genome, the molecular mechanism(s) of ICLR is not yet entirely clear. ICLR is a multistep, sequential assembly of repair enzymes and involves distinct subpathways depending on the cell cycle phase and type of ICL. Most ICLs are repaired during S-phase, which requires the concerted action of different DNA repair systems, including the Fanconi anemia (FA) and homologous recombination (HR) repair pathways, NER and translesion synthesis (TLS). This replication-dependent ICLR is proposed to be initiated when two replication forks converge on an ICL. This leads to the helicase heterodimer FANCM/FAAP24-dependent recruitment of the FA-core complex and monoubiquitylation of the FANCD2-FANCI heterodimer (23, 24). Experiments using *Xenopus laevis* egg extract and *in vitro* modelled ICL-containing replication structures suggest that ERCC1-XPF is then recruited, depending on its interaction with the scaffold protein SLX4 that stimulates its function (2, 25, 26). ERCC1-XPF incises the lagging strand to unhook the ICL, possibly together with another endonuclease or together with the exonuclease SNM1A that digests past the ICL (27). The resulting single stranded gap is filled by TLS and is used as homology template for repair of the remaining double strand break by HR (28, 29). The unhooked crosslink is likely repaired by NER. Certain types of ICLs, such as for instance induced by psoralens, appear to be preferentially unhooked by DNA glycosylase NEIL3-mediated cleavage of one of the two *N-glycosyl* bonds forming the crosslink, which circumvents the need for FA factors and incision of the DNA backbone (30). Other forms of ICLR probably exist that are independent of replication, such as in slowly or non-replicating cells, but these are only poorly understood. Replication-independent ICLR is proposed to involve GG-NER and/or TC-NER factors, likely

depending on the type of crosslinked chemical, including ERCC1-XPF to unhook the ICL (31–35). TLS then fills the resulting gap while a second round of NER removes the remaining ICL from the opposite DNA strand (22, 28).

Understanding how ERCC1-XPF is recruited to sites of DNA damage is necessary to understand how ERCC1-XPF protects against different types of DNA damage, including those induced by commonly used chemotherapeutics, how it helps to prevent cancer and how its inherited deficiency can cause different diseases. Previous imaging studies by us and others have highlighted the importance of XPA in regulating ERCC1-XPF recruitment to UV damage and have shown that patient-derived mutations within XPF can differentially affect its subcellular localization or recruitment to UV-induced DNA damage, explaining phenotypic differences observed in diseases associated with NER dysfunction, such as XP and XPCS complex (16, 17, 36, 37). However, XPA is not implicated in replication-dependent ICLR and not much is known about how ERCC1-XPF is recruited to ICLs in human cells. Here we used imaging of wild type and ICLR-defective XPF to investigate how ERCC1-XPF is distinctly recruited to psoralen-DNA crosslinks repaired by NER or by ICLR. Our results substantiate that FANCD2 is required for recruitment of the complex to ICLs and suggest that XPF ICLR-defective mutants are unable to efficiently associate with ICLs.

Material and methods

Cell culture and siRNA

U2OS cells expressing ERCC1-GFP, XPF-GFP and XPF-C236R, XPF-R689S and XPF-S786F were previously described (37, 38). To knockout XPA, U2OS cells expressing ERCC1-GFP or XPF-GFP were transfected with pLentiCRISPR-V2 plasmid (39) encoding the sgRNA GGCGGCTTTAGAGCAACCCG, targeting the first exon of the *XPA* gene. Transfected cells were selected with puromycin and individual XPA KO clones were screened by immunoblot and sequencing and analyzed using Tracking Indels by DEcomposition as described (40). All cell lines were cultured in standard condition: DMEM/F10 supplemented with 10% fetal calf serum (FCS) and 1% penicillin-streptomycin (PS) at 37°C and 5% CO_2. For siRNA treatment, cells were transfected using RNAiMax (Invitrogen) with control siRNA (Dharmacon, D-001210-05), siRNA targeting XPA (Dharmacon,

MJAWM-000011) or FANCD2 (Dharmacon, D-016376-02), 48 h before UVC or 8-MOP treatment.

Immunoprecipitation

Immunoprecipation of chromatin-enriched nuclear extracts (Figure 2D) was performed as described (41). ERCC1-GFP cells were seeded in 14 cm culture dishes and irradiated with 20 J/m^2 UVC (254 nm lamp, Philips) or left untreated. After 1 h, cells were harvested by scraping in 3 ml cold PBS containing protease inhibitor cocktail (Roche), centrifuged for 10 min at 1500 rpm and washed again with PBS. Cell pellet was then incubated in HEPES buffer (10 mM HEPES pH 7.6, 1.5 mM $MgCl_2$, 10 mM KCl, 0.5 mM DTT, protease inhibitor cocktail) for 10 min on ice. Dounce Homogenizer with a type A pestle was used to isolate the nuclei prior to centrifugation at 3000 rpm for 10 min at 4°C. Next, cell pellets were resuspended in HEPES buffer (100 mM HEPES pH 7.6, 1.5 mM $MgCl_2$, 150 mM NaCl, 0.5 mM DTT, 25% glycerol, protease inhibitor cocktail) and subsequently dounced using a type B pestle. 25 U Microccocal nuclease (MNase, Sigma) was used to digest chromatin extracts for 1 h at 4°C so to obtain mononucleosomal size material by centrifugation at 15000 rpm for 15 min.

Immunoprecipitation of benzonase treated lysates (Figure 5C) was performed as described (Pines *et al*, 2018). Briefly, cells were lysed using IP buffer (30 mM Tris pH 7.5, 150 mM NaCl, 2 mM MgCl2, 0.5% Triton X-100, protease inhibitor cocktail (Roche) supplemented with 250 U/mL Benzonase® nuclease.

In both cases, GFP-Trap®_A beads (Chromotek) were used to immunoprecipitate GFP-tagged proteins. Cell lysate and immunoprecipitated samples were analyzed by immunoblot or mass spectrometry. For mass spectrometry beads from UVC- and mock-treated cells were combined in a 1:1 ratio and label swapping was used to validate the biological findings and exclude contaminants.

Immunoblot

Protein lysates were prepared by scraping cells in 2x sample buffer (125 mM Tris-HCl pH 6.8, 20% Glycerol, 10% 2-β-Mercaptoethanol, 4% SDS, 0.01% Bromophenol Blue) and boiled at 98°C for 5 min. Proteins were separated by SDS-PAGE and transferred to a PVDF membrane (0.45 µm, Merck Millipore). Subsequently, membranes were blocked in 2% BSA and incubated with primary antibodies and secondary antibodies conjugated with CF IRDye 680 and 770 (Sigma) for 1 h or overnight. Primary antibodies used were anti-XPA (sc-853,

Santa Cruz Biotechnology), anti-SNF2H (ab3749, Abcam), anti-Tubulin (T6074, Sigma), anti-FANCD2 (nb100-316, Novus Biologicals), anti-GFP (ab290, Abcam), anti-SLX4 (NBP1-28680, Novus Biologicals), anti-ERCC1 (ab129267, Abcam), anti-H2B (07-371, Millipore), anti-RPA70 (2267, Cell signaling). Secondary antibodies were visualized using the Odyssey CLx Infrared Imaging System (LI-COR Biosciences).

Clonogenic survival assays

To analyze the UV sensitivity of the ERCC1-GFP and XPF-GFP XPA-deficient cells, we seeded 500 cells in 6-well plates in triplicate. After 24 h, cells were irradiated with the indicated doses of UV (254 nm UVC lamp, Philips). 5 to 7 days after irradiation, cells were fixed and stained with 50% Methanol, 7% Acetic Acid, 0.1 % Brilliant Blue R (Sigma). Colonies were counted using the integrated colony counter GelCount (Oxford Optronix). The number of colonies in the non-treated cells was set to 100% and the number of colonies after UV treatment was normalized to the number of colonies in untreated samples and plotted as percentage survival.

UV-, psoralen-treatment and immunofluorescence

To analyze the localization of proteins to LUD, cells seeded on coverslips were irradiated with 60 J/m^2 (254 nm UVC lamp, Philips) through an 8 μm microporous filter (Millipore) and fixed with 2% paraformaldehyde supplemented with 0.1% Triton X-100, 1 h after irradiation. Next, cells were permeabilized with 0.1% Triton X-100 for 20 min, incubated with 0.07 M NaOH for 5 min (to visualize CPDs) and washed in PBS containing 0.15% glycine and 0.5% BSA before proceeding with immunofluorescence. Analysis of protein localization to psoralen-induced DNA damage was performed as described (43, 44). Briefly, cells were seeded on coverslips and incubated with 50 μM 8-methoxypsoralen (8-MOP, Sigma) for 2 h. 8-MOP was locally activated in stripes along the cell nuclei by a 355 nm UVA laser coupled to a PALM Laser Dissection microscope (Zeiss) through a 40x 0.60 NA Korr LD Plan Neofluar objective. Cells were then fixed with 2% paraformaldehyde supplemented with 0.1% Triton X-100 and washed in PBS containing 0.15% glycine and 0.5% BSA before proceeding with immunofluorescence. For immunofluorescence, cells were stained with primary antibodies for 2 h and then incubated with secondary antibodies conjugated to ALEXA fluorochromes 488, 555 and 633 (Invitrogen) for 1 h. Primary antibodies used were against: GFP

(ab290, Abcam), CPD (CAC-NM-DND-001; Cosmo Bio), XPA (sc-853, Santa Cruz Biotechnology), FANCD2 (nb100-316, Novus Biologicals), SLX4 (NBP1-28680, Novus Biologicals), γH2AX (ab11174, Abcam or 05-636, Millipore), XPF (sc-136153, Santa Cruz Biotechnology). DAPI Vectashield (Vector Laboratories) was used to mount the coverslips. Cells were imaged using an LSM700 microscope equipped with a 40x Plan-apochromat 1.3 NA oil immersion lens (Carl Zeiss). The software Image J was used to quantify fluorescence intensity. Fold accumulation was calculated as the ratio between fluorescence intensity at the site of damage and fluorescence intensity in the cell nucleus, measured in at least 60 cells per condition in two or more separate experiments. Statistical analysis of the differences in GFP intensity at sites of local damage (Figure 2C, 4B, 4D, 5B) was performed using a one-way ANOVA followed by post-hoc analysis by Bonferroni's test.

SILAC-based mass spectrometry analysis

For SILAC, cells were cultured in DMEM containing 10% dialyzed FBS (Gibco), 10% GlutaMAX (Life Technologies), penicillin/streptomycin (Life Technologies), unlabeled L-arginine-HCl and L-lysine-HCL ("light") or $^{13}C_6$,$^{15}N_4$l-arginine-HCl and $^{13}C_6$,$^{15}N_2$l-lysine-2HCl ("heavy") (Cambridge Isotope Laboratories). For the "Forward" experiment, immunoprecipitation extracts derived from "light"-labeled mock-treated cells were mixed with extracts derived from "heavy" UVC-treated (20 J/m^2) cells; for the "Reverse" experiment, extracts derived from "light"-labeled UVC-treated (20 J/m^2) treated cells were mixed with extracts derived from "heavy" mock-treated cells. After protein separation, SDS-PAGE gel was cut into 2 mm slices and subjected to in-gel reduction with dithiothreitol, alkylation with iodoacetamide (98%; D4, Cambridge Isotope Laboratories) and digested with trypsin (sequencing grade; Promega). Samples were analyzed by mass spectrometry using an Orbitrap Fusion™ Tribrid™ mass spectrometer and EASY-nLC™ 1000 (Thermo). MaxQuant software was used to analyze the data.

Results

ERCC1-XPF recruitment to sites of UV damage is XPA-dependent

To investigate how the activity of ERCC1-XPF in response to ICLs is regulated in cells, we studied how the complex is recruited to sites of locally induced psoralen-DNA crosslinks independently of NER. ERCC1-XPF binding to damaged DNA during NER critically depends on its interaction with XPA (15–19). Therefore, we generated XPA knockout (KO) cell lines by transfecting a plasmid encoding Cas9 and an sgRNA targeting exon 1 of XPA in previously generated U2OS cells expressing ERCC1-GFP (38) and U2OS XPF KO cells expressing XPF-GFP (37). Sequencing and Tracking Indels by DEcomposition analysis (40) revealed multiple indel mutations in the *XPA* gene of a selected ERCC1-GFP-expressing and a selected XPF-GFP-expressing XPA KO clone (data not shown). The absence of XPA in these clones was confirmed by immunoblot (Figure 1A, B), while strong UV hypersensitivity (Figure 1C, D) showed that these cells indeed lack functional NER.

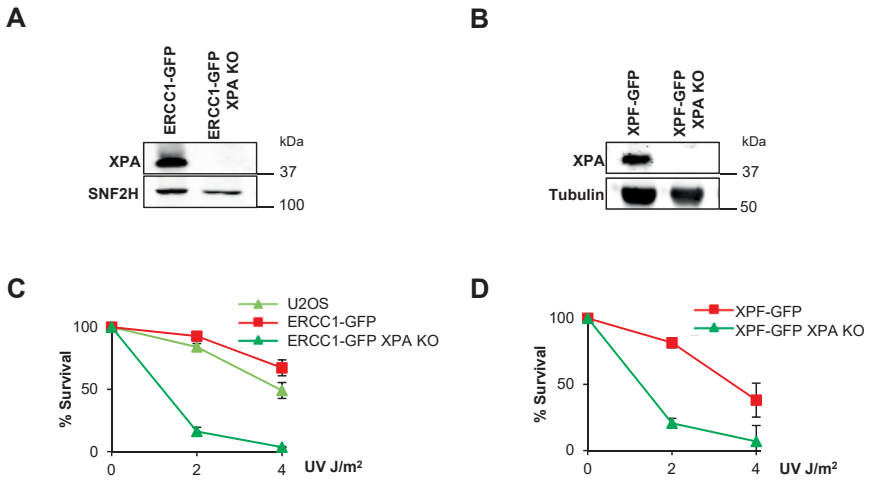

Figure 1. Generation of XPA knockout in ERCC1-GFP and XPF-GFP expressing cells. (**A**) Immublot showing XPA expression levels in XPA-proficient and XPA knockout (XPA KO) U2OS cells expressing GFP-tagged ERCC1. SNF2H was used as loading control. (**B**) Immublot showing XPA expression levels in XPA-proficient and XPA knockout (XPA KO) U2OS cells expressing GFP-tagged XPF. Tubulin was used as loading control. (**C**) Clonogenic UV survival assays of wild type U2OS cells without any transgene (U2OS) and XPA-proficient and XPA KO U2OS cells expressing ERCC1-GFP. Results are plotted as average of three independent experiments, each performed in triplicate. (**D**) Clonogenic UV survival assays of XPA-proficient and XPA KO U2OS cells expressing XPF-GFP. Results are plotted as average of at least two independent experiments, each performed in triplicate. In (C) and (D), error bars represent the SEM.

To show the validity of these cells in discerning between ERCC1-XPF activity in NER and in ICLR, we tested ERCC1-GFP and XPF-GFP recruitment to local UV damage (LUD) in XPA-proficient and XPA KO cells by immunofluorescence, after UVC irradiation through an 8 μm microporous filter (Figure 2A, C). While both ERCC1 and XPF were clearly recruited to LUD in XPA-proficient cells, we could not observe clear recruitment in XPA KO cells. Depletion of FANCD2 in XPA-proficient and XPA KO cells expressing XPF-GFP, by a 48 h siRNA treatment (Figure S1A), did not reduce XPF-GFP LUD recruitment as compared to control siRNA-treated cells (Figure 2B, C). Our data confirm that ERCC1-XPF engagement in NER is completely dependent on XPA (45) and not regulated by FANCD2, indicating that the XPA KO cells can be used to study ERCC1-XPF activity outside NER.

To determine whether any additional, as-of-yet unidentified factors regulate ERCC1-XPF recruitment to UV damage, we combined ERCC1-GFP immunoprecipitation with stable isotope labeling by amino acids in cell culture (SILAC)-based quantitative proteomics (including label-swapping, i.e. "forward" and "reverse" replicate experiments). To this end, SILAC-labeled ERCC1-GFP expressing U2OS cells were mock-treated or exposed to UVC (20 J/m^2) and 1 h after treatment chromatin-enriched nuclear extracts were subjected to GFP-mediated immunoprecipation and mass spectrometry analysis. Interestingly, and as expected, this showed that after UV irradiation, ERCC1-XPF interacts with multiple components of the TFIIH complex, RPA and XPG (Figure 2D and Table 1). Also XPA was identified as interactor of ERCC1, but only in one of the replicate experiments and therefore not depicted in Figure 2D. However, no additional new factors were identified, suggesting that no major or essential unknown factors exist that regulate ERCC1-XPF involvement in NER. Moreover, SLX4 was identified as a constitutive interaction partner of the endonuclease complex, in line with previous observations (2, 25, 26). However, the interaction ratio of this partner did not change upon UV-irradiation, in line with its specific role in ICLR.

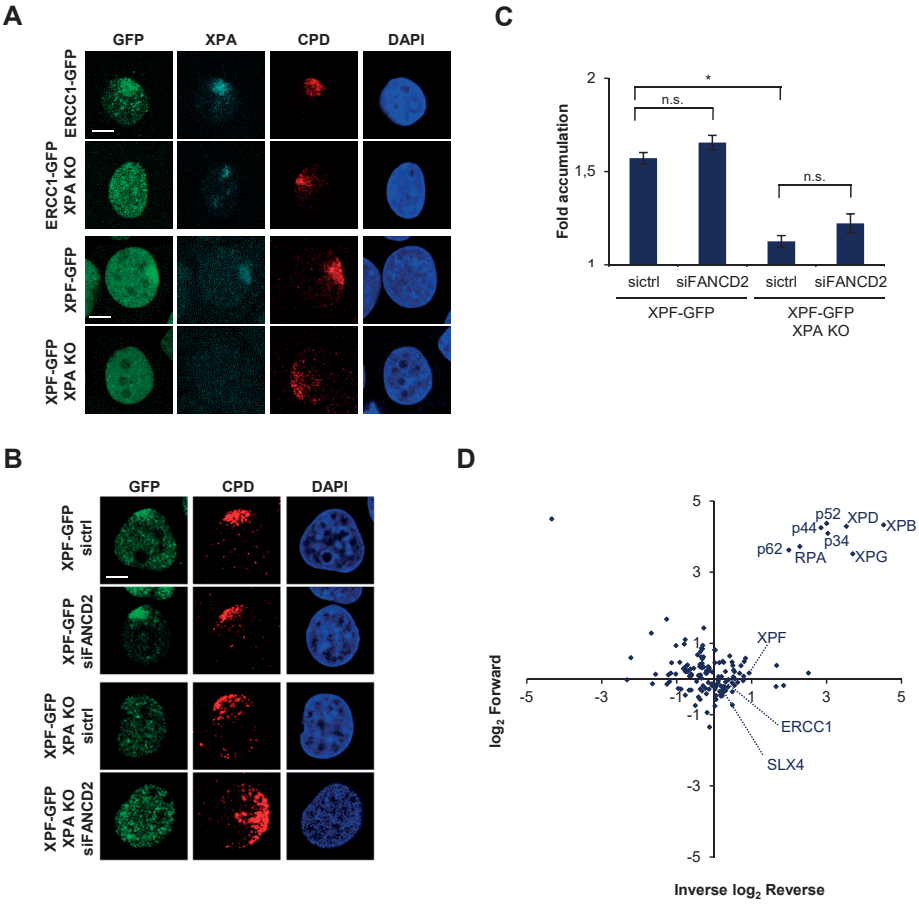

Figure 2. XPF recruitment to LUD is XPA-dependent. (**A**) Immunofluorescence images showing LUD recruitment of ERCC1-GFP (top panel) or XPF-GFP (lower panel) and endogenous XPA in XPA-proficient and XPA KO U2OS cells, 1 h after 60 J/m^2 UVC irradiation through an 8 µm microporous filter. Cells were immunostained against XPA and CPD, as damage marker. The GFP signal was not amplified using antibody staining. Scale bar: 5 µm. (**B**) Immunofluorescence images showing XPF-GFP LUD recruitment 1 h after 60 J/m^2 UVC through an 8 µm microporous filter in XPA-proficient and XPA KO U2OS cells treated with non targeting siRNA (sictrl) or siRNA targeting FANCD2 (siFANCD2). Cells were immunostained against GFP and CPD, which was used as damage marker. Scale bar: 5 µm. Error bars represent the SEM. (**C**) Quantification of XPF-GFP LUD recruitment in XPA-proficient and XPA KO cells, as determined by immunofluorescence experiments shown in (B). The fold accumulation at sites of local damage was calculated over the nuclear background and plotted as average of at least 100 cells per condition from two independent experiments. Statistical significant difference ($p<0.05$) is indicated by *, n.s. non-significant. (**D**) Scatter plot of the $\log_2$ SILAC ratio of the Forward and Reverse SILAC ERCC1-GFP immunoprecipations experiments, comparing ERCC1-GFP interactors with and without UVC treatment (20 J/m^2, 1 h). UV-specific interactors are depicted in the upper right quadrant.

Table 1: UV-dependent ERCC1-GFP interacting proteins identified by SILAC-MS

Protein names	Unique peptides	Ratio H/L Forward	Ratio L/H Reverse	Average
XPB/ERCC3	18	22.991	20.10	21.55
XPD/ERCC2	24	11.55	19.57	15.56
p52/GTF2H4	8	8.0175	20.70	14.36
XPG/ERCC5	14	12.985	11.45	12.22
p34/GTF2H3	11	8.1806	17.08	12.63
p44/GTF2H2	13	7.2274	19.04	13.14
XPA	2		9.14	9.14
RPA1	7	4.8773	13.23	9.05
p62/GTF2H1	11	3.9822	12.33	8.15
XPF/ERCC4	51	1.9116	1.13	1.52
ERCC1	21	1.3952	0.93	1.16
SLX4	27	1.1329	0.72	0.93

Unique peptides and normalized ratios of the forward and reverse experiment of the top interacting proteins with ERCC1 1 h after 20 J/m^2 UV irradiation. Also, peptides and ratios for ERCC1, XPF and SLX4 are shown.
H: heavy; L: light

ICLR and NER core factors localize to psoralen-induced DNA damage

In order to analyze ERCC1-XPF recruitment to ICLs, we combined the use of the psoralen 8-methoxypsoralen (8-MOP) with UVA laser micro-irradiation along a user-defined track across the cell nucleus (44, 46), to activate the 8-MOP and induce local psoralen-DNA crosslinks. UVA activation of intercalated 8-MOP generates both monoadducts as well as ICLs in DNA (47–51). The efficiency of this method to induce ICLs was shown by the clear recruitment of endogenous FANCD2 and SLX4 to local psoralen adducts, marked by γH2AX co-staining, as visualized by immunofluorescence in U2OS cells (Figure 3A, 8-MOP+Laser). Importantly, we did not observe recruitment of FANCD2 or SLX4 or induction of γH2AX in cells that were only UVA microirradiated but not treated with 8-MOP (Laser), indicating that the applied UVA laser by itself did not generate DNA damage that leads to γH2AX signaling or is recognized by FANCD2. Furthermore, we observed clear recruitment of XPA to local psoralen adducts, as marked by γH2AX (Figure 3B), indicative of targeting of the core NER machinery to psoralen adducts and suggesting the induction of NER subtrate lesions. As monoadducts formed by psoralen are known NER substrates (52, 53), XPA is likely recruited to psoralen monoadducts as part of the NER machinery. However, as NER is also implicated in replication-dependent and -independent ICLR (31, 32), XPA may be recruited to psoralen-ICLs as well. Moreover, also endogenous XPF as well as

ERCC1-GFP and XPF-GFP were clearly recruited to psoralen adducts. Because of the induction of multiple types of DNA damage, this accumulation likely reflects the engagement of ERCC1-XPF in both active NER as well as ICLR.

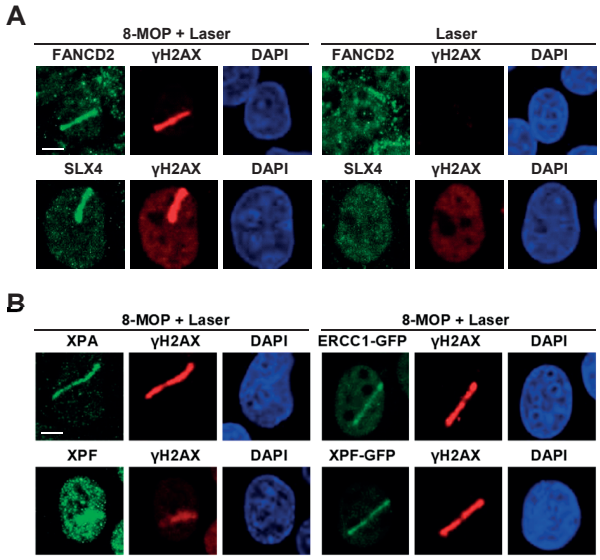

Figure 3. ICLR and NER core factors are recruited to psoralen-induced DNA damage. (**A**) Immunofluorescence images showing recruitment of endogenous FANCD2 and SLX4 to sites of local UVA laser microirradiation in untreated (Laser) or psoralen-treated (8-MOP + Laser, 50 μM 8-MOP, 2 h) U2OS cells. Cells were immunostained against FANCD2, SLX4 and γH2AX, which was used as damage marker. Scale bar: 5 μm. (**B**) Immunofluorescence images showing recruitment to sites of local UVA laser microirradiation in psoralen-treated U2OS cells (8-MOP + Laser, 50 μM 8-MOP, 2 h) of endogenous XPA and XPF (left panels) and in psoralen-treated U2OS cells expressing ERCC-GFP or XPF-GFP (right panels). Cells were immunostained against XPA, XPF, GFP and γH2AX, which was used as damage marker. Scale bar: 5 μm.

ERCC1-XPF recruitment to psoralen adducts is XPA- and FANCD2-dependent

To test whether ERCC1-XPF recruitment to ICLs is dependent on FANCD2, we studied the recruitment of the complex to local psoralen adducts in ERCC1-GFP- and XPF-GFP-expressing XPA-proficient and KO cells, depleted of FANCD2 by siRNA (Figure 4). In XPA-proficient cells, XPF-GFP recruitment to psoralen adducts was reduced after siFANCD2 treatment compared to control siRNA-treated cells (Figure 4A, B). Also, ERCC1-GFP recruitment was slightly reduced in siFANCD2-treated cells compared to control siRNA-treated cells (Figure 4C, D). This was less pronounced than for XPF, possibly because of competition

with endogenous ERCC1 that is still present in these cells (and which we did not visualize). These observations suggest that ERCC1-XPF recruitment to psoralen adducts is partially dependent on FANCD2. Furthermore, the absence of XPA also induced a strong reduction in ERCC1-GFP and XPF-GFP localization to psoralen adducts that was further reduced by additional FANCD2 depletion (Figure 4). Our data therefore suggest that, in response to psoralen adducts, ERCC1-XPF is recruited both by XPA to participate in NER and by FANCD2 to function in ICLR. These observations in human cells are in accordance with chromatin immunoprecipation (ChIP) studies in *Xenopus* egg extracts suggesting that FANCD2 preceeds and is needed for ERCC1-XPF recruitment to an ICL (2).

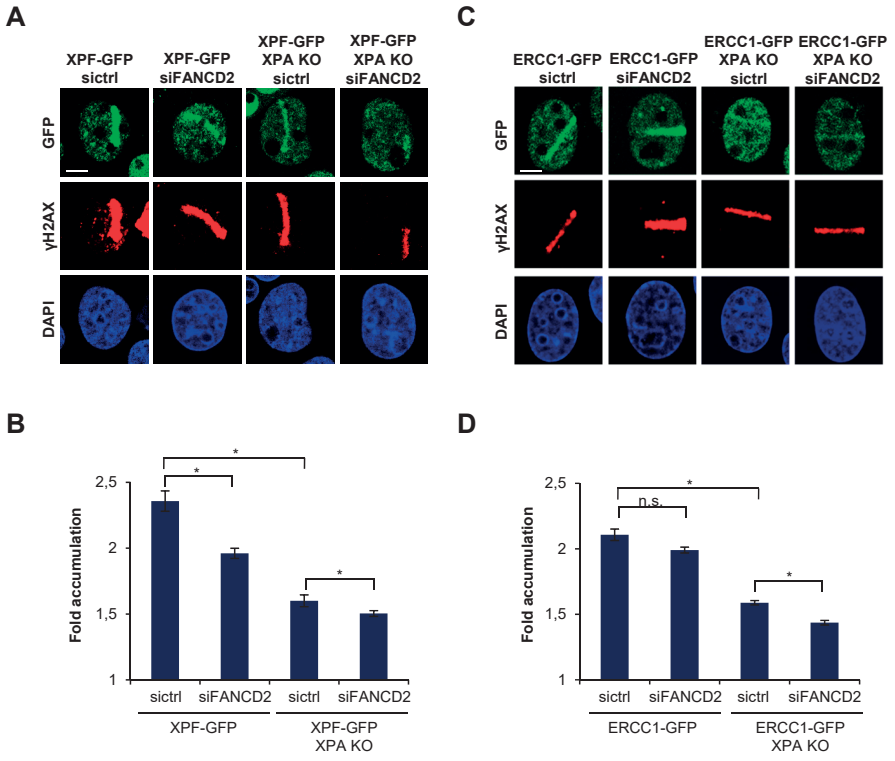

Figure 4. ERCC1-XPF recruitment to psoralen-induced DNA damage is XPA- and FANCD2-dependent. (**A**) Immunofluorescence images showing XPF-GFP recruitment to sites of local UVA laser microirradiation in psoralen-treated (50 μM 8-MOP, 2 h) XPA-proficient and XPA KO U2OS cells treated with nontargeting siRNA (sictrl) or siRNA targeting FANCD2 (siFANCD2). Cells were immunostained against GFP and γH2AX, which was used as damage marker. Scale bar: 5 μm. (**B**) Quantification of XPF-GFP recruitment to sites of local UVA laser microirradiation in psoralen-treated XPA-proficient and XPA KO U2OS cells, as determined by immunofluorescence experiments shown in (A). The fold accumulation at sites of local

damage was calculated over the nuclear background and plotted as average of at least 80 cells per condition from three independent experiments. Error bars represent the SEM. Statistical significant difference ($p<0.05$) is indicated by *. (**C**) Immunofluorescence images showing ERCC1-GFP recruitment to sites of local UVA laser microirradiation in psoralen-treated (50 μM 8-MOP, 2 h) XPA-proficient and XPA KO U2OS cells treated with nontargeting siRNA (sictrl) or siRNA targeting FANCD2 (siFANCD2). Cells were stained against GFP and γH2AX, which was used as damage marker. Scale bar: 5 μm. (**D**) Quantification of ERCC1-GFP recruitment to sites of local UVA laser microirradiation in psoralen-treated XPA-proficient and XPA KO U2OS cells, as determined by immunofluorescence experiments shown in (C). The fold accumulation at sites of local damage was calculated over the nuclear background and plotted as average of at least 100 cells per condition from two independent experiments. Error bars represent the SEM. Statistical significant difference ($p<0.05$) is indicated by *, n.s. non-significant.

The stronger reduction in ERCC1-XPF recruitment due to XPA KO as compared to siFANCD2 could be because of incomplete FANCD2 depletion by siRNA. However, considering that we obtained efficient FANCD2 knockdown (Figure S1A) this is likely better explained by the observation that psoralen-ICLs are preferentially repaired via unhooking by the DNA glycosylase NEIL3, which is independent of FANCD2-FANCI (30). Moreover, XPA, but not FANCD2, is implicated in replication-independent ICLR as well (31, 33, 35). Knockout of XPA will therefore also impair ERCC1-XPF engagement in this pathway. Importantly, this implies that even though in our experiments we did not distinguish between different cell cycle phases of the cells under study (which were rapidly dividing U2OS cells), the FANCD2-dependent recruitment of ERCC1-XPF reflects its engagement in replication-dependent ICLR. Finally, we observed residual ERCC1-XPF recruitment even in the absence of both XPA and FANCD2. It is thus possible that the ERCC1-XPF complex can still be targeted to psoralen adducts, albeit less efficient, even in the absence of both of these factors. Alternatively, it could be that this residual targeting reflects a function of the complex in yet another DNA repair pathway, possibly the repair of DSBs (5).

R689S and S786F mutant XPF recruitment to psoralen adducts is XPA-dependent

Several of the XPF mutations reported in patients have been described to disrupt ICLR. Among these are: C236R, located in the SF2 helicase-like domain and associated with XPCS-complex with FA features (7); R689S, located in the nuclease domain and associated with FA (8); S786F, also located in the nuclease domain and identified in a breast cancer (54). Cells carrying the R689S or S786F mutant XPF alleles are hypersensitive to MMC but not to UV irradiation, suggesting that the R689S and S786F mutations only impair XPF function in ICLR (8, 37, 54). Conversely, C236R renders cells hypersensitive to both MMC and UV irradiation,

indicating that this mutation impairs XPF function in both ICLR and NER (7, 37). Moreover, previous incision assays and ChIP experiments in *Xenopus* egg extracts showed that all three mutations impair the unhooking of a sequence-specific cisplatin-DNA ICL by XPF but not its recruitment to this lesion (55). Therefore, we determined whether in human cells these mutations affect ERCC1-XPF recruitment to psoralen adducts.

We previously generated U2OS XPF KO cell lines that stably expressed GFP-tagged XPF mutants carrying the amino acid substitutions C236R (XPF-C236R), R689S (XPF-R689S) and S786F (XPF-S786F) (37). To study their ability to be recruited to psoralen adducts repaired by NER or repaired by ICLR, we treated these cells with control, XPA and FANCD2 siRNA (Figure S1A, B) and applied local UVA laser microirradiation after 8-MOP treatment. XPF-C236R was clearly recruited to sites of damage (Figure 5A, B), which was reduced after FANCD2 and, even more, after XPA depletion. These results indicate that this XPF mutant is recruited to psoralen adducts as part of both the NER and the replication-dependent ICLR machinery, similarly as wild type XPF (Figure 4A, B). Conversely, XPF-S786F and, even more so, XPF-R689S were recruited less efficiently to psoralen adducts. Strikingly, their recruitment was only strongly reduced after XPA depletion but not significantly after FANCD2 depletion. This suggests that ERCC1-XPF carrying R689S or S786F can still be normally recruited as part of the NER machinery, in line with previous immunofluorescence and fluorescence recovery after photobleaching experiments that showed efficient binding of these mutants to UV-induced DNA damage (37). However, the absence of a significant dependency on FANCD2 suggests that these mutants cannot efficiently be recruited to or stably associate with psoralen-DNA ICLs, which is in line with the MMC hypersensitivity of cells expressing these mutants (8, 37, 54). Interestingly, the less efficient recruitment to psoralen adducts of XPF-R689S compared to XPF-S786F may indicate that this mutation has a more deleterious effect on XPF function in ICLR. This is in line with the stronger MMC hypersensitivity observed in cells expressing XPF with this mutation (37) and the stronger nuclease and ICL-unhooking defect found with purified *Xenopus* XPF carrying this mutation (55).

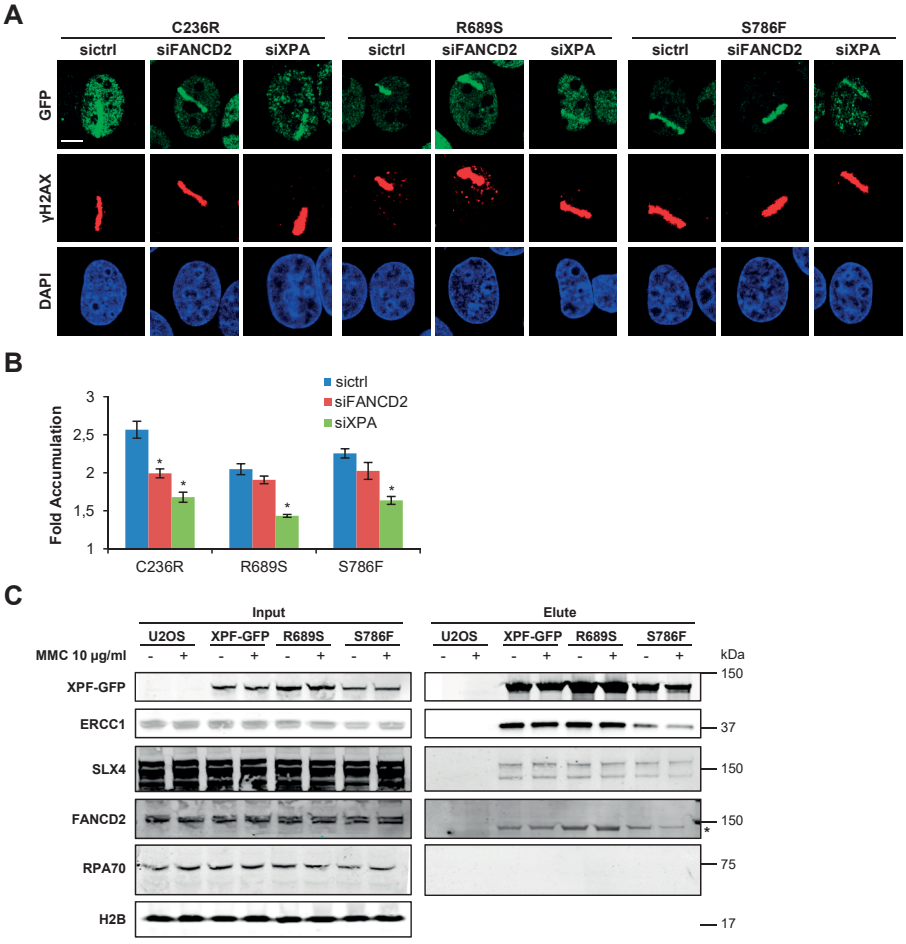

Figure 5. R689S and S786F mutant XPF is recruited to psoralen adducts in an XPA-dependent and FANCD2-independent manner. (**A**) Immunofluorescence images showing XPF recruitment to sites of local UVA laser microirradiation in psoralen-treated (50 μM 8-MOP, 2 h) U2OS XPF KO cells expressing GFP-tagged XPF carrying the amino acid mutations C236R, R689S or S786F, treated with nontargeting siRNA (sictrl) or siRNA targeting XPA (siXPA) or FANCD2 (siFANCD2). Cells were immunostained against GFP and γH2AX, which was used as damage marker. Scale bar: 5 μm. (**B**) Quantification of mutant XPF-GFP recruitment to sites of local UVA laser microirradiation in psoralen-treated U2OS XPF KO cells expressing GFP-tagged XPF carrying the amino acid mutations C236R, R689S or S786F, as determined by immunofluorescence experiments shown in (A). The fold accumulation at sites of local damage was calculated over the nuclear background and plotted as average of at least 60 cells per condition from three independent experiments. Error bars represent the SEM. Statistical significant difference ($p<0.05$) compared to sictrl of each cell line is indicated by *. (**C**) Immunoblot analysis of cell lysate (Input) and GFP immunoprecipitation samples (Elute) from wild type U2OS cells (U2OS) and XPF KO U2OS cells expressing GFP-tagged wild type XPF (XPF-GFP) or XPF carrying the amino acid mutations R689S or S786F. Samples were analyzed with antibodies against GFP, ERCC1, SLX4, FANCD2, RPA70 and H2B (as loading control). Cells were mock treated (-) or incubated with 10 μg/ml MMC for 1 h before lysis. In the FANCD2 immunoblot, the asterisk indicates aspecific staining.

In an effort to understand why XPF-R689S and XPF-S786F are inefficiently recruited, we tested whether these XPF mutants showed reduced interaction with known or hypothesized XPF-interacting proteins. To this end, we performed GFP-immunoprecipitation experiments on benzonase-treated lysate (i.e. to avoid isolation of DNA-mediated interactions/associations) from cells expressing GFP-tagged wild type, R689S or S786F mutant XPF that were either mock-treated or exposed to MMC. Importantly, we found that the mutant XPF proteins interacted normally with ERCC1 (Figure 5C), which is in line with previous observations that these mutants stabilize, and thus bind ERCC1 (8, 37, 55). Moreover, treatment with the crosslinking agent MMC did not alter the ratio of the interaction between XPF and ERCC1. It is currently unclear through which protein interactions ERCC1-XPF is recruited to ICLs, except that this depends on binding to its partner SLX4 (2, 25, 26), which was suggested to interact with mono-ubiquitylated FANCD2 (56). Therefore, we tested whether these interactions were affected due to the XPF mutations. Strikingly, we did not observe any change in the interaction of XPF with SLX4, neither upon MMC exposure nor in the presence of the two XPF mutations. Moreover, we were unable to co-immunoprecipitate FANCD2 with XPF, suggesting that these proteins do not interact directly. Because *in vitro* ERCC1-XPF activity in ICLR is stimulated by RPA (27, 57), we also tested whether RPA directly interacts with wild type or R689S or S786F mutant XPF. However, GFP-tagged XPF was unable to co-immunoprecipitate RPA70, the largest subunit of the heterotrimeric RPA complex, suggesting that stimulation of XPF activity by RPA is not via a direct physical interaction between the proteins. In summary, it remains unclear how exactly ERCC1-XPF, in complex with SLX4, is recruited to ICLs and how specific mutations in XPF could affect this. We observed that, even in presence of both FANCD2 and XPA, recruitment of XPF-S786F and XPF-R689S is impaired. It was previously proposed that R689S and S786F affect the positioning of the XPF nuclease domain around the ICL rather than the actual catalytic activity itself (55, 58). It is therefore possible that this incorrect positioning impairs a stable association of ERCC1-XPF with DNA at the lesion site, leading to inefficient visual recruitment at ICL sites as observed in our immunofluorescence experiments.

Discussion

In this study, we show that in human cells ERCC1-XPF is involved in the repair of the multiple types of lesions induced by psoralen-DNA crosslinking, as part of the NER machinery via XPA, and as part of replication-dependent ICLR via FANCD2. Our results highlight and help to better understand the multifaceted activity and regulation of ERCC1-XPF in DNA repair, which is essential for a better comprehension of how the multiple DNA repair pathways in which ERCC1-XPF is involved tightly collaborate to protect against cancer and promote health. Moreover, our data encourage to seriously consider the activation of multiple DNA repair pathways when evaluating the (side) effects of using DNA crosslinking agents as therapeutic drugs.

It would be interesting to further investigate the kinetics of ERCC1-XPF recruitment to ICLs, to determine how this changes over time in accord with unhooking and repair of the lesions. Moreover, considering the different mechanisms involved in replication-dependent and replication-independent ICLR and the different activities that NER might have in both pathways, it would be useful to study the roles of ERCC1-XPF in these two different mechanisms by investigating how the complex is recruited to ICLs specifically in S-phase and non-S-phase cells. Additionally, the interaction and interdependency of ERCC1-XPF with other ICLR, NER and HR factors should be determined in a cell cycle phase specific manner, to precisely elucidate the multistep processes that lead to ICL removal. Possibly, ICLR factors that we did not investigate or unknown factors influence the recruitment of ERCC1-XPF and could help explain why the recruitment of XPF-R689S and XPF-S786F to ICLs is inefficient.

Acknowledgements

The authors would like to thank Dr. Christophe Lachaud and Dr. John Rouse for help with setting up the technique to locally induce psoralen-DNA crosslinks, the Erasmus Proteomics Center for mass spectrometry and the Erasmus MC Optical Imaging Center for support with microscopes. This work was supported by the Marie Curie Initial Training Network 'aDDRess' funded by the European Commission 7th Framework Programme (grant 316390), a European Research Council Advanced Grant (grant 340988-ERC-ID), an EMBO long-term fellowship

(ALTF 663-2014) and the Dutch Cancer Society (KWF grant 10506). This work is part of the Oncode Institute which is partly financed by the Dutch Cancer Society.

Author contribution

MS, AP and HL performed all experiments and analyzed data. JS contributed reagents. MS, HL and WV designed experiments and wrote the manuscript. All authors reviewed the manuscript.

Conflict of interest

The authors declare no competing financial interests.

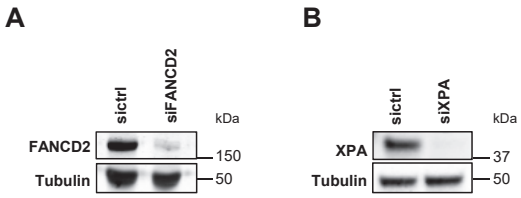

Supplementary Figure S1. ERCC1, XPF and XPA recruitment in ERCC1 and XPF wt or XPA KO cells. (**A**) Immunoblot showing FANCD2 expression in XPF KO U2OS cells expressing XPF-GFP treated with nontargeting control (sictrl) or FANCD2 siRNA (siFANCD2). Tubulin was used as loading control. (**B**) Immunoblot showing XPA expression in XPF KO U2OS cells expressing XPF-GFP treated with nontargeting control (sictrl) or XPA siRNA (siXPA). Tubulin was used as loading control.

References

1. Sijbers AM, et al. (1996) Xeroderma pigmentosum group F caused by a defect in a structure-specific DNA repair endonuclease. *Cell* 86(5):811–822.
2. Klein Douwel D, et al. (2014) XPF-ERCC1 Acts in Unhooking DNA Interstrand Crosslinks in Cooperation with FANCD2 and FANCP/SLX4. *Mol Cell* 54(3):460–471.
3. Wang AT, et al. (2011) Human SNM1a and XPF-ERCC1 collaborate to initiate DNA interstrand cross-link repair. *Genes Dev* 25(17):1859–1870.
4. Bhagwat N, et al. (2009) XPF-ERCC1 participates in the Fanconi anemia pathway of cross-link repair. *Mol Cell Biol* 29(24):6427–37.
5. Ahmad A, et al. (2008) ERCC1-XPF Endonuclease Facilitates DNA Double-Strand Break Repair. *Mol Cell Biol* 28(16):5082–5092.
6. Muñoz P, Blanco R, Flores JM, Blasco MA (2005) XPF nuclease-dependent telomere loss and increased DNA damage in mice overexpressing TRF2 result in premature aging and cancer. *Nat Genet* 37(10):1063–1071.
7. Kashiyama K, et al. (2013) Malfunction of nuclease ERCC1-XPF results in diverse clinical manifestations and causes Cockayne syndrome, xeroderma pigmentosum, and Fanconi anemia. *Am J Hum Genet* 92(5):807–819.
8. Bogliolo M, et al. (2013) Mutations in ERCC4, encoding the DNA-repair endonuclease XPF, cause Fanconi anemia. *Am J Hum Genet* 92(5):800–806.
9. Niedernhofer LJ, et al. (2006) A new progeroid syndrome reveals that genotoxic stress suppresses the somatotroph axis. *Nature* 444(7122):1038–1043.
10. Jaspers NGJ, et al. (2007) First Reported Patient with Human ERCC1 Deficiency Has Cerebro-Oculo-Facio-Skeletal Syndrome with a Mild Defect in Nucleotide Excision Repair and Severe Developmental Failure. *Am J Hum Genet* 80(3):457–466.
11. Marteijn JA, Lans H, Vermeulen W, Hoeijmakers JHJ (2014) Understanding nucleotide excision repair and its roles in cancer and ageing. *Nat Rev Mol Cell Biol* 15(7):465–481.
12. Schärer OD (2013) Nucleotide excision repair in Eukaryotes. *Cold Spring Harb Perspect Biol* 5(10):a012609–a012609.
13. Sugasawa K, et al. (2009) Two-step recognition of DNA damage for mammalian nucleotide excision repair: Directional binding of the XPC complex and DNA strand scanning. *Mol Cell* 36(4):642–53.
14. Staresincic L, et al. (2009) Coordination of dual incision and repair synthesis in human nucleotide excision repair. *EMBO J* 28(8):1111–1120.
15. Tsodikov O V, et al. (2007) Structural basis for the recruitment of ERCC1-XPF to nucleotide excision repair complexes by XPA. *EMBO J* 26(22):4768–4776.
16. Orelli B, et al. (2010) The XPA-binding domain of ERCC1 is required for nucleotide excision repair but not other DNA repair pathways. *J Biol Chem* 285(6):3705–3712.
17. Volker M, et al. (2001) Sequential assembly of the nucleotide excision repair factors in vivo. *Mol Cell* 8(1):213–224.
18. Li L, Elledge SJ, Peterson CA, Bales ES, Legerski RJ (1994) Specific association between the human DNA repair proteins XPA and ERCC1. *Proc Natl Acad Sci U S A* 91(11):5012–6.
19. Park CH, Sancar A (1994) Formation of a ternary complex by human XPA, ERCC1, and ERCC4(XPF) excision repair proteins. *Proc Natl Acad Sci U S A* 91(11):5017–5021.
20. Enzlin JH, Schärer OD (2002) The active site of the DNA repair endonuclease XPF-ERCC1 forms a highly conserved nuclease motif. *EMBO J* 21(8):2045–2053.
21. Pontel LB, et al. (2015) Endogenous Formaldehyde Is a Hematopoietic Stem Cell Genotoxin and Metabolic Carcinogen. *Mol Cell* 60(1):177–188.
22. Clauson C, Scharer OD, Niedernhofer L (2013) Advances in Understanding the Complex Mechanisms of DNA Interstrand Cross-Link Repair. *Cold Spring Harb Perspect Biol* 5(10):a012732–a012732.
23. Smogorzewska A, et al. (2007) Identification of the FANCI Protein, a Monoubiquitinated FANCD2 Paralog Required for DNA Repair. *Cell* 129(2):289–301.

24. Knipscheer P, et al. (2009) The fanconi anemia pathway promotes replication-dependent DNA interstrand cross-link repair. *Science (80-)* 326(5960):1698–1701.
25. Muñoz IM, et al. (2009) Coordination of Structure-Specific Nucleases by Human SLX4/BTBD12 Is Required for DNA Repair. *Mol Cell* 35(1):116–127.
26. Hodskinson MRG, et al. (2014) Mouse SLX4 Is a Tumor Suppressor that Stimulates the Activity of the Nuclease XPF-ERCC1 in DNA Crosslink Repair. *Mol Cell* 54(3):472–484.
27. Abdullah UB, et al. (2017) RPA activates the XPF-ERCC1 endonuclease to initiate processing of DNA interstrand crosslinks. *EMBO J* 36(14):2047–2060.
28. Roy U, Schärer OD (2016) Involvement of translesion synthesis DNA polymerases in DNA interstrand crosslink repair. *DNA Repair (Amst)* 44:33–41.
29. Long DT, Räschle M, Joukov V, Walter JC (2011) Mechanism of RAD51-dependent DNA interstrand cross-link repair. *Science (80-)* 333(6038):84–87.
30. Semlow DR, Zhang J, Budzowska M, Drohat AC, Walter JC (2016) Replication-Dependent Unhooking of DNA Interstrand Cross-Links by the NEIL3 Glycosylase. *Cell* 167(2):498-511.e14.
31. Wang X, et al. (2001) Involvement of nucleotide excision repair in a recombination-independent and error-prone pathway of DNA interstrand cross-link repair. *Mol Cell Biol* 21(3):713–20.
32. Sarkar S, Davies AA, Ulrich HD, McHugh PJ (2006) DNA interstrand crosslink repair during G1 involves nucleotide excision repair and DNA polymerase zeta. *EMBO J* 25(6):1285–94.
33. Enoiu M, Jiricny J, Schärer OD (2012) Repair of cisplatin-induced DNA interstrand crosslinks by a replication-independent pathway involving transcription-coupled repair and translesion synthesis. *Nucleic Acids Res* 40(18):8953–64.
34. Zheng H, et al. (2003) Nucleotide Excision Repair- and Polymerase -Mediated Error-Prone Removal of Mitomycin C Interstrand Cross-Links. *Mol Cell Biol* 23(2):754–761.
35. Muniandy PA, Thapa D, Thazhathveetil AK, Liu S ting, Seidman MM (2009) Repair of laser-localized DNA interstrand cross-links in G1 phase mammalian cells. *J Biol Chem* 284(41):27908–27917.
36. Ahmad A, et al. (2010) Mislocalization of XPF-ERCC1 nuclease contributes to reduced DNA repair in XP-F patients. *PLoS Genet* 6(3):e1000871.
37. Sabatella M, et al. (2018) Repair protein persistence at DNA lesions characterizes XPF defect with Cockayne syndrome features. *Nucleic Acids Res* 46(18):9563–9577.
38. Van Cuijk L, et al. (2015) SUMO and ubiquitin-dependent XPC exchange drives nucleotide excision repair. *Nat Commun* 6(1):7499.
39. Sanjana NE, Shalem O, Zhang F (2014) Improved vectors and genome-wide libraries for CRISPR screening. *Nat Methods* 11(8):783–784.
40. Brinkman EK, Chen T, Amendola M, Van Steensel B (2014) Easy quantitative assessment of genome editing by sequence trace decomposition. *Nucleic Acids Res* 42(22):e168.
41. Aydin ÖZ, et al. (2014) Human ISWI complexes are targeted by SMARCA5 ATPase and SLIDE domains to help resolve lesion-stalled transcription. *Nucleic Acids Res* 42(13):8473–85.
42. Pines A, et al. (2018) TRiC controls transcription resumption after UV damage by regulating Cockayne syndrome protein A. *Nat Commun* 9(1):1040.
43. Lachaud C, et al. (2014) Distinct functional roles for the two SLX4 ubiquitin-binding UBZ domains mutated in Fanconi anemia. *J Cell Sci* 127(13):2811–2817.
44. Slyskova J, et al. (2018) Base and nucleotide excision repair facilitate resolution of platinum drugs-induced transcription blockage. *Nucleic Acids Res* 46(18):9537–9549.
45. Sugitani N, Sivley RM, Perry KE, Capra JA, Chazin WJ (2016) XPA: A key scaffold for human nucleotide excision repair. *DNA Repair (Amst)* 44:123–135.
46. Thazhathveetil AK, Liu ST, Indig FE, Seidman MM (2007) Psoralen conjugates for visualization of genomic interstrand cross-links localized by laser photoactivation. *Bioconjug Chem* 18(2):431–437.
47. Tessman JW, Isaacs ST, Hearst JE (1985) Photochemistry of the Furan-Side 8-Methoxypsoralen-Thymidine Monoadduct Inside the DNA Helix. Conversion to Diadduct and to Pyrone-Side Monoadduct. *Biochemistry* 24(7):1669–1676.
48. Sage E, Moustacchi E (1987) Sequence Context Effects on 8-Methoxypsoralen Photobinding to Defined DNA Fragments. *Biochemistry* 26(12):3307–3314.

49. Hearst JE, Isaacs ST, Kanne D, Rapoport H, Straub K (1984) The reaction of the psoralens with deoxyribonucleic acid. *Q Rev Biophys* 17(1):1–44.
50. Cao H, Hearst JE, Corash L, Wang Y (2008) LC - MS / MS for the Detection of DNA Interstrand Cross-Links Formed by 8-Methoxypsoralen and UVA Irradiation in Human Cells. 80(8):2932–2938.
51. Lai C, et al. (2008) Quantitative analysis of DNA interstrand cross-links and monoadducts formed in human cells induced by psoralens and UVA irradiation. *Anal Chem*. doi:10.1021/ac801520m.
52. Wood RD, Robins P, Lindahl T (1988) Complementation of the xeroderma pigmentosum DNA repair defect in cell-free extracts. *Cell* 53(1):97–106.
53. Kaye J, Smith CA, Hanawalt PC (1980) DNA Repair in Human Cells Containing Photoadducts of 8-Methoxypsoralen or Angelicin. *Cancer Res*.
54. Osorio A, et al. (2013) Evaluation of Rare Variants in the New Fanconi Anemia Gene ERCC4 (FANCQ) as Familial Breast/Ovarian Cancer Susceptibility Alleles. *Hum Mutat* 34(12):1615–1618.
55. Klein Douwel D, Hoogenboom WS, Boonen RA, Knipscheer P (2017) Recruitment and positioning determine the specific role of the XPF-ERCC1 endonuclease in interstrand crosslink repair. *EMBO J* 36(14):2034–2046.
56. Yamamoto KN, et al. (2011) Involvement of SLX4 in interstrand cross-link repair is regulated by the Fanconi anemia pathway. *Proc Natl Acad Sci* 108(16):6492–6496.
57. Mu D, et al. (2000) DNA interstrand cross-links induce futile repair synthesis in mammalian cell extracts. *Mol Cell Biol* 20(7):2446–2454.
58. Su Y, Orelli B, Madireddy A, Niedernhofer LJ, Schärer OD (2012) Multiple DNA binding domains mediate the function of the ERCC1-XPF protein in nucleotide excision repair. *J Biol Chem* 287(26):21846–21855.

CHAPTER 4

Tissue-specific DNA repair activity of ERCC-1/XPF-1 in *C. elegans*

Mariangela Sabatella[1,2], Karen L. Thijssen[1,2], Wim Vermeulen[1,2], Hannes Lans[1,2]

[1]. Department of Molecular Genetics, Erasmus MC, University Erasmus Medical Center Rotterdam, 3000 CA, The Netherlands
[2]. Oncode Institute, Erasmus MC, University Erasmus Medical Center Rotterdam, 3000 CA, The Netherlands

Abstract

Hereditary DNA repair defects affect tissues differently, suggesting that *in vivo* cells can deal differently with DNA damage. Knowledge of the DNA damage response, however, is largely based on *in vitro* and cell culture studies and it is currently unclear whether DNA repair changes depending on the cell type. Here, we used *in vivo* imaging of the nucleotide excision repair (NER) endonuclease ERCC-1/XPF-1 in *C. elegans* to demonstrate tissue-specific NER activity. In oocytes, XPF-1 functions as part of global genome NER to ensure extremely rapid removal of DNA-helix distorting lesions throughout the genome. In contrast, in post-mitotic neurons, XPF-1 participates in NER of transcribed genes only. Strikingly, no activity of XPF-1 was observed in muscle cells. These results suggest a tissue-specific organization of the DNA damage response and may help to better understand pleiotropic and tissue-specific consequences of accumulating DNA damage.

Introduction

Cells of all organisms continuously acquire DNA damage from exposure to environmental pollutants, radiation and the cell's own metabolism. DNA damage poses a serious threat to health because it interferes with genome function and leads to accumulation of mutations, causing cancer, aging and genetic disease. The DNA damage response (DDR) is an intricate network of DNA damage repair and signaling pathways that deals with these lesions depending on their type and genomic location and the cell cycle phase (1). In addition, it is becoming increasingly clear that also the cell type, and its developmental and differentiation state within an organism, determines how lesions are dealt with (2). Most knowledge of DDR mechanisms, however, is based on *in vitro* experimentation and/or analysis of single cell organisms and cells in culture and not much is known on how the DDR is organized *in vivo*.

Hereditary mutations in DNA repair pathways lead to different diseases characterized by cancer predisposition, developmental defects, neurodegeneration and/or progeroid features (3). Typically, not all tissues are equally affected, suggesting that DDR acts differently according to the function of each tissue (4). Even mutations in the same DNA repair gene can give rise to different diseases in which tissues are differently affected. A prime example is inherited deficiency of the structure-specific endonuclease complex ERCC1-XPF, which plays a pivotal role in DNA damage excision during nucleotide excision repair (NER), unhooking of interstrand crosslinks (ICLs) as part of the Fanconi anemia (FA) pathway and removal of DNA overhangs during double strand break (DSB) repair (5–9). Mutations that affect ERCC1-XPF activity in NER give rise to high incidence of skin cancers and, in some cases, progressive neurological degeneration, as observed in Xeroderma Pigmentosum (XP) patients (10), or to additional symptoms such as severe neurodegeneration, dwarfism, sensorineural impairment and early death, as observed in Cockayne Syndrome (CS) patients (12). Conversely, mutations that affect ERCC1-XPF activity in ICL repair mainly give rise to hematological abnormalities and developmental failure, as observed in FA patients (13). It is currently not understood why defects in the same gene, which impair different DDR pathways, cause symptoms in different tissues and whether this reflects a tissue-specific activity of the complex.

NER removes many diverse DNA helix-distorting lesions, including those induced by UV light, i.e. cyclobutane-pyrimidine dimers (CPDs) and 6-4 pyrimidine-pyrimidone photoproducts (6-4PPs) (14). NER consists of two sub-pathways: global genome NER (GG-NER), that deals with damage located anywhere in the genome and is initiated when damage is detected by the UV-DDB and XPC-RAD23B-CETN2 complexes; and transcription-coupled NER (TC-NER), that specifically deals with damage that blocks transcription and is initiated by stalling of RNA polymerase II and recruitment of the CSA, CSB and UVSSA proteins. Upon damage detection, transcription factor TFIIH and DNA binding proteins XPA and RPA are recruited to unwind DNA, check for damage and facilitate the positioning of endonucleases ERCC1-XPF and XPG that excise 22-30 nt of the damaged strand flanking the lesion. DNA synthesis and ligation fill and seal the gap.

Although GG-NER and TC-NER are both active in mammalian cells in culture, the contribution of both pathways to repair and/or cellular survival may not necessarily be similar in different cell types *in vivo.* For instance, *in vitro* differentiation experiments have suggested that upon terminal differentiation, cells retain the ability to repair damage in transcribed genes but lose the ability to repair lesions in non-transcribed regions of the genome (15, 16). In line with these results, pluripotent mouse ES cells were found to rely more on GG-NER than on TC-NER for their survival upon UV irradiation, but this was reversed in embryonic fibroblasts (17). These results suggest that there may be a cell type-specific organisation of NER *in vivo*.

To better understand tissue-specific consequences of DNA repair deficiency, it is necessary to determine how DDR is organized *in vivo*. The nematode *C. elegans* has emerged as an ideal model organism to study *in vivo* cell-type-specific differences in DDR organisation (2). The essential role of many DDR mechanisms including NER is highly conserved in *C. elegans* (18, 19) in particular also ERCC-1/XPF-1 function in NER as well as in ICL and DSB repair (20–23). *ercc-1* and *xpf-1* mutant animals also show features reminiscent of ERCC1-XPF deficiency in mammals, including growth arrest, developmental failure and reduced lifespan (20, 24–26). Moreover, previous UV survival experiments have suggested that GG-NER is the main pathway that preserves genomic integrity in germ cells and early embryos, whereas TC-NER only becomes essential for cellular function in post-mitotic

somatic cells (27). However, it remains unclear to what extent these differentiation-driven changes are due to altered activity of NER itself or to differences in the way cell types respond to DNA damage. Here, we use imaging of fixed and living *C. elegans* to show that XPF-1 exhibits a tissue-specific spatiotemporal response to UV damage, suggestive of a difference between the activity of GG-NER and TC-NER in meiotic germ cells, muscles and neurons.

Material and methods

C. elegans strains

C. elegans was cultured according to standard methods (28). The wild type strain was Bristol N2. Mutant strains and alleles are summarized in Table S1. All mutants were backcrossed three to five times against wild type and genotyped by PCR and sequencing. To generate *xpf-1::gfp* knock-in animals, a 542 bp left and 482 bp right homology arm were amplified from wild type genomic DNA and cloned into plasmid pDD282 (a gift from Bob Goldstein (29)), flanking *gfp*, after which the 'self-excising cassette' was removed. The plasmid was injected together with trcRNA and crRNA (targeting ATTTCGGAAGAAAATAACAC; both from Integrated DNA technologies) in the Cas9^{dPiRNA} expressing strain HCL67 (a kind gift from Heng-Chi Lee (30)). Knock-in animals were verified by genotyping PCR and sequencing, after which the Cas9 was removed by backcrossing against wild type.

To generate strains expressing XPF-1::GFP under control of tissue-specific promoters, the MosSCI technology (31) was used. Promoter fragments of *unc-119* and *aex-3* (to drive expression in neurons (32, 33)), *myo-3* and *hlh-1* (to drive expression in muscles (34, 35)), *lin-26* (to drive expression in hypodermis (36)) were PCR amplified from wild type genomic DNA (*myo-3*: 2499 bp upstream of ATG, *unc-119*: 2194 bp upstream of ATG, *hlh-1*: 3116 bp upstream of ATG, *aex-3*: 1343 bp upstream of ATG and *lin-26*: 3740 bp upstream of ATG) and recombined into pDONRP4-P1R using BP clonase (Invitrogen). For the *mex-5* promoter (driving expression in germ cells (37)) and *gfp::ttb-2* sequences, entry vectors pJA252 and pJA256 (gifts from Julie Ahringer) were used, respectively (37). *xpf-1* cDNA was generated by PCR amplification of wild type cDNA and was cloned into pDONR201. To generate expression vectors, promoter entry vectors,

xpf-1 cDNA and *gfp::ttb-2* vectors were recombined with plasmid pCFJ201 (37) using LR clonase II (Invitrogen). Resulting vectors were verified by sequencing. The constructs were injected in the MosSCI strain EG6250 to generate transgenic worms which were selected after heat shock based on rescue of the *unc-119* phenotype and genotyping. All strains were backcrossed against *xpf-1(tm2842) II* animals.

DNA repair survival assays

Germ cell and embryo survival assays were performed as previously described (27). Briefly, staged young adults were washed and irradiated on empty agar plates at the indicated UVB dose (Philips TL-12 tubes, 40W). Following a 24 h recovery period on OP50 bacteria, three to five adults were allowed to lay eggs for 3 h on 6 cm plates seeded with HT115 bacteria, in quadruple for each UVB dose. 24 h later, the amount of hatched and unhatched (dead) eggs was counted and survival percentage calculated. Results are plotted as average of at least eight independent experiments. Statistical difference was calculated using a one-way ANOVA followed by post-hoc analysis by Bonferroni's test. L1 larvae survival assays were performed as previously described (27). Briefly, eggs collected from adult animals after hypochlorite treatment were plated onto agar plates seeded with HT115 bacteria, in quadruple for each UV dose. 16 h later, L1 larvae were irradiated at the indicated doses of UVB (Philips TL-12 tubes, 40 W) and allowed to recover for 48 h. Animals arrested at the L1/L2 stages and surviving animals that developed beyond the L2 stage were counted to determine the survival percentage. During all assays, animals were kept at 20°C. Results are plotted as average of at least eight independent experiments. Statistical difference was calculated using a one-way ANOVA followed by post-hoc analysis by Bonferroni's test.

CPD immunofluorescence and imaging of fixed animals

To image XPF-1::GFP in fixed animals, unperturbed or irradiated (using two Philips TL-12 tubes, 40 W, emitting UVB) adults were fixed on Poly-L-lysine hydrobromide (Sigma) slides with 4% paraformaldehyde in PBS containing 0.1% Tween. Animals were then incubated with DAPI (Sigma) for 10 min and coverslips were mounted using Vectashield (Vector laboratories). To visualize CPDs lesions (Figure 4D), adult animals were dissected by cutting heads and tails, exposing gonads and embryos which were freeze cracked and incubated in cold methanol. Upon fixation in 4% paraformaldehyde in PBS containing 0.1% Tween, gonads

were blocked with PBS containing 0.5% BSA and 0.1% Tween and incubated with 0.07 M NaOH to denature DNA. Next, gonads were incubated with CPD antibody (TDM-2; Cosmobio) overnight and with Alexa555-conjugated secondary antibody (Invitrogen) for 2 h. DAPI Vectashield (Vector Laboratories) was used to mount coverslips. Animals and oocytes were imaged using an LSM700 confocal microscope equipped with a 40x Plan-apochromat 1.3 NA oil immersion lens (Carl Zeiss). Fluorescence intensity of the CPD staining was quantified in at least 30 bivalents/condition in two independent experiments using Image J software. Statistical difference was calculated using a one-way ANOVA followed by post-hoc analysis by Bonferroni's test.

Real-time imaging and FRAP in *C. elegans*

To image XPF-1::GFP in living animals, adults were immobilized in a mix of M9 buffer and polystyrene beads (Polyscience Inc.) on 6% agarose pads on microscope slides. When indicated, adults were irradiated with 300 J/m^2 UVB (Philips TL-12 tubes, 40 W) on coverslips. After mounting of coverslips on microscope slides, animals were imaged using a Leica TCS SP5 confocal microscope equipped with a 63x/1.4 NA HCX PL APO CS oil immersion lens (Leica Microsystems). To perform FRAP, nuclei of oocytes, neurons and muscles were imaged at 700 Hz every 37 ms using a 488 nm laser at low power until steady-state levels were reached. Next, GFP-derived fluorescence in a small square (0.8 x 0.8 µm on a bivalent in oocytes; 0.3 x 0.3 µm for neurons and muscles, zoom 9) was photobleached using high (80-100%) laser power. Photobleaching in the small square was optimized such that reduction in the overall nuclear fluorescence signal was minimized (Figure S2B). Recovery of the fluorescence signal was measured at low laser power every 37 ms until steady-state levels were reached. In oocytes, the bivalent position was tracked by simultaneous imaging of mCherry::H2B using a 561 nm laser. Fluorescent signals were normalized to the average fluorescence intensity before bleaching and bleach depth and plotted as average of at least 12 animals per condition, except for oocytes between 10 and 20 min after UV for which 5 animals were averaged. For real-time imaging of XPF-1::GFP LUD recruitment, nuclei in immobilized animals were imaged using a 100x quartz objective coupled to a Leica TCS SP5 confocal microscope. Local DNA damage was inflicted using a UVC laser (266 nm, Rapp OptoElectronic, Hamburg GmbH) as previously described (38). In oocytes, the UVC laser was specifically directed on one of the bivalents. Fluorescence intensities at sites of local damage were normalized

to average fluorescence intensities before irradiation and plotted as average of at least 5 animals per condition from two independent experiments. All real-time imaging was performed at room temperature. LAS AF software (Leica) was used for imaging and Image J software to compensate for movement of cells and for quantification. Deconvoluted images of -1 oocytes in living animals (Figure 4B) were generated using The Huygens software.

Human cell culture and siRNA

Human XPF knockout osteosarcoma U2OS cells complemented with GFP-tagged XPF were previously described (39) and cultured in DMEM/F10 supplemented with 10% fetal calf serum (FCS) and 1% penicillin-streptomycin (PS) at 37°C and 5% CO_2. For siRNA treatment, cells were transfected using RNAiMax (Invitrogen) with control siRNA (Dharmacon, D-001210-05) or siRNA targeting XPC (custom, CUGGAGUUUGAGACAUAUCUU), 48 h before UVC treatment.

Real-time imaging in human cells

To measure XPF-GFP recruitment to laser-induced LUD in human cells, XPF-GFP expressing cells were seeded on coverslips and imaged using a 100x quartz objective coupled to a Leica TCS SP5 confocal microscope. Local DNA damage was inflicted using a UVC laser (266 nm, Rapp OptoElectronic, Hamburg GmbH) as previously described (38). Fluorescence intensity at sites of local damage was normalized to the average fluorescence intensity before irradiation. Results are plotted as average of at least 10 cells from two independent experiments. During imaging, cells were kept in culture medium at 37°C and 5% CO_2. LAS AF software (Leica) was used for imaging and Image J software for quantification.

Immunofluorescence in human cells

For immunofluorescence, human cells were seeded on coverslips and irradiated with 60 J/m^2 (254 nm UVC lamp, Philips) through an 8 μm microporous filter (Millipore) to create LUD. Cells were fixed at the indicated times after irradiation with 2% paraformaldehyde and 0.1% Triton X-100 in PBS, and permeabilized for 20 min with 0.1 % triton X-100 in PBS. DNA was denatured with 0.07 M NaOH in PBS for 5 min. PBS containing 0.15% glycine and 0.5% BSA was used to wash cells prior to 2 h incubation with primary antibodies and 1 h incubation with secondary antibodies conjugated to Alexa Fluor 488, 555 and 633 (Invitrogen). DAPI Vectashield (Vector Laboratories) was used to mount the coverslips that were subsequently imaged using an LSM700 microscope equipped with a 40x Plan-

apochromat 1.3 NA oil immersion lens (Carl Zeiss). Primary antibodies used were anti-XPF (3F2/3, Santa Cruz), anti-XPC (home-made fraction 5), anti-GFP (ab290, Abcam), anti-CPD (TDM-2; Cosmobio). Accumulation of XPF at sites of damage was measured in at least 100 cells per condition in two independent experiments.

Results

Tissue-specific expression of GFP-tagged XPF-1 in *C. elegans*

We first determined the tissue distribution of the ERCC-1/XPF-1 complex by generating a knock-in animal expressing XPF-1 tagged at the C-terminus with GFP using CRISPR/Cas9-mediated homology directed repair. Knock-in animals revealed that XPF-1 is expressed in nuclei of all tissues, i.e. neurons, muscles, hypodermis and intestine, as well as in germ cells and embryos (Figure 1).

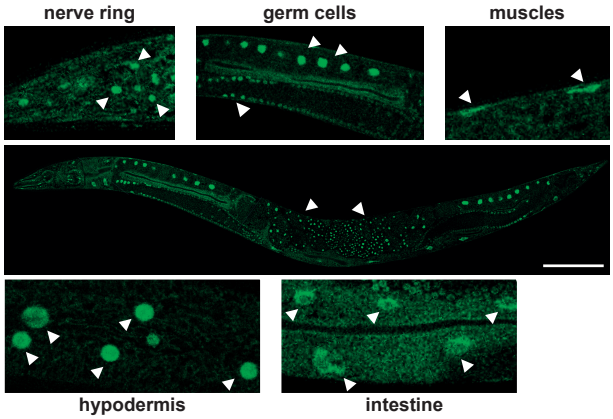

Figure 1. Representative fluorescence image of a fixed animal (middle panel) showing XPF-1::GFP expression in nuclei of multiple cell types of an *xpf-1::gfp* knock-in animal. Scale bar: 100 µm. Upper and lower panels depict zoomed-in areas showing XPF-1::GFP expression in the indicated tissues. Arrowheads indicate nuclei of the indicated cell types.

To be able to study XPF-1 function in specific cell types, we stably integrated *gfp* tagged *xpf-1* as single copy transgene under the control of tissue-specific promoters in *xpf-1* null mutant animals (*tm2842)* (20). We generated an *xpf-1* strain expressing XPF-1::GFP driven by the *mex-5* promoter, i.e. specifically in proliferating and meiotic cells of the germ line, including oocytes, and early

embryo (these *xpf-1*; *P(mex-5)::xpf-1::gfp* animals will be, for simplicity, referred to as *mex-5::xpf-1* animals). Furthermore, we generated *xpf-1* strains expressing XPF-1::GFP driven by the *unc-119* promoter, i.e in non-proliferating neuronal cells (for simplicity, referred to as *unc-119::xpf-1* animals) or expressing XPF-1::GFP driven by the *myo-3* promoter, i.e. in muscle cells (for simplicity, referred to as *myo-3::xpf-1* animals) (Figure 2A). The GFP tag did not compromise the functionality of XPF-1, as its expression in the germ line rescued embryonic lethality of *xpf-1* mutants, due to a function of *xpf-1* in meiotic recombination (23), and UVB sensitivity of *xpf-1* mutant embryos, as shown by germ cell and embryo survival assays (Figure 2B). Next, we crossed *mex-5::xpf-1* animals with an *ercc-1* loss-of-function mutant strain. *ercc-1* deficiency strongly reduced expression levels of XPF-1::GFP (Figure 2C) and abolished its ability to rescue embryonic lethality and UV hypersensitivity of *xpf-1* mutant animals (Figure 2B). This shows that XPF-1 stability and functionality is dependent on its obligate partner ERCC-1, as previously shown in human cells (39–41) and that in these *C. elegans* strains GFP-tagged XPF-1 is in complex with ERCC-1.

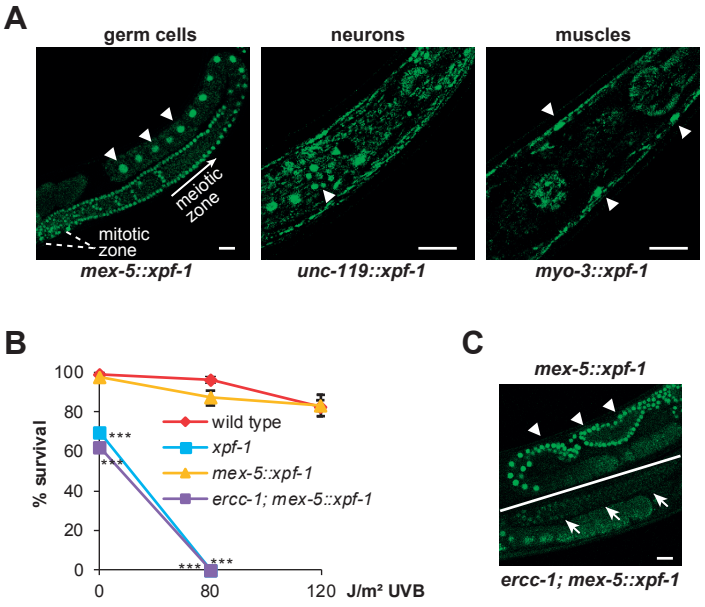

Figure 2. Generation of *C. elegans* strains with XPF-1::GFP tissue-specific expression. (**A**) Representative pictures showing expression of XPF-1::GFP in fixed adult animals specifically in nuclei (indicated by white arrowheads) of germ cells (*mex-5::xpf*), neurons (*unc-119::xpf*) and muscles (*myo-3::xpf*). Mitotic and meiotic zone of the gonad are also indicated. Scale bar: 20 µm. (**B**) Germ cell and embryo survival assay after

UVB irradiation of germ cells in young adult wild type animals, *xpf-1* mutants, *xpf-1* mutants expressing XPF-1::GFP in the germ line (*mex-5::xpf-1*) and *ercc-1; xpf-1* double mutants expressing XPF-1::GFP in the germ line (*ercc-1; mex-5::xpf-1)*. The percentages of hatched eggs (survival) are plotted against the applied UVB doses as average of eight independent experiments. Error bars represent the SEM. ***P<0.001 (one-way ANOVA followed by post-hoc analysis by Bonferroni's test) indicates statistically significant difference compared to wild type for each dose. (**C**) Confocal images of living worms, showing clear expression of XPF-1::GFP in meiotic germ cells (indicated with arrowheads) of an adult animal with intact *ercc-1* (top; *mex-5::xpf-1*) and strongly reduced expression of XPF-1::GFP in meiotic cells (indicated with arrows) of an adult *ercc-1* mutant animal (bottom; *ercc-1; mex-5::xpf-1)*. Scale bar: 20 μm.

XPF-1 protects against UVB in oocytes and neurons, but not in muscles

To study how XPF-1::GFP expression impacts NER activity in different tissues, we tested UV sensitivity of *mex-5::xpf-1, unc-119::xpf-1* or *myo-3::xpf-1* animals using two different survival assays. The first is the 'germ cell and embryo survival assay' that measures UV survival of proliferating germ and early embryonic cells, which mostly depends on GG-NER. With this assay, we had found that *mex-5*-driven XPF-1::GFP rescues UV hypersensitivity of *xpf-1* embryos (Figure 2B). The second is the 'L1 larvae survival assay', which measures UV sensitivity of post-mitotic somatic cells, i.e. continuation of larval development, which mostly depends on TC-NER (18, 27). *xpf-1* mutant animals are strongly UV hypersensitive in both assays, due to the essential function of *xpf-1* in GG-NER and TC-NER (9, 20). In the germ cell and embryo survival assay both *unc-119::xpf-1* and *myo-3::xpf-1* were as hypersensitive to UV as *xpf-1* mutant animals, in contrast to *mex-5::xpf-1* worms (Figure 2B and 3A), which is as expected because in these animals XPF-1::GFP is not expressed in the germ line. In the L1 larvae survival assay, we surprisingly observed that only XPF-1::GFP expression in neurons, i.e. in *unc119::xpf-1* animals, rescued the UV hypersensitivity of *xpf-1* mutants, but XPF-1::GFP expression in muscles, i.e. in *myo-3::xpf-1,* did not (Figure 3B). To verify this unexpected result, we transiently expressed XPF-1::GFP in *xpf-1* mutants under control of alternative neuronal (*aex-3*) and muscular (*hlh-1*) promoters. Strikingly, the L1 larvae survival assay again showed that neuronal expression of XPF-1 rescued *xpf-1* UV hypersensitivity whereas muscular expression did not (Figure 3C). Rescue of UV hypersensitivity by the *aex-3* driven XPF-1::GFP expression was likely only partial because of the transient (and therefore mosaic) expression of the transgene. These data indicate that NER activity in the germ line and developing embryo suffices to rescue embryonic lethality of *xpf-1*-deficient animals upon UVB irradiation. Remarkably, however, for *xpf-1* mutant L1 larvae, the expression of XPF-1::GFP in neuronal cells only, as opposed to exclusive expression in muscle cells, is sufficient to fully rescue the UV hypersensitivity. Together, these data suggest that in UV irradiated animals, neuronal NER activity and functionality is more important than that of muscle cells.

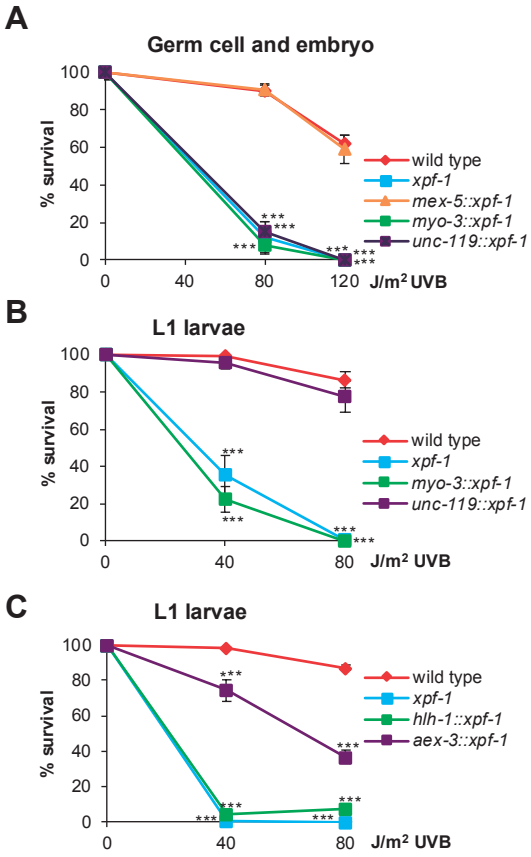

Figure 3. XPF-1 protects against UV in oocytes and neurons, but not in muscles. (**A**) Germ cell and embryo survival assay after UVB irradiation of germ cells in young adult wild type, xpf-1, mex-5::xpf-1 (germ line), myo-3::xpf-1 (muscles) and unc-119::xpf-1 (neurons) animals. The percentages of hatched eggs (survival) after UVB irradiation are plotted against the applied UVB doses. Results are plotted as average of eight independent experiments. (**B**, **C**) L1 larvae survival assay after UVB irradiation of (B) L1 wild type, xpf-1, myo-3::xpf-1 (muscles) and unc-119::xpf-1 (neurons) animals and (C) L1 animals transiently expressing XPF-1::GFP under the control of the hlh-1 (muscles) or aex-3 (neurons) promoters. The percentages of animals that developed beyond the L2 stage (survival) after irradiation are plotted against the applied UVB doses. Results are plotted as average of eight independent experiments. Error bars represent the SEM. ***P<0.001 (one-way ANOVA followed by post-hoc analysis by Bonferroni's test) indicates statistically significant difference compared to wild type for each dose.

In oocytes, XPF-1 quickly repairs damaged DNA in a GG-NER dependent manner

We next investigated the dynamic behavior of XPF-1::GFP in different tissues and focused our attention first on germ cells. *C. elegans* germ cells are arranged in a spatiotemporal gradient of differentiation in two gonad arms, which at their

proximal ends harbor diakinesis stage oocytes that are readily discernable by microscopy. In these oocytes, DNA is highly condensed and organized in six pairs of homologous chromosomes (called bivalents), which allows a straightforward visualization of protein binding to DNA. To study binding of XPF-1::GFP to UV-damaged DNA in these cells, we determined its sub-nuclear localization in animals fixed with paraformaldehyde at different time points after UVB irradiation. We observed clear localization of XPF-1::GFP to bivalents 5 and 15 min after UVB irradiation (Figure 4A), indicating that XPF-1::GFP is targeted to UV-damaged chromatin and thus reflecting active NER. Strikingly, however, XPF-1::GFP was redistributed throughout the whole nucleus already 30 min after UVB irradiation. This fast redistribution of XPF-1::GFP was surprising considering that in mammalian cells in culture ERCC1-XPF is only redistributed from sites of UV damage after more than 4 h (42). Indeed, immunofluorescence analysis of the recruitment of human XPF to sites of local UV damage (LUD) in U2OS cells, generated by UVC irradiation through a microporous filter, revealed that XPF was still clearly bound to damaged DNA 2 h after irradiation (Figure S1A; (39)). To confirm the rapid XPF-1::GFP re-localization to and from UV-damaged bivalents in living oocytes, we crossed *mex-5::xpf-1* animals with worms expressing mCherry-tagged histone H2B driven by the germ line-specific *pie-1* promoter, as live cell chromatin marker. Deconvoluted images of living oocytes closest to the uterus (the -1 oocytes) showed distribution of XPF-1::GFP throughout the nucleoplasm, away from bivalents, in untreated animals (Figure 4B). Conversely, clear accumulation of the protein to damaged bivalents was visible 5 and 15 min after UVB irradiation, which quickly disappeared between 25 and 45 min.

Previously, we have shown that in *C. elegans* germ cells GG-NER but not TC-NER predominantly protects against UV damage (27). To show that accumulation of XPF-1::GFP on UV-damaged bivalents reflects the repair activity of the GG-NER pathway, we crossed *mex-5::xpf-1* with *xpc-1* and *csb-1* mutants to test XPF-1 bivalent accumulation in UVB-irradiated animals lacking functional GG-NER or TC-NER, respectively. XPF-1::GFP clearly accumulated on damaged DNA in oocytes of *csb-1* mutants but its accumulation was almost completely absent in *xpc-1* mutant oocytes (Figure 4C), indicating that XPF-1::GFP binds to bivalents mainly because of GG-NER activity. This, in combination with its relatively rapid dissociation from bivalents, may therefore suggest that GG-NER of UV photolesions in oocytes is completed within ~30 min. Such a fast repair is surprising

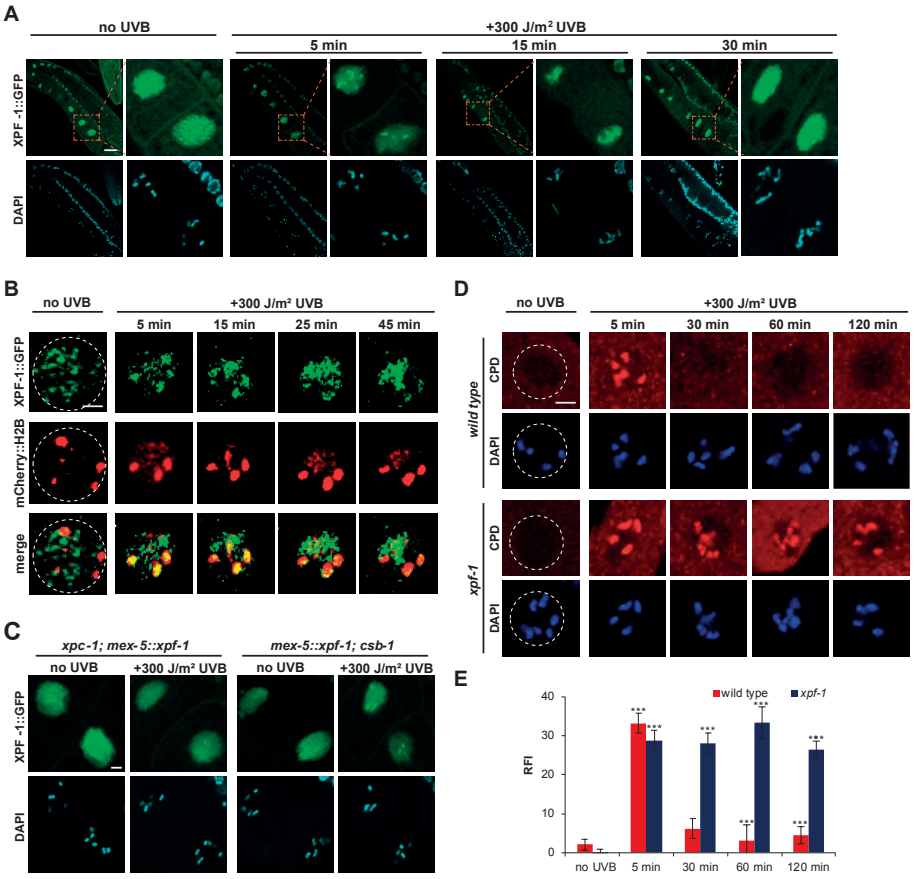

Figure 4. In oocytes, XPF-1 is quickly recruited to damaged DNA in a GG-NER dependent manner. (**A**) Representative pictures of UVB-damaged bivalent recruitment of XPF-1::GFP in oocytes of adult *mex-5::xpf-1* (germ line) animals fixed without irradiation (no UVB) or fixed 5, 15 or 30 min after global irradiation with 300 J/m^2 UVB. Animals were stained with DAPI as DNA marker. Scale bar: 5 µm. The right panel of each set of pictures shows an enlargement of the area indicated with the dashed red box. (**B**) Deconvoluted pictures of -1 oocytes of living adult *mex-5::xpf-1* (germ line) animals showing XPF-1::GFP distribution after no treatment (no UVB) or 5, 15, 25 and 45 min after global irradiation with 300 J/m^2 UVB. *mex-5::xpf-1* animals were crossed with animals carrying the allele *P(pie-1)::mCherry::H2B* to use mCherry::H2B as chromatin marker. Scale bar: 5 µm. Dashed white circle represents the edge of the nucleus. (**C**) Representative pictures of UVB-damaged bivalent recruitment of XPF-1::GFP in adult *xpc-1*;*mex-5::xpf-1* and *mex-5::xpf-1;csb-1* (germ line) mutants without treatment (no UVB) or 5 min after global irradiation with 300 J/m^2 UVB. Animals were stained with DAPI as DNA marker. Scale bar: 5 µm. (**D**) Representative immunofluorescence pictures of -1 oocytes of adult wild type and *xpf-1* mutants without treatment (no UVB) or 5, 30, 60 and 120 min after global irradiation with 120 J/m^2 UVB. Oocytes in dissected gonads were stained with antibodies against CPD photolesions and DAPI, as DNA marker. Scale bar: 5 µm. Dashed white circle represents the edge of the nucleus. (**E**) Quantification of CPD staining on bivalents as determined by immunofluorescence experiments shown in D. CPD staining intensity, corrected for nuclear background staining, is plotted as average of at least 30 bivalents per condition from two independent experiments. RFI indicates relative fluorescence intensity. Error bars represent the SEM. ***P<0.001 (one-way ANOVA followed by post-hoc analysis by Bonferroni's test) indicates statistically significant difference compared to respective untreated sample.

and uncommon, when compared to NER rates in human cells (43) or in *C. elegans* embryos, larvae and adults (44, 45). To test whether indeed such fast repair occurs, we measured the clearance of CPDs by immunostaining of non-irradiated and UVB-irradiated wild type and *xpf-1* oocytes with anti-CPD antibody. In wild type *C. elegans*, CPD staining was clearly detectable on the bivalents 5 min after UVB irradiation (Figure 4D), but, remarkably, not anymore after 30 min (Figure 4D, E). In contrast, in *xpf-1* mutant oocytes strong CPD staining persisted up to 2 h after UV, due to lack of repair. Furthermore, CPD lesions were also still observed 2 h after UV in nuclei of wild type mitotic germ cells at the distal tip of the gonad arm and in nuclei of early embryos (Figure S1B, C), indicating that in these cells repair is slower than in oocytes. Together, these observations indicate that in irradiated *C. elegans* oocytes, XPF-1 engages in GG-NER to excise UV photolesions in an unprecedented fast manner.

XPF-1 quickly localizes to local UV damage in oocytes but not in neurons and muscles

In nuclei of somatic cells, the DNA is not organized into discernable condensed structures making it difficult to assess XPF-1 recruitment to damaged DNA after global UV irradiation. Therefore, we optimized the use of 266 nm UVC microbeam laser irradiation (46) to inflict sub-nuclear LUD in cells of adult, living *C. elegans*, immobilized using polystyrene beads on agarose pads and imaged by confocal microscopy. To validate this system, we first directed the UVC laser specifically on only one bivalent in -1 oocytes of *mex-5::xpf-1* animals. XPF-1::GFP quickly localized to UVC laser-induced LUD, showing readily visible and quantifiable recruitment within seconds after damage infliction (Figure 5A, B). Again, we observed that XPF-1::GFP recruitment mainly reflects functional GG-NER and not TC-NER, as it was absent in *xpc-1*-deficient but clearly observed in *csb-1*-deficient animals (Figure 5C, D). Moreover, this rapid accumulation suggests that GG-NER-mediated damage detection in *C. elegans* oocytes occurs relatively fast. Similar UVC laser-induced recruitment of human GFP-tagged XPF expressed in XPF knockout U2OS cells (39) shows that in human cells, XPF recruitment is initially slower and takes longer to reach a steady-state level (Figure S1D).

Next, we investigated XPF-1 recruitment to UVC laser-induced LUD in nuclei of body wall muscle and ventral nerve cord cells, in respectively *myo-3::xpf-1* and *unc-119::xpf-1* animals. Strikingly, in neither cell type could we observe

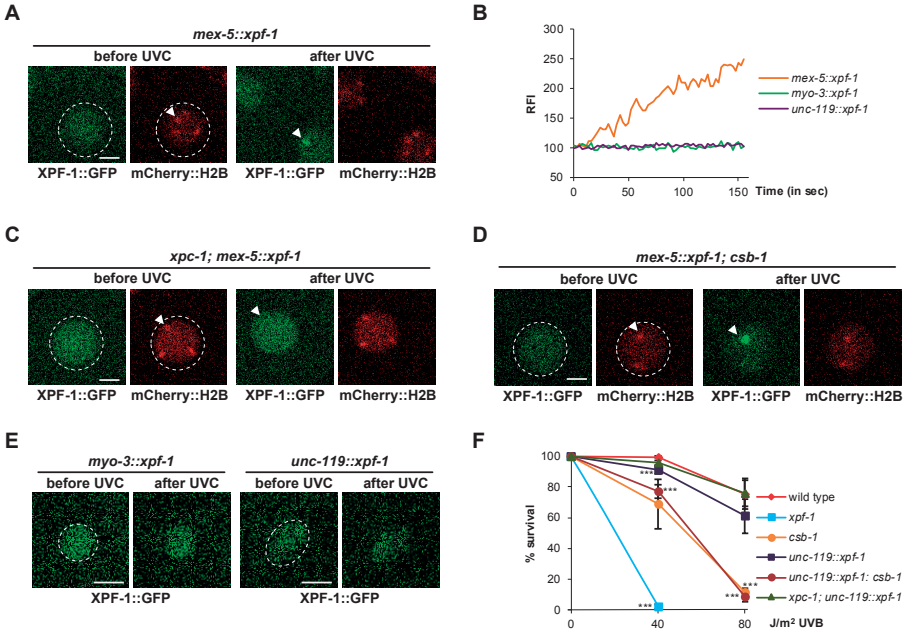

Figure 5. XPF-1 quickly re-localized to local UV damage in oocytes but not in neurons and muscles. (**A**) Representative pictures of real-time imaging of XPF-1::GFP recruitment to local UV damage in -1 oocytes of *mex-5::xpf-1* (germ line) animals expressing *pie-1* promoter driven *mCherry::H2B* as well, before and 160 sec after UV damage induction. Local UV damage was induced using 266 nm UVC laser microbeam irradiation. Scale bar: 5 µm. Arrowhead indicates the bivalent on which the laser was directed. Dashed white circle represents the edge of the nucleus. The shifted position of the nuclei (right panel) after UV is due to contraction of the gonad and pharyngeal pumping of the living animals. Low resolution of the images is due to high magnification and the relatively poor optical performance of the quartz lens that needs to be used for optimal transmission of the UVC wave-length. (**B**) Quantification of XPF-1::GFP recruitment to local UVC laser-induced DNA damage, as determined by real-time imaging shown in A and E. GFP fluorescence intensity at sites of local damage was measured for 150 sec and normalized to pre-damage values. Results are plotted as average of at least 5 animals per condition from at least three independent experiments. Damage was inflicted at t=0. RFI indicates relative fluorescence intensity. (**C**, **D**) Representative pictures of real-time imaging of XPF-1::GFP recruitment to local UV damage in (C) *xpc-1; mex-5::xpf-1* and (D) *mex-5::xpf-1; csb-1* animals each expressing *pie-1* promoter driven *mCherry::H2B* as well, before and 160 sec after local UVC damage induction by 266 nm laser. Scale bar: 5 µm. Arrowheads indicate the bivalents on which the laser was directed. Dashed white circle represents the edge of the nucleus. (**E**) Representative pictures of real-time imaging of XPF-1::GFP recruitment to local UV damage in body wall muscle cells of *myo-3::xpf-1* (left panel) and ventral cord neurons of *unc-119::xpf-1* (right panel) animals before and 160 sec after UV damage induction. Local UV damage was induced using 266 nm UVC laser microbeam irradiation. Scale bar: 5 µm. Dashed white circle represents the edge of the nucleus. (**F**) L1 larvae survival assay after UVB irradiation of L1 wild type, *xpf-1, csb-1* and *unc-119::xpf-1* (neurons) animals and the double mutants *unc-119::xpf-1; csb-1* and *xpc-1; unc-119::xpf-1*. The percentages of animals that developed beyond the L2 stage (survival) after irradiation are plotted against the applied UVB doses. Results are plotted as average of eight independent experiments, normalized to untreated conditions. Error bars represent the SEM. ***P<0.001 (one-way ANOVA followed by post-hoc analysis by Bonferroni's test) indicate statistically significant difference compared to wild type for each dose.

recruitment of XPF-1::GFP to damaged DNA (Figure 5B-E). An explanation for this lack of visible XPF-1::GFP recruitment could be that in these non-cycling somatic cell types the response to UV mostly relies on TC-NER. Since TC-NER only takes place in transcribed genes, i.e. in only a minor portion of the entire genome, this will require much less XPF-1 proteins at LUD as when also GG-NER in the entire genome takes place. Typically, in UV irradiated human cells in culture only ~10% of NER activity is due to TC-NER (47) and it is therefore very hard to visualize engagement of repair proteins in this NER sub-pathway by measuring LUD recruitment (48). Indeed, we observed in U2OS cells that recruitment of human GFP-tagged XPF to LUD induced through a microporous filter was hardly visible when only TC-NER was active, i.e. when GG-NER was impaired by siRNA-mediated XPC knockdown (Figure S1E, F). Thus, similar to these siRNA-treated human cells, it is likely that the lack of visible XPF-1::GFP recruitment to LUD in the differentiated *C. elegans* cells is caused by the absence of active GG-NER. To verify that in neurons XPF-1 mainly acts through the TC-NER pathway, we determined if the rescued L1 larvae UV survival of *unc-119::xpf-1* animals (Figure 3B) depends on TC-NER or GG-NER by crossing these animals with *csb-1* or *xpc-1* mutants, respectively. Strikingly, neuronal XPF-1::GFP expression still fully rescued UV sensitivity in *xpc-1*-deficient animals, but not in *csb-1*-deficient animals (Figure 5F). Hence, XPF-1 expression in neurons protects against UV damage through its activity in repair of transcribed genes.

XPF-1 damage binding is tissue-specific

To better understand the apparent difference in XPF-1 activity in oocytes, neurons and muscle cells, we investigated the XPF-1::GFP mobility, i.e. its ability to freely move through the nucleus, in unperturbed and UV-irradiated cells using Fluorescence Recovery After Photobleaching (FRAP). Previous FRAP analysis in mammalian cells in culture has shown that human ERCC1-XPF freely diffuses through the nucleus in the absence of DNA damage and becomes partially immobilized upon UV irradiation, reflecting its binding to damaged DNA and engagement in NER (39, 42). Surprisingly, in unperturbed *C. elegans* cells *in vivo*, we observed only partial recovery of fluorescence in the photobleached area, suggesting that a significant fraction of XPF-1 was immobilized. Importantly, we noted mobility differences between different tissues, indicating that the amount of proteins that (freely) diffuse through the nucleus depends on the tissue type (Figure 6A-D). In particular, XPF-1::GFP showed the highest mobility in neurons (Figure 6D; in *unc-119::xpf-1*), slightly less mobility in oocytes (Figure 6A; in *mex-*

5::xpf-1) and hardly any mobility in muscle cells (Figure 6C; in *myo-3::xpf-1)*. In oocytes, XPF-1::GFP showed a clear additional UV-dependent immobilization directly after UVB treatment, indicative of its involvement in NER (Figure 6A) (49). However, already within 10 to 20 min after UV irradiation, the XPF-1::GFP mobility returned to a level comparable to that in unperturbed cells (Figure 6B). This transient UV-induced immobilization is in line with our previous results suggestive of a fast repair reaction in oocytes, as lesion removal will coincide with the dissociation of XPF-1::GFP from damaged DNA. In muscle cells, we did not observe any change in the already low XPF-1 mobility after UV treatment (Figure 6C), suggesting that NER might not be active in this tissue. Interestingly, in neurons we consistently observed only a very slightly increased immobilization of XPF-1::GFP after UV treatment (Figure 6D). This small immobilized fraction is likely derived from its engagement in repair of transcribed genes only, since NER in the entire genome does not seem to be active in these cells. Similarly, only minor UV-induced immobilization in FRAP is observed in human cells for TC-NER factors (50, 51), but not for GG-NER factors (52). Taken together, our results suggest that ERCC-1/XPF-1 displays a tissue-specific repair activity *in vivo*.

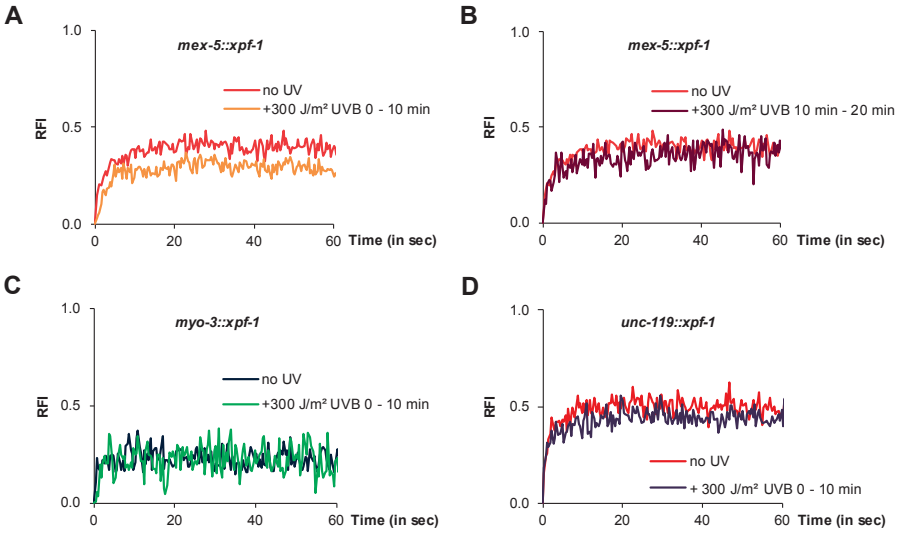

Figure 6. XPF-1 exhibits tissue-specific mobility and damaged DNA binding. (**A-D**) FRAP analysis showing XPF-1::GFP mobility in unperturbed (no UV) and UVB irradiated (+300 J/m^2) animals. FRAP was measured in a small square (as explained in the methods) in nuclei of oocytes of *mex-5::xpf-1*, of body wall muscle cells of *myo-3::xpf-1* and of ventral cord neurons of *unc-119::xpf-1* animals, 0 to 10 min or 10 to 20 min after irradiation, as indicated. Each curve represents the average of 4 to 10 animals per condition from at least two independent experiments. RFI indicates relative fluorescence intensity.

Discussion

In order to reveal tissue-specific DNA repair activities, we developed a sophisticated *in vivo* imaging platform that allows visualization and quantification of DNA damage binding of DNA repair factors in single cells of living *C. elegans.* To do so, we combined tissue-specific expression of a fluorescent repair protein with real-time confocal imaging in living organisms after DNA damage infliction by (1) a dedicated UVC micro-irradiation system, to inflict UV photolesions in a user-defined sub-nuclear area of individual cells, and (2) global UVB irradiation of living animals, to reveal DNA damage binding properties by live and fixed-tissue imaging and FRAP analysis.

C. elegans germ cells constitute an immortal and totipotent cell lineage in which the entire genome needs to be protected from DNA damage to ensure faithful transmission of genetic information to the next generation (2). Using our imaging platform, we show that in oocytes the DNA repair activity of the NER endonuclease ERCC-1/XPF-1 fully depends on GG-NER. These results are in line with previous observations by us and others that specifically GG-NER, but not TC-NER, protects against DNA damage-induced germ cell proliferation and meiotic maturation defects and embryonic lethality (18, 27, 53). Importantly, we observed that in oocytes, XPF-1::GFP very quickly localizes and binds to damaged DNA, which was, surprisingly, not observed anymore within 30 min after irradiation. This rapid disappearance of XPF binding to DNA damage coincides with the unprecedented short time it took to completely remove all UV-induced CPDs in wild type animals, which was *xpf-1* and thus NER-dependent. Strikingly, such rapid repair speed contrasts to the much slower global genome CPD repair observed in yeast and human cells in culture (39, 43, 54) and in other *C. elegans* cell types (Figure S1B, C) (44, 45) and may therefore be oocyte-specific. Mammalian oocytes do exhibit UV-induced unscheduled DNA repair synthesis indicative of NER (55) and are likely well able to efficiently repair many different types of DNA damage (56), but it is unknown how fast NER operates in mammalian oocytes. Studies using UV irradiated DNA plasmids in *Xenopus laevis* oocytes or oocyte extracts, however, which show rapid removal of CPD lesions within 1- 2 h, support the idea that NER proceeds with high efficiency and speed in these types of germ cells (57, 58).

It is currently unclear which mechanisms drive this unprecedented fast NER *in vivo*. Possibly, differences in chromatin conformation and/or remodeling, which impact and regulate formation and repair of UV lesions (14, 59, 60), play a role. Alternatively, the activity of GG-NER-specific factors such as XPC may be enhanced by oocyte-specific post-translational modifications, known to stimulate its damage detection efficiency (14). Moreover, in *C. elegans* oocytes, 30 minutes is also about the time that the proximal -1 oocyte, in which we measured XPF-1 and CPD repair kinetics, needs to mature and ovulate (61), at which time the nuclear envelope breaks down to allow bivalents to complete diakinesis of the first meiotic prophase upon fertilization. Therefore, oocytes probably need to quickly repair DNA damage to allow the release of DNA-bound proteins not needed for or even interfering with the subsequent meiotic and embryonic cell divisions and ensure a faithful transmission of undamaged genetic information. Indeed, shortly after fertilization and completion of meiosis I and II, the first embryonic cell divisions occur for which proper timing becomes more important than faithful genome maintenance. During this early phase of embryogenesis, the DNA damage checkpoint is suppressed and DNA damage is bypassed by translesion polymerases rather than repaired by NER (62, 63). Therefore, it will be very urgent for oocytes to be able to efficiently repair lesions and preserve genomic integrity. The higher expression of NER genes in germ cells as compared to somatic cells (64) is a likely requisite to allow the efficient and rapid maintenance of the entire genome by GG-NER.

Contrarily to oocytes, XPF-1 expression in neurons protected L1 animals against UV irradiation in a TC-NER but not in a GG-NER dependent manner, in line with our previous observations (27). These results suggest that somatic cells only preserve genetic information contained in genes that are actively transcribed and needed for proper cell functionality. It was previously observed that as animals develop, the amount of UV lesions repaired in time declines and that the repair rate is highest in more actively transcribed genomic regions (44, 45). These developmental-stage-specific changing repair activities might be explained by this differentiation-driven switch from GG-NER to TC-NER. This switch is also observed in mammalian cells, which lose their global-genome repair capacity, but retain repair in active genes, upon *in vitro* differentiation (15, 16). It was suggested that this switch is regulated by differentiation-driven changes in phosphorylation of the ubiquitin-activating enzyme E1 (65). Importantly, *in vivo* imaging of

the spatiotemporal properties of *C. elegans* XPF-1 shows that in neurons XPF-1 behaves similarly to TC-NER factors in mammalian cells in culture. XPF-1 is not visibly recruited at LUD and, like human CSB, is only slightly immobilized upon UV irradiation in FRAP (50, 51). These data exemplify the importance of TC-NER rather than GG-NER for maintaining transcriptional integrity and cell functionality in post-mitotic neurons, which also likely correlates to the fact that neurodegeneration is a typical feature of human patients carrying mutations in TC-NER factors (1, 14, 66).

L1 larvae arrest development upon UV irradiation due to transcription arrest, mediated by ERK1/2 MAP kinase signaling (18, 67, 68). Considering the importance of TC-NER in somatic cells, it is striking to note that loss of *csb-1*, in a wild type or *unc-119::xpf-1* background, does not completely impair UV survival of L1 larvae (Figure 5F). Apparently, XPF-1 expressed in neurons can still partially rescue UV survival in the absence of TC-NER. This can be explained by results from previous UV survivals showing that in somatic cells GG-NER becomes crucial to recover UV-blocked transcription and promote L1 larvae survival only when TC-NER is deficient (27, 69). Thus, GG-NER is active in somatic cells, but only in the maintenance of transcribed genes. Such transcription-specific GG-NER activity has been previously described for *in vitro* differentiated human cell types including neurons and has been dubbed 'transcription domain-associated repair' (16, 70). Considering that in *C. elegans* neurons, XPF-1::GFP recruitment to UVC laser-induced UV damage is not visible, it is therefore likely that XPF-1 functions only to maintain transcribed genes, which in wild type cells is mostly mediated by TC-NER but which may also be mediated by GG-NER, as backup system or in the absence of TC-NER.

Remarkably, we find that the activity of XPF-1, and therefore likely also that of the whole NER machinery, is not similar in every differentiated somatic cell type. Strikingly, expression of XPF-1::GFP in muscle cells did not protect against UV as in neurons. It could be that in the L1 larvae UV survival assay used, which actually measures arrested development of the whole animal, the contribution of muscle cell types to survival is not as big or as important as that of neurons. Pan-neural promoters *unc-119* and *aex-3* were used to drive XPF-1::GFP expression in all neurons, which in the L1 larvae make up over one third of the animals cells (71). In contrast, *myo-3* and *hlh-1* drove XPF-1 expression in body wall muscles

and anal and gonadal contractile sheath muscles, which together make up less than one fifth of the animal's cells. Still, it is unexpected that expression of XPF-1 in only part of the animal (*i.e.* in neurons) can fully rescue UV survival. We also observed partial rescue of UV sensitivity when XPF-1::GFP was transiently expressed by the *lin-26* promoter, which drives specific expression in glial and hypodermal cells that make up less than one fourth of the total amount of cells in L1 larvae (Figure S2A); (36). DNA damage in *C. elegans* leads to upregulation of adaptive stress and survival responses (20, 72, 73) and in germ cells triggers a non-cell autonomous systemic response that promotes stress resistance of somatic cells (74). Also, persistent DNA damage in somatic cells leads to activation of the FOXO transcription factor DAF-16 that together with GATA transcription factor EGL-27 regulates and promotes development and growth (53). It is thus conceivable that similar systemic responses to control developmental growth act in neurons (and hypodermal cells) but not in muscles. Nevertheless, in unperturbed conditions, XPF-1::GFP was much more immobile in muscle cells than in oocytes or neurons or compared to mammalian cells in culture (39, 42). Also, after UV irradiation there was no measurable difference in XPF-1 mobility, in striking contrast to oocytes, neurons and mammalian cells in culture. The low muscle mobility of XPF-1 is, however, reminiscent of a similar low mobility observed for TFIIH in organotypic cultures of mouse differentiated cell types (75) and is therefore suggestive of a tissue-specific differential organization of NER *in vivo*. Our observations could therefore indicate that genome maintenance is less important in muscles to the point that NER is not or hardly active. This is in line with multiple studies that have addressed repair capacity in differentiated rodent muscle cell types showing a decrease in repair capacity upon differentiation (76, 77). This possibly correlates to the fact that TC-NER deficiency has less negative impact on the muscular system than on the nervous system and that even CS symptoms displayed in the musculoskeletal system derive from denervation myopathy and disuse atrophy rather than from a direct dysfunction of the muscular tissue itself (66). However, why and how NER, which is important to preserve physiological gene expression programs, displays reduced activity or is not functional in muscles, is currently not clear.

In summary, we conclude that NER displays tissue-specific activity which may explain the differential impact of DNA lesions on different tissues. It will be interesting to determine if similar tissue-specific repair activities are also present

in tissues of higher organisms *in vivo* and whether these can explain part of the tissue-specific symptoms associated with hereditary NER deficiency.

Acknowledgements
We thank Dr. Gert Jansen for providing an injection microscope, Dr. Bob Goldstein and Dr. Julie Ahringer for pJA252, pJA256 and pDD282 plasmids, Dr. Heng-Chi Lee for the *Cas9*-expressing *C. elegans* strain and Dr. Gert van Cappellen and the Erasmus MC Optical Imaging Center for support with microscopes. Some strains were provided by the *Caenorhabditis* Genetics Center (funded by NIH Office of Research Infrastructure Programs P40 OD010440) and the National Bioresource Project for the nematode. Our work was funded by the Marie Curie Initial Training Network 'aDDRess' funded by the European Commission 7th Framework Programme (grant 316390) and a European Research Council Advanced Grant (grant 340988-ERC-ID). Oncode Institute is partly financed by the Dutch Cancer Society and was funded by the gravitation program CancerGenomiCs.nl from the Netherlands Organization for Scientific Research (NWO).

Author contribution
MS, KT and HL performed experiments. MS, KT, WV and HL designed experiments, analyzed data and wrote the manuscript.

Conflict of interests
The authors declare no competing financial interests.

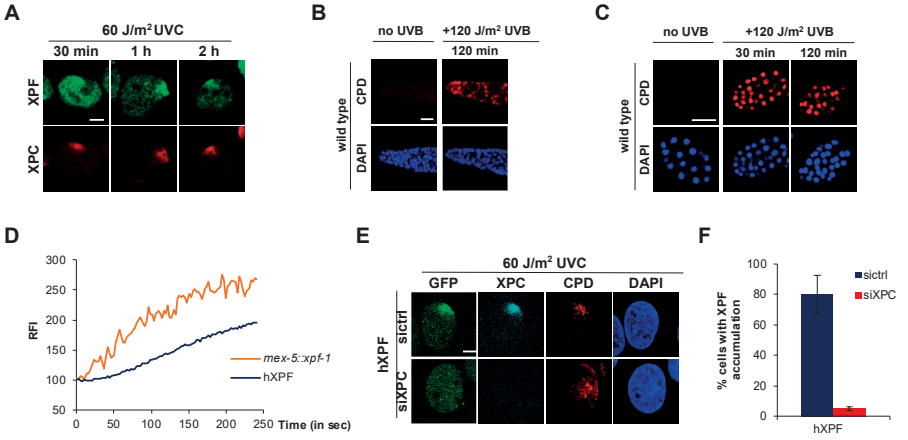

Supplementary Figure S1. Recruitment of human XPF to sites of local UV damage in U2OS cell line. (**A**) Representative immunofluorescence pictures of human XPF recruitment to local UV damage in U2OS cells 30 min, 1 and 2 h after irradiation with 60 J/m^2 UVC through an 8 μm microporous filter. Cells were stained with antibodies against XPF and XPC, as damage marker. Scale bar: 5 μm. (**B**) Representative immunofluorescence pictures of mitotic germ cells in the distal tip of dissected gonads of adult wild type animals without treatment (no UVB) or 120 min after global irradiation with 120 J/m^2 UVB. Dissected gonads were stained with antibodies against CPD photolesions and DAPI, as DNA marker. Scale bar: 5 μm. (**C**) Representative immunofluorescence pictures of wild type embryos without treatment (no UVB) or 30 and 120 min after global irradiation with 120 J/m^2 UVB. Embryos were stained with antibodies against CPD photolesions and DAPI, as DNA marker Scale bar: 5 μm. (**D**) Local UVC laser-induced DNA damage recruitment of XPF-1::GFP in oocytes of *mex-5::xpf-1* (germ line) animals (depicted also in Figure 5B) is shown in comparison to recruitment of GFP-tagged human wild type XPF (hXPF) expressed in XPF knockout U2OS cells. GFP fluorescence intensities at sites of local damage were measured in real-time for 250 sec and normalized to pre-damage values. Results are plotted as average of at least 5 animals and 20 cells from at least two independent experiments. Damage was inflicted at t=0. RFI indicates relative fluorescence intensity. (**E**) Representative immunofluorescence pictures of the UV damage recruitment of human XPF-GFP expressed in XPF knockout U2OS cells (hXPF) treated with non-targeting (sictrl) and XPC (siXPC) siRNAs, 1 h after irradiation with 60 J/m^2 UVC through an 8 μm microporous filter. Cells were stained with antibodies against XPC and CPD, as damage marker. Scale bar: 5 μm. (**F**) Percentage of cells showing clear co-localization of XPF-GFP and CPD in cells treated with non-targeting (sictrl) and XPC (siXPC) siRNAs, as determined by immunofluorescence experiments shown in (E). Results are plotted as average of at least 190 cells from two independent experiments. Error bars represent the SEM.

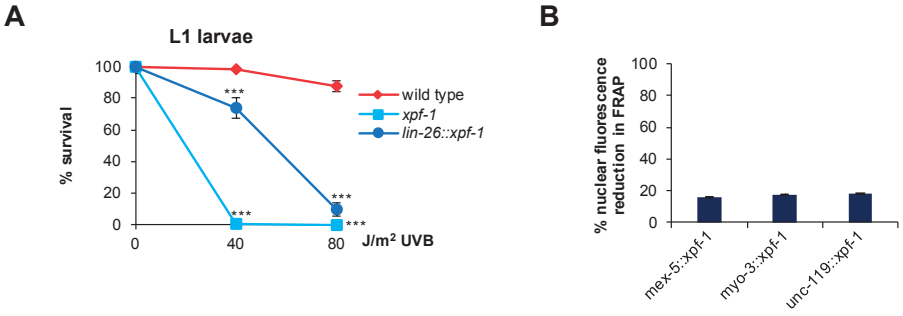

Supplementary Figure S2. XPF-1 partially protects against UV in hypodermis. (**A**) L1 larvae survival assay after UVB irradiation of wild type and *xpf-1 L1* larvae and L1 larvae transiently expressing XPF-1::GFP under the control of the *lin-26* (hypodermis) promoter. The percentages of animals that developed beyond the L2 stage (survival) after irradiation are plotted against the applied UVB doses. Results are plotted as average of eight independent experiments, normalized to untreated conditions. (**B**) Reduction in overall XPF::GFP fluorescence signal after photobleaching in a small square during FRAP experiments shown in Figure 6 in nuclei of oocytes of *mex-5::xpf-1*, of body wall muscle cells of *myo-3::xpf-1* and of ventral cord neurons of *unc-119::xpf-1* animals. Error bars represent the SEM. ***P<0.001 (one-way ANOVA followed by post-hoc analysis by Bonferroni's test) indicates statistically significant difference compared to wild type for each dose.

Table S1: ***C. elegans*** **strains used in this study**

Strain	Genotype
EG6250	*unc-119(ed3) III; cxTi10882 IV*
GJ1564	*xpf-1(tm2842)II*
GJ1519	*csb-1(ok2335)X*
HAL20	*xpf-1(tm2842)II; emcSi7[P(mex-5)::xpf-1::GFP] IV*
HAL21	*ercc-1(tm 2073)I; xpf-1(tm2842)II; emcSi7[P(mex-5)::xpf-1::GFP] IV*
HAL42	*xpf-1(tm2842)II; xpc-1(tm3886) emcSi7[P(mex-5)::xpf-1::GFP] IV; itIs37[P(pie-1):: mCherry::H2B]*
HAL43	*xpf-1(tm2842)II; emcSi7[P(mex-5)::xpf-1::GFP] IV; itIs37[P(pie-1):: mCherry::H2B]; csb-1(ok2335)X*
HAL44	*xpf-1(tm2842)II; emcSi7[P(mex-5)::xpf-1::GFP] IV; itIs37[P(pie-1):: mCherry::H2B]*
HAL62	*xpf-1(tm2842)II; emcSi24[P(myo-3)::xpf-1::GFP]IV*
HAL63	*xpf-1(tm2842)II; emcSi27[P(unc-119)::xpf-1::GFP]IV*
HAL69	*xpf-1(tm2842)II; emcEx42[P(aex-3)::xpf-1::GFP myo-3::mCherry]*
HAL75	*xpf-1(tm2842)II; emcEx48[P(lin-26)::xpf-1::GFP myo-2::mCherry elt-2::mCherry]*
HAL77	*xpf-1(tm2842)II; emcEx50[P(hlh-1)::xpf-1::GFP myo-2::mCherry elt-2::mCherry]*
HAL100	*emcSi57[xpf::GFP::xpf]II*
HAL128	*xpf-1(tm2842)II; emcIs27[P(unc-119)::xpf-1::GFP]IV; csb-1(ok2335)X*
HAL130	*xpf-1(tm2842)II; xpc-1(tm3886) emcSi27[P(unc-119)::xpf-1::GFP] IV*
HCL67	*Is[Peft-3::Cas9 dPiRNA::tbb-2 3'utr; cbunc-119(+)] II; unc-119(ed3) III*

References

1. Hoeijmakers JHJ (2009) DNA Damage, Aging, and Cancer. *N Engl J Med* 361(15):1475–1485.
2. Lans H, Vermeulen W (2015) Tissue specific response to DNA damage: C. elegans as role model. *DNA Repair (Amst)* 32:141–148.
3. Keijzers G, Bakula D, Scheibye-Knudsen M (2017) Monogenic Diseases of DNA Repair. *N Engl J Med* 377(19):1868–1876.
4. Niedernhofer LJ (2008) Tissue-specific accelerated aging in nucleotide excision repair deficiency. *Mech Ageing Dev* 129(7–8):408–15.
5. Ahmad A, et al. (2008) ERCC1-XPF Endonuclease Facilitates DNA Double-Strand Break Repair. *Mol Cell Biol* 28(16):5082–5092.
6. De Silva IU, McHugh PJ, Clingen PH, Hartley JA (2000) Defining the Roles of Nucleotide Excision Repair and Recombination in the Repair of DNA Interstrand Cross-Links in Mammalian Cells. *Mol Cell Biol* 20(21):7980–7990.
7. Klein Douwel D, et al. (2014) XPF-ERCC1 Acts in Unhooking DNA Interstrand Crosslinks in Cooperation with FANCD2 and FANCP/SLX4. *Mol Cell* 54(3):460–471.
8. Manandhar M, Boulware KS, Wood RD (2015) The ERCC1 and ERCC4 (XPF) genes and gene products. *Gene* 569(2):153–161.
9. Sijbers AM, et al. (1996) Xeroderma pigmentosum group F caused by a defect in a structure-specific DNA repair endonuclease. *Cell* 86(5):811–822.
10. Digiovanna JJ, Kraemer KH (2012) Shining a light on xeroderma pigmentosum. *J Invest Dermatol* 132(3 PART 2):785–796.
11. Garinis GA, van der Horst GTJ, Vijg J, Hoeijmakers JHJ (2008) DNA damage and ageing: New-age ideas for an age-old problem. *Nat Cell Biol* 10(11):1241–1247.
12. Natale V, Raquer H (2017) Xeroderma pigmentosum-Cockayne syndrome complex. *Orphanet J Rare Dis* 12(1):65.
13. Bogliolo M, et al. (2013) Mutations in ERCC4, encoding the DNA-repair endonuclease XPF, cause Fanconi anemia. *Am J Hum Genet* 92(5):800–806.
14. Marteijn JA, Lans H, Vermeulen W, Hoeijmakers JHJ (2014) Understanding nucleotide excision repair and its roles in cancer and ageing. *Nat Rev Mol Cell Biol* 15(7):465–481.
15. Nouspikel T, Hanawalt PC (2002) DNA repair in terminally differentiated cells. *Thierry Nouspikel, Philip C Hanawalt 2002 DNA repair Termin Differ cells DNA Repair 1 59-75* 1(1):59–75.
16. van der Wees C, et al. (2007) Nucleotide excision repair in differentiated cells. *Mutat Res Mol Mech Mutagen* 614(1–2):16–23.
17. de Waard H, et al. (2008) Cell-type-specific consequences of nucleotide excision repair deficiencies: Embryonic stem cells versus fibroblasts. *DNA Repair (Amst)* 7(10):1659–1669.
18. Lans H, Vermeulen W (2011) Nucleotide Excision Repair in Caenorhabditis elegans. *Mol Biol Int* 2011:1–12.
19. Rieckher M, Bujarrabal A, Doll MA, Soltanmohammadi N, Schumacher B (2017) A simple answer to complex questions: Caenorhabditis elegans as an experimental model for examining the DNA damage response and disease genes. *J Cell Physiol* 233(4):2781–2790.
20. Lans H, et al. (2013) DNA damage leads to progressive replicative decline but extends the life span of long-lived mutant animals. *Cell Death Differ* 20(12):1709–1718.
21. Pontier DB, Tijsterman M (2009) A Robust Network of Double-Strand Break Repair Pathways Governs Genome Integrity during C. elegans Development. *Curr Biol* 19(16):1384–1388.
22. Ward JD, Barber LJ, Petalcorin MIR, Yanowitz J, Boulton SJ (2007) Replication blocking lesions present a unique substrate for homologous recombination. *EMBO J* 26(14):3384–3396.
23. Saito TT, Youds JL, Boulton SJ, Colaiácovo MP (2009) Caenorhabditis elegans HIM-18/SLX-4 interacts with SLX-1 and XPF-1 and maintains genomic integrity in the germline by processing recombination intermediates. *PLoS Genet* 5(11):e1000735.

24. Gurkar AU, et al. (2018) Dysregulation of DAF-16/FOXO3A-mediated stress responses accelerates oxidative DNA damage induced aging. *Redox Biol* 18:191–199.
25. Niedernhofer LJ, et al. (2006) A new progeroid syndrome reveals that genotoxic stress suppresses the somatotroph axis. *Nature* 444(7122):1038–1043.
26. Jaspers NGJ, et al. (2007) First Reported Patient with Human ERCC1 Deficiency Has Cerebro-Oculo-Facio-Skeletal Syndrome with a Mild Defect in Nucleotide Excision Repair and Severe Developmental Failure. *Am J Hum Genet* 80(3):457–466.
27. Lans H, et al. (2010) Involvement of global genome repair, transcription coupled repair, and chromatin remodeling in UV DNA damage response changes during developm. *PLoS Genet* 6(5):e1000941.
28. Brenner S (1974) The genetics of Caenorhabditis elegans. *Genetics* 77(1):71–94.
29. Dickinson DJ, Pani AM, Heppert JK, Higgins CD, Goldstein B (2015) Streamlined genome engineering with a self-excising drug selection cassette. *Genetics* 200(4):1035–1049.
30. Zhang D, et al. (2018) The piRNA targeting rules and the resistance to piRNA silencing in endogenous genes. *Science (80-)* 359(6375):587–592.
31. Frøkjær-Jensen C, et al. (2008) Single-copy insertion of transgenes in Caenorhabditis elegans. *Nat Genet* 40(11):1375–1383.
32. Maduro M, Pilgrim D (1995) Identification and cloning of unc-119, a gene expressed in the Caenorhabditis elegans nervous system. *Genetics* 141(3):977–988.
33. Iwasaki K, Staunton J, Saifee O, Nonet M, Thomas JH (1997) aex-3 encodes a novel regulator of presynaptic activity in C. elegans. *Neuron* 18(4):613–622.
34. Ardizzi JP, Epstein HF (1987) Immunochemical localization of myosin heavy chain isoforms and paramyosin in developmentally and structurally diverse muscle cell types of the nematode Caenorhabditis elegans. *J Cell Biol* 105(6 I):2763–2770.
35. Krause M, Harrison SW, Xu SQ, Chen L, Fire A (1994) Elements regulating cell- and stage-specific expression of the C. elegans myod family homolog hlh-1. *Dev Biol* 166(1):133–148.
36. Labouesse M, Hartwieg E, Horvitz HR (1996) The Caenorhabditis elegans LIN-26 protein is required to specify and/or maintain all non-neuronal ectodermal cell fates. *Development* 122(9):2579–2588.
37. Zeiser E, Frøkjær-Jensen C, Jorgensen E, Ahringer J (2011) MosSCI and gateway compatible plasmid toolkit for constitutive and inducible expression of transgenes in the c. elegans germline. *PLoS One* 6(5):3–8.
38. Aydin ÖZ, et al. (2014) Human ISWI complexes are targeted by SMARCA5 ATPase and SLIDE domains to help resolve lesion-stalled transcription. *Nucleic Acids Res* 42(13):8473–85.
39. Sabatella M, et al. (2018) Repair protein persistence at DNA lesions characterizes XPF defect with Cockayne syndrome features. *Nucleic Acids Res* 46(18):9563–9577.
40. van Vuuren AJ, et al. (1993) Evidence for a repair enzyme complex involving ERCC1 and complementing activities of ERCC4, ERCC11 and xeroderma pigmentosum group F. *EMBO J* 12(9):3693–701.
41. Biggerstaff M, Szymkowski DE, Wood RD (1993) Co-correction of the ERCC1, ERCC4 and xeroderma pigmentosum group F DNA repair defects in vitro. *EMBO J* 12(9):3685–92.
42. Houtsmuller AB (1999) Action of DNA Repair Endonuclease ERCC1/XPF in Living Cells. *Science (80-)* 284(5416):958–961.
43. Mitchell DL, Haipek CA, Clarkson JM (1985) (6–4)Photoproducts are removed from the DNA of UV-irradiated mammalian cells more efficiently than cyclobutane pyrimidine dimers. *Mutat Res - Mutat Res Lett* 143(3):109–112.
44. Hartman PS, Hevelone J, Dwarakanath V, Mitchell DL (1989) Excision repair of UV radiation-induced DNA damage in Caenorhabditis elegans. *Genetics* 122(2):379–385.
45. Meyer JN, et al. (2007) Decline of nucleotide excision repair capacity in aging Caenorhabditis elegans. *Genome Biol* 8(5):R70.
46. Dinant C, et al. (2007) Activation of multiple DNA repair pathways by sub-nuclear damage induction methods. *J Cell Sci* 120(15):2731–2740.
47. Limsirichaikul S, et al. (2009) A rapid non-radioactive technique for measurement of repair synthesis in primary human fibroblasts by incorporation of ethynyl deoxyuridine (EdU). *Nucleic Acids Res* 37(4):e31.

48. Schwertman P, et al. (2012) UV-sensitive syndrome protein UVSSA recruits USP7 to regulate transcription-coupled repair. *Nat Genet* 44(5):598–602.

49. Vermeulen W (2011) Dynamics of mammalian NER proteins. *DNA Repair (Amst)* 10(7):760–771.

50. Van Den Boom V, et al. (2004) DNA damage stabilizes interaction of CSB with the transcription elongation machinery. *J Cell Biol* 166(1):27–36.

51. Anindya R, et al. (2010) A Ubiquitin-Binding Domain in Cockayne Syndrome B Required for Transcription-Coupled Nucleotide Excision Repair. *Mol Cell* 38(5):637–648.

52. Hoogstraten D, et al. (2008) Versatile DNA damage detection by the global genome nucleotide excision repair protein XPC. *J Cell Sci* 121(23):3991–3991.

53. Mueller MM, et al. (2014) DAF-16/FOXO and EGL-27/GATA promote developmental growth in response to persistent somatic DNA damage. *Nat Cell Biol* 16(12):1168–1179.

54. Teng Y, Li S, Waters R, Reed SH (1997) Excision repair at the level of the nucleotide in the Saccharomyces cerevisiae MFA2 gene: Mapping of where enhanced repair in the transcribed strand begins or ends and identification of only a partial Rad16 requisite for repairing upstream control sequenc. *J Mol Biol* 267(2):324–337.

55. Masui Y, Pedersen RA (1975) Ultraviolet Light-induced unscheduled DNA synthesis in Mouse oocytes during meiotic maturation. *Nature* 257(5528):705–706.

56. Stringer JM, Winship A, Liew SH, Hutt K (2018) The capacity of oocytes for DNA repair. *Cell Mol Life Sci* 75(15):2777–2792.

57. Hays JB, Ackerman EJ, Pang QS (1990) Rapid and apparently error-prone excision repair of nonreplicating UV-irradiated plasmids in Xenopus laevis oocytes. *Mol Cell Biol* 10(7):3505–3511.

58. Adair JE, Kwon Y, Dement GA, Smerdon MJ, Reeves R (2005) Inhibition of nucleotide excision repair by high mobility group protein HMGA1. *J Biol Chem* 280(37):32184–32192.

59. Lans H, Marteijn JA, Vermeulen W (2012) ATP-dependent chromatin remodeling in the DNA-damage response. *Epigenetics and Chromatin* 5(1):4.

60. Mao P, Wyrick JJ, Roberts SA, Smerdon MJ (2017) UV-Induced DNA Damage and Mutagenesis in Chromatin. *Photochem Photobiol* 93(1):216–228.

61. McCarter J, Bartlett B, Dang T, Schedl T (1999) On the Control of Oocyte Meiotic Maturation and Ovulation inCaenorhabditis elegans. *Dev Biol* 205(1):111–128.

62. Roerink SF, Koole W, Stapel LC, Romeijn RJ, Tijsterman M (2012) A broad requirement for TLS polymerases η and κ, and interacting sumoylation and nuclear pore proteins, in lesion bypass during C. elegans embryogenesis. *PLoS Genet* 8(6):e1002800.

63. Holway AH, Kim S-H, La Volpe A, Michael WM (2006) Checkpoint silencing during the DNA damage response in Caenorhabditis elegans embryos. *J Cell Biol* 172(7):999–1008.

64. Boyd WA, et al. (2010) Nucleotide excision repair genes are expressed at low levels and are not detectably inducible in Caenorhabditis elegans somatic tissues, but their function is required for normal adult life after UVC exposure. *Mutat Res - Fundam Mol Mech Mutagen* 683(1–2):57–67.

65. Nouspikel T, Hanawalt PC (2006) Impaired nucleotide excision repair upon macrophage differentiation is corrected by E1 ubiquitin-activating enzyme. *Proc Natl Acad Sci* 103(44):16188–16193.

66. Karikkineth AC, Scheibye-Knudsen M, Fivenson E, Croteau DL, Bohr VA (2017) Cockayne syndrome: Clinical features, model systems and pathways. *Ageing Res Rev* 33:3–17.

67. Astin JW, O'Neil NJ, Kuwabara PE (2008) Nucleotide excision repair and the degradation of RNA pol II by the Caenorhabditis elegans XPA and Rsp5 orthologues, RAD-3 and WWP-1. *DNA Repair (Amst)* 7(2):267–280.

68. Bianco JN, Schumacher B (2018) MPK-1/ERK pathway regulates DNA damage response during development through DAF-16/FOXO. *Nucleic Acids Res* 46(12):6129–6139.

69. Babu V, Hofmann K, Schumacher B (2014) A C. elegans homolog of the Cockayne syndrome complementation group A gene. *DNA Repair (Amst)* 24:57–62.

70. Nouspikel TP, Hyka-Nouspikel N, Hanawalt PC (2006) Transcription Domain-Associated Repair in Human Cells. *Mol Cell Biol* 26(23):8722–8730.

71. Sulston JE, Horvitz HR (1977) Post-embryonic cell lineages of the nematode, Caenorhabditis elegans. *Dev Biol* 56(1):110–156.

72. Arczewska KD, et al. (2013) Active transcriptomic and proteomic reprogramming in the C. elegans nucleotide excision repair mutant xpa-1. *Nucleic Acids Res* 41(10):5368–5381.
73. Edifizi D, et al. (2017) Multilayered Reprogramming in Response to Persistent DNA Damage in C. elegans. *Cell Rep* 20(9):2026–2043.
74. Ermolaeva MA, et al. (2013) DNA damage in germ cells induces an innate immune response that triggers systemic stress resistance. *Nature* 501(7467):416–420.
75. Giglia-Mari G, et al. (2009) Differentiation driven changes in the dynamic organization of basal transcription initiation. *PLoS Biol* 7(10):e1000220.
76. Ho L, Hanawalt PC (1991) Gene-specific DNA repair in terminally differentiating rat myoblasts. *Mutat Res Repair* 255(2):123–141.
77. Lampidis TJ, Schaiberger GE (1975) Age-related loss of DNA repair synthesis in isolated rat myocardial cells. *Exp Cell Res* 96(2):412–416.

CHAPTER 5

Exploring TTDN1 function in genome maintenance and transcription

Arjan F. Theil[1,2], Mariangela Sabatella[1,2,*], Alex Pines[1,2,*], Maximilian A.K. Rätze[1], Anja Raams[1,2], Hannes Lans[1,2], Wim Vermeulen[1,2]

1. Department of Molecular Genetics, Erasmus MC, 3015 GE, Rotterdam, The Netherlands
2. Oncode Institute, Erasmus MC, 3015 GE, Rotterdam, The Netherlands

* These authors contributed equally to this work

Abstract

Trichothiodystrophy (TTD) syndrome patients express a heterogeneous and broad spectrum of clinical features including brittle hair, photosensitivity, ichthyosis, impaired intelligence, microcephaly, developmental delay and anemia. Part of the TTD phenotype is thought to be caused by defects in gene expression. About half of the TTD patients are photosensitive and carry mutations in the *XPD*, *XPB* or *TTDA* genes, encoding for subunits of DNA repair and transcription factor TFIIH. Non-photosensitive TTD is caused by mutations in the transcription factor *TFIIEβ,* the spliceosome-associated protein encoded by *RNF113A* or *MPLKIP/TTDN1* genes. TFIIEβ and RNF113A are both involved in gene expression, corroborating the proposed link to the TTD phenotype. However, no obvious link between TTDN1 and transcription or DNA repair has been identified and its biological role remained enigmatic. Here, we show by mass spectrometry analysis that TTDN1 is likely functionally linked to mRNA splicing and/or maturation. Furthermore, genotoxicity and DNA damage recruitment assays suggest that TTDN1 participates in the DNA damage response to interstrand-crosslinks and/or DNA strand breaks. These novel findings are a first step in understanding the exact activities of TTDN1 that are impaired in non-photosensitive TTD.

Introduction

Trichothiodystrophy (TTD) is a rare recessive multi-system developmental disorder, characterized by brittle hair and nails that are due to a low content of sulfur-rich proteins in keratinocytes. Patients present a variable combination of additional symptoms including photosensitivity, ichthyosis, impaired intelligence, decreased fertility, microcephaly, developmental delay and anemia (1). Approximately 50% of the TTD patients are photosensitive, which is caused by biallelic mutations in genes encoding TFIIH subunits, such as the *XPB*, *XPD* or *TTDA* genes (2–4). Since TFIIH is essential for both transcription initiation and nucleotide excision repair (NER) (5), it is expected that these mutations impair both processes. Indeed, photosensitive TTD patients are characterized by defective NER (6, 7) and impaired transcription (8, 9).

The other 50% of TTD cases display non-photosensitive TTD (NPS-TTD). We previously hypothesized that most of the clinical features associated with this NER-proficient NPS-TTD arise from defects in gene expression (10). Indeed, recently mutations in *TFIIEβ* were found to be causative for NPS-TTD and lead to decreased levels and phosphorylation of transcription factor TFIIE, impairing transcription (11, 12). In addition, a mutation in *RNF113A* (13) and mutations in *MPLKIP/TTDN1*, found in multiple patients (14), have been shown to cause NPS-TTD. RNF113A was found associated with spliceosomal protein complexes and implicated in activating the spliceosome (15, 16). However, thus far, no link between TTDN1 and gene expression or DNA repair has been identified and its exact function has remained unclear (17).

TTDN1 is a 179 amino acid protein that is only conserved in vertebrates and is expressed at various levels in many different human cell types. The protein has a glycine/proline-rich region but no obvious functional domains or predicted putative functions have been identified (6) (Figure 1A). TTDN1 was previously found to interact with the mitosis regulating polo-like kinase 1 (PLK1) and based on this it was hypothesized to act in cell cycle progression (18). However, cells derived from TTDN1-patients, including patients with a complete absence of the *TTDN1* gene do not display any obvious defect in cell cycle progression, suggesting that it is not essential for cell proliferation and viability despite its obvious important function in promoting health (6, 14).

To obtain a better understanding of the function of TTDN1 and how its mutation leads to TTD symptoms, we expressed GFP-tagged TTDN1 in TTDN1-deficient fibroblasts to investigate its interactome and a potential role in DNA repair. Our mass spectrometry (MS)-based quantitative proteomics identified splicing factors and an RNA/DNA helicase as novel TTDN1 interactors, suggesting a role of the protein in RNA processing. Furthermore, we provide evidence that TTDN1 might function in DNA repair pathways other than NER, as cells that lack TTDN1 are hypersensitive to the DNA interstrand crosslinks (ICLs) inducing agent mitomycin C (MMC) and because TTDN1 itself is recruited to DNA damage.

Material and methods

Cell culture, generation of TTDN1-GFP expressing cell lines

Wild type SV40-immortalized MRC5, C5RO and patient fibroblasts TTD9PV, TTD10RO and TTD11RO were cultured in F10 supplemented with 15% FCS and 1% PS at 37°C and 5% CO_2. U2OS cells and XP4PA-SV40 expressing XPC-GFP (19) were cultured in DMEM/F10 supplemented with 10% fetal calf serum (FCS) and 1% penicillin-streptomycin (PS) at 37°C and 5% CO_2. To generate TTD11RO stably expressing TTDN1-GFP, TTDN1 cDNA was fused to GFP at its C-terminus and cloned into pLenti-CMV-Puro-DEST (Addgene plasmid #17452) (20). Cloning details are available upon request. Cells were transfected with siRNA using Lipofectamine RNAiMAX Reagent (Invitrogen) 48 h prior to the experiment. siRNAs used were: control (Dharmacon, D-001210-05-20), MPLKIP/TTDN1 (Dharmacon, L-016379-02-0005), AQR (9716) (Dharmacon, D-022214-01-0005). For PARP inhibitor treatment, cells were incubated for 1 h with 10 mM KU 0058948 (Axon Medchem).

Immunofluorescence

For immunofluorescence experiments, cells were seeded on coverslips, fixed with 2% paraformaldehyde and 0.1% Triton X-100 and permeabilized for 20 min using 0.1% Triton X-100 in PBS. PBS containing 0.15% glycine and 0.5% BSA was used to wash cells, followed by incubation with primary antibodies for 2 h. Cells were again washed with PBS containing 0.1% Triton X-100 and 0.5% BSA and incubated with Alexa Fluor conjugated secondary antibodies (555, Invitrogen) for 1 h. Coverslips were mounted using DAPI Vectashield (Vector Laboratories)

and imaged using an LSM700 microscope equipped with a 40x Plan-apochromat 1.3 NA oil immersion lens (Carl Zeiss). Antibodies used were against TTDN1 (ab34309, Abcam) and SLX4 (NBP1-28680, Novus Biologicals).

Immunoprecipitation

Immunoprecipitation was performed as previously described (21). Briefly, cell lysate was prepared using IP buffer (30 mM Tris pH 7.5, 150 mM NaCl, 2 mM MgCl2, 0.5% Triton X-100, protease inhibitor cocktail (Roche)) supplemented with 250 U/mL Benzonase® nuclease. GFP-Trap®_A beads (Chromotek) were used to precipitate GFP-tagged proteins. All the fractions were then analyzed by immunoblot or mass spectrometry (see below).

Immunoblot

To analyze lysate extract, cells were collected in 2x sample buffer (125 mM Tris-HCl pH 6.8, 20% Glycerol, 10% 2-β-Mercaptoethanol, 4% SDS, 0.01% Bromophenol Blue) and boiled at 98°C for 5 min. Protein lysate was separated by SDS-PAGE and transferred to a PVDF membrane (0.45 µm, Merck Millipore). The membrane was blocked in 2% BSA and then incubated with primary and secondary antibodies for 2 h or overnight. Antibodies used were anti-TTDN1 (ab34309, Abcam), anti-GFP (11814460001, Roche), anti-Tubulin (T5168, Santa Cruz Biotechnology), anti-XAB2 (sc-271037, Santa Cruz Biotechnology), anti-AQR (A302-547A, Bethyl Laboratories). Secondary antibodies were conjugated with CF IRDye 680 or 770 (Sigma) and visualized using the Odyssey CLx Infrared Imaging System (LI-COR Biosciences).

Identification of TTDN1 interactors by SILAC-based MS analysis

Sample treatment was performed as previously described (21).

For SILAC, cells were cultured in DMEM containing 10% dialyzed FBS (Gibco), 10% GlutaMAX (Life Technologies), penicillin/streptomycin (Life Technologies), unlabeled L-arginine-HCl and L-lysine-HCL (control, "light") or $^{13}C_6$,$^{15}N_4$l-arginine-HCl and $^{13}C_6$,$^{15}N_2$l-lysine-2HCl (TTDN1-GFP, "heavy") (Cambridge Isotope Laboratories). After immunoprecipitation, cell extracts were separated on SDS-PAGE gel cut into 2-mm slices and subjected to in-gel reduction with dithiothreitol, alkylation with iodoacetamide (98%; D4, Cambridge Isotope Laboratories) and digested with trypsin (sequencing grade; Promega). To perform a nanoflow liquid chromatography tandem mass spectrometry (LC-MS/MS), an

1100 series capillary liquid chromatography system (Agilent Technologies) coupled to a Q-Exactive mass spectrometer (Thermo Scientific) operating in positive mode was used. ReproSil C18 reversed phase column (1.5 cm × 100 μm) at a rate of 8 μl/min was used to trap the peptide mixtures that was then separated by a linear gradient of 0–80% acetonitrile (in 0.1% formic acid) during 60 min at a rate of 200 nl/min using a splitter. The eluate was sprayed into the electrospray ionization (ESI) source of the mass spectrometer and spectra were acquired in continuum mode while a data-dependent mode was used to perform fragmentation of the peptides. MaxQuant software (version 1.1.1.25) was used to analyze the data.

Transcription measured by EU incorporation

To measure transcription levels, cells were seeded onto 24 mm coverslips and cultured for 24 h prior to incubation with EU for 1 h. Cells were fixed in 4% paraformaldehyde and permeabilized with 0.1% Triton X-100 in PBS. EU incorporation was visualized by incubating the cells in Click-it buffer containing Atto 594 Azide (60 μM, Atto Tec.), Tris-HCl (50 mM, pH 7.6), $CuSO_4$*$5H_2O$ (4 mM, Sigma) and ascorbic acid (10 mM, Sigma) for 1 h and washing with PBS containing 0.1% Triton X-100. DAPI (Sigma) was used to stain DNA and coverslips were mounted using Aqua-Poly/Mount (Polysciences, Inc.). Images were acquired using an LSM700 confocal microscope equipped with a 40x Plan-apochromat 1.3 NA oil immersion lens (Carl Zeiss Micro Imaging Inc.). EU levels were quantified by averaging the total nuclear fluorescence intensities of at least 50 cells per experiment with FIJI image analysis software and normalization to fluorescence levels in control conditions.

Induction of localized UV-, 8-MOP and multiphoton damage

To measure spatiotemporal redistribution of GFP-tagged XPC and TTDN1 to local UV laser-induced DNA damage, cells were seeded on quartz coverslips and imaged using a 100x quartz objective coupled to a Leica TCS SP5 confocal microscope. Local UV damage was inflicted using a UVC laser (266 nm, Rapp OptoElectronic, Hamburg GmbH) as previously described (22). Fluorescence intensities at the site of local damage, measured in real-time, were analyzed using the software Image J and were normalized to the average nuclear fluorescence intensities before irradiation. Results are plotted as average of at least 6 cells per condition from 2 independent experiments. SLX4 and TTDN1-GFP redistribution to 8-MOP induced DNA damage was performed as described (23, 24, chapter 3).

Briefly, cells were seeded on coverslips and incubated with 50 μM (8-MOP, Sigma) for 2 h. Cells were micro-irradiated along a nuclear track by a 355 nm UVA laser coupled to a PALM Laser Dissection microscope (Zeiss) through a 40x 0.60 NA Korr LD Plan Neofluar objective to activate the 8-MOP and induce local ICLs. Cells were then subjected to immunofluorescence, as described. To measure TTDN1-GFP redistribution to localized MP-induced DNA damage, cells were seeded on coverslips 24 h prior to the experiment. An MP laser coupled to a Leica TCS SP5 confocal microscope, set to obtain an 800 nm pulse, was used to irradiate a region of 1,5 μm x 1,5 μm for 220 ms in the nucleus of the cells. Fluorescence intensities at the site of local damage, measured in real-time, were analyzed using the software Image J and normalized to the average fluorescence intensities before irradiation. Results are plotted as average of a representative experiment performed with 10 cells per condition.

Clonogenic survival assays

MMC sensitivity was determined by seeding 500 cells in triplicate in 6-well plates. 24 h after seeding, cells were treated with increasing concentrations of MMC, as indicated (Sigma). After 5 to 7 days, cells were fixed and stained with 50% Methanol, 7% Acetic Acid, 0.1 % Brilliant Blue R (Sigma) and counted using the integrated colony counter GelCount (Oxford Optronix). The number of colonies after treatment was normalized to the number in non-treated conditions and plotted as average survival percentage.

Results

TTDN1-GFP interacts with core spliceosome factors

To investigate the function of TTDN1 in more detail, we first generated SV40-immortalized fibroblasts derived from patients with distinct TTDN1-inactivating mutations to characterize the TTDN1 protein expression (Figure 1A). As expected, in TTD10RO cells (genomic deletion of at least 150kb; (25)) no TTDN1 protein could be detected by immunoblotting (Figure 1B) and in situ immunostaining of cells (Figure 1C), since the TTDN1 gene is completely lacking in these patients. Strikingly, also in cells of patients with different truncation mutations, i.e. TTD11RO (p.Ser93Profs*60; (26)) and TTD9PV (deletion of part of exon 1 and entire exon 2; (14)), no TTDN1 protein could be detected (Figure 1B).

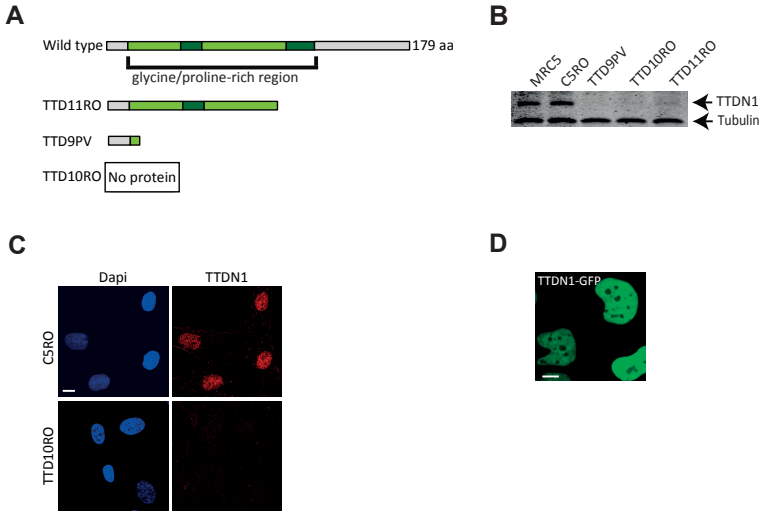

Figure 1. TTDN1-deficient and TTDN1-GFP expressing patient fibroblasts. (**A**) Schematic representation of the predicted TTDN1 wild type and truncated TTDN1 proteins, as expressed in TTD9PV, TTD10RO and TTD11RO patient fibroblasts. Light green, dark green and grey blocks indicate different predicted domain of the protein. (**B**) Immunoblot analysis showing TTDN1 protein levels in whole cell extracts from wild type fibroblasts (MRC5, C5RO) and TTDN1-deficient patient fibroblast. Tubulin staining is shown as loading control. (**C**) Immunofluorescence images showing endogenous TTDN1 expression in C5RO and TTD10RO patient fibroblasts. Scale bar: 20 μm. (**D**) Live cell image showing TTDN1-GFP stably expressed in TTD11RO fibroblasts. Scale bar: 20 μm.

Next, we stably expressed GFP-tagged TTDN1 (TTDN1-GFP) in TTD11RO-SV40 cells and observed that, like endogenous TTDN1, the fusion protein is predominantly localized in nuclei (Figure 1D). To identify the TTDN1-interacting proteins, we used the GFP-tag as affinity bait to immunoprecipitate TTDN1 and its associated proteins. To this end, we performed differential Stable Isotope Labeling by Amino Acids in Cell Culture (SILAC) of parental and TTDN1-GFP expressing TTD11RO-SV40 cells. SILAC-based quantitative MS was performed on GFP-pull down samples from whole cell extracts of both cell lines (Figure 2A). Among the main interacting proteins, depicted in Figure 2B, we identified PLK1, confirming an earlier report (18) and validating our approach. In addition, we identified AQR, XAB2, ISY1, PPIE, DBR1, CWF19L1, DHX9 and PRMT1 as novel TTDN1 interactors. Surprisingly, most of these factors are associated with the splicing machinery acting at late stages of pre-mRNA processing. For instance, debranching enzyme DBR1 and its homolog CWF19L1 (also called Drn1) are responsible for the turnover of lariat-intermediates and lariat-introns,

finalizing splicing and intron degradation (27–29). XAB2, ISY1, AQR and PPIE are all core components of the PRP19-associated and XAB2 complexes which have been implicated in mediating spliceosome assembly and activation (30–32). We confirmed the interaction of TTDN1-GFP with the tetratricopeptide repeat protein XAB2 by GFP pull down and subsequent immunoblotting (Figure 2C). Previously, XAB2 was shown to interact with elongating RNA polymerase II and to promote nascent RNA synthesis (30, 33). Therefore, we hypothesized that likewise TTDN1, in complex with XAB2, might promote RNA synthesis. To test this, we quantified transcription levels in TTDN1 depleted C5RO and U2OS cells, compared to control siRNA-treated cells, by measuring the incorporation of 5-ethynyluridine (EU). Remarkably, siTTDN1 treatment induced a clear reduction in EU levels (Figure 2D), suggesting that, indeed, TTDN1 is somehow necessary to promote normal transcription.

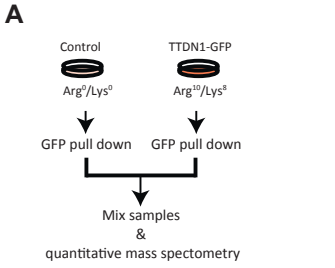

B

Protein Numbers	Unique peptides	Ratio H/L normalized
DBR1	29	16.2
AQR	37	14.2
XAB2	26	11.6
MPLKIP/TTDN1	6	10.5
CWF19L1	12	10.0
ISY1	3	8.7
PPIE	8	6.7
DHX9	41	6.5
PRMT1	6	5.4
PLK1	11	3.9

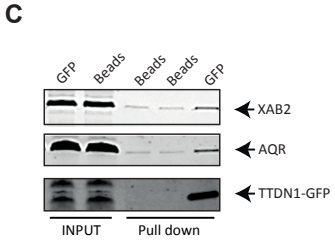

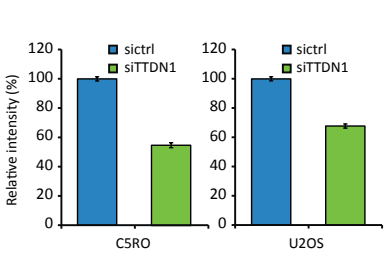

Figure 2. TTDN1 functions in splicing and transcription. (**A**) Workflow of a SILAC-based MS approach. C5RO cells were grown in light (Arg^0/Lys^0) medium and TTDN1-GFP-expressing TTD11RO cells in heavy (Arg^{10}/Lys^6) medium. After GFP pull down, proteins were mixed in a 1:1 ratio and analyzed by MS. (**B**) TTDN1-GFP interacting proteins identified by MS are listed in the table, along with the amount of unique peptides identified and the normalized ratio of heavy (H) over light (L) medium. (**C**) Immunoblot analysis of input samples, beads only and GFP immunoprecipitation (IP) from TTDN1-GFP-expressing TTD11RO cells, to validate MS results, Samples were analyzed with antibodies against XAB2, AQR and GFP. (**D**) Quantification of EU incorporation, as measure of transcription levels, in C5RO and U2OS cells treated with control siRNA (sictrl) or siRNA against TTDN1 (siTTDN1), averaged from at least 50 cells per experiment.

TTDN1 response to DNA damage

We also confirmed the interaction of TTDN1-GFP with the spliceosomal putative RNA helicase AQR (also known as IBP160) by co-immunoprecipitation and immunoblotting (Figure 2C) (34, 35). Previously, it was shown that depletion of mRNA-processing factors such as AQR leads to R-loop formation, which causes DNA damage that robustly triggers the DNA damage response (DDR) (36–38). Also, UV-induced transcription stalling was shown to cause chromatin displacement of late-stage co-transcriptional spliceosome factors, leading to R-loop formation and activation of ATM-mediated DNA damage signaling (39). Considering that TTDN1 appears to be associated with late-stage spliceosomes, we wondered if TTDN1 might also be displaced from chromatin in response to UV-induced transcription arrest. To test this, we determined the spatiotemporal response of TTDN1 to UVC laser-induced local DNA damage. A typical NER factor such as XPC is strongly recruited to local UV damage sites (40) (Figure 3A). Strikingly, but similar to late-acting core splicing factors (39), TTDN1 moves away from the site of damage (Figure 3A, B). Since most, if not all, NER factors are swiftly recruited to local UV-induced DNA damage (41), these results further confirm that TTDN1 is likely not directly involved in NER (6), in contrast to the TFIIH-associated factors implicated in TTD. However, the novel identified interactors, XAB2 and AQR, the reduced transcription induced by TTDN1 depletion and the UV-induced chromatin displacement of TTDN1 suggest that TTDN1 promotes gene expression, either directly by regulating transcription or indirectly by regulating mRNA splicing or processing.

To study TTDN1's reactivity to other types of DNA damage, we tested its response to local multiphoton (MP) laser treatment in TTD11RO fibroblasts expressing TTDN1-GFP. MP-laser irradiation induces an array of different DNA lesions, ranging from oxidative base damage, single and double strand breaks to intrastrand crosslinked pyrimidine dimers (42–45). Strikingly, and in strong contrast to local UVC-induced damage, we observed a clear recruitment of TTDN1-GFP to sites of local MP damage (Figure 3C, D), suggesting a role of TTDN1 in the DDR. To test whether this TTDN1 response to DNA damage might be coupled to its function in transcription regulation and/or splicing, we evaluated how AQR depletion affected TTDN1 recruitment. Remarkably, AQR depletion strongly enhanced TTDN1 recruitment to MP damage (Figure 3D). As recruitment of many repair proteins to or near DNA lesions is influenced by the activity of the

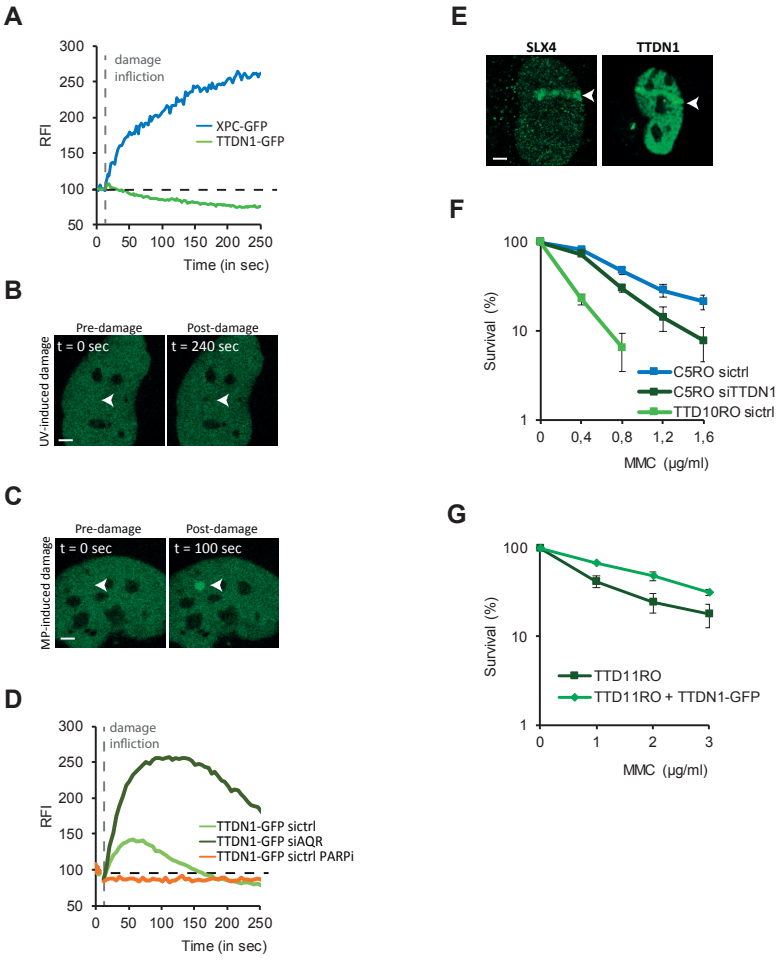

Figure 3. TTDN1 is recruited to DNA damage. (**A**) Quantification of XPC-GFP and TTDN1-GFP accumulation at local UVC laser DNA damage infliction, as determined by live cell imaging experiments shown in Figure 3B. RFI indicates relative fluorescence intensity. (**B**) Representative live cell images showing TTDN1-GFP distribution before (pre-damage) and 240 s after (post-damage) local UVC laser DNA damage infliction. Scale bar: 5 µm. (**C**) Representative live cell images showing TTDN1-GFP distribution before (pre-damage) and 100 sec after (post-damage) local DNA damage inflicted using MP laser. Scale bar: 5 µm. (**D**) Quantification of TTDN1-GFP accumulation at local MP DNA damage, as determined by live cell imaging and shown in Figure 3C. Cells were treated with control siRNA (sictrl) or AQR siRNA (siAQR), with or without PARP inhibitor (PARPi) treatment. RFI indicates relative fluorescence intensity. (**E**) Immunofluorescence pictures showing recruitment of endogenous SLX4 and TTDN1-GFP to DNA damage-induced along a track in the nucleus by 360 nm laser micro-irradiation in 8-MOP treated U2OS cells and TTD11RO fibroblasts, respectively. Scale bar: 5 µm. (**F**) Clonogenic survival assays showing MMC sensitivity of TTD10RO (TTDN1-deficient) cells and C5RO cells treated with control siRNA (sictrl) or siRNA targeting TTDN1 (siTTDN1). Results are plotted as average of three independent experiments, each performed in triplicate. (**G**) Clonogenic survival assays showing MMC sensitivity of TTD11RO (TTDN1-deficient) cells and TTD11RO cells complemented with TTDN1-GFP.

poly(ADP-ribose) polymerase PARP1 (46, 47), we additionally tested if PARP1 inhibition affected TTDN1 recruitment. Strikingly, we observed that treatment with PARP inhibitor completely suppressed TTDN1 recruitment to MP-induced DNA damage (Figure 3D).

We further investigated the recruitment of TTDN1-GFP to DNA damage by analyzing its recruitment to sites of locally psoralen-induced intrastrand crosslinks and ICLs. To this end, TTD11RO cells expressing TTDN1-GFP and U2OS cells were incubated for 2 h with 8-methoxypsoralen (8-MOP), which was subsequently locally activated using 355 nm laser micro-irradiation to induce DNA crosslinks along a track in the cell nuclei (Figure 3E) (23, 24, chapter 3). We first tested the recruitment of SLX4 to ICL-repair sites by immunostaining. SLX4 is a core Fanconi anemia factor acting as scaffold protein required for the coordinated recruitment and action of the ERCC1-XPF endonuclease (48–51). We observed clear recruitment of SLX4 to local psoralen-induced DNA crosslinks (Figure 3E), demonstrating the validity of our system to induce ICLs. Surprisingly, also TTDN1-GFP was clearly recruited to these sites of DNA crosslinks, suggestive of a putative function of TTDN1 in response to intrastrand crosslinks and/or ICLs.

To examine the functional relevance of the TTDN1 localization to psoralen-DNA crosslinks, we tested the sensitivity of TTDN1-deficient cells to the DNA crosslinking agent mitomycin C (MMC) (52). Strikingly, both TTDN1-deficient TTD10RO patient-derived fibroblasts as well as wild type C5RO fibroblasts treated with siRNA against TTDN1 showed strong sensitivity to MMC (Figure 3F). Moreover, we observed that expression of TTDN1-GFP in TTDN11RO cells reduced the MMC sensitivity of these cells (Figure 3G). Altogether, these data support the hypothesis that TTDN1 plays a role in the response to DNA damage, which is likely linked with its role in splicing via its interaction with AQR.

Discussion

The majority of NPS-TTD patients carry mutations in the *TTDN1* gene but the function of the encoded TTDN1 protein is up to date largely unknown. Here, we show that TTDN1 co-purifies with known spliceosome factors, is recruited to DNA damage and protects against MMC toxicity. This suggests that the protein

has a function in splicing or transcript processing and the DDR, which may, as we argue below, be related to each other. It is still unclear whether TTDN1 acts as part of a specific DNA repair pathway or whether it is otherwise involved in DDR. The MMC sensitivity of TTDN1-deficient cells and recruitment of TTDN1 to psoralen-induced DNA crosslinks suggests that TTDN1 may function as part of an ICL-repair pathway. However, MMC treatment also induces DNA strand breaks in replicating cells (52) and TTDN1 was recruited to MP-induced DNA damage as well, in a PARP1-dependent manner. This suggests that, alternatively, TTDN1 could participate in the repair of single and/or double strand breaks. In this regard, it is interesting to note that several of the proteins we identified as novel TTDN1 interactors, including XAB2, ISY1 and AQR, as well as other splicing factors, were recently suggested to function in homologous recombination repair of DNA double strand breaks (53–55).

We identified XAB2 as novel TTDN1 interactor. XAB2 has both been implicated in splicing, via its interaction with the PRP19-associated complex (31, 32), as well as DNA repair, i.e. in homologous recombination (55) and in NER, via its interaction with transcription-coupled NER proteins CSA, CSB, RNAP2 and XPA (30, 33). However, unlike most transcription-coupled NER factors (22, 56, 57) TTDN1 did not accumulate at sites of UVC laser-induced DNA damage. This, together with the non-photosensitive phenotype of TTDN1-deficient TTD patients and absence of UV sensitivity of patient fibroblasts, strongly suggests that TTDN1 does not function in NER. Rather, we observed that TTDN1 dissociates from sites of UV damage, similar to core splicing factors (39), and that TTDN1 depletion leads to reduced transcription levels, like depletion of XAB2 (30). These results confirm its putative role in splicing and or transcript maturation.

TTDN1 furthermore interacts with the spliceosomal protein AQR. Interestingly, the recruitment of TTDN1 to MP-induced DNA damage was strongly enhanced in the absence of AQR, suggesting that its function in splicing might be somehow linked to its function at sites of DNA damage. AQR is part of a subfamily of RNA/DNA helicases that includes Senataxin/SETX and its yeast ortholog Sen1, which were shown to prevent transcription-associated genome instability and promote efficient transcription termination by resolving R-loops (58–60). AQR itself has also been shown to prevent transcription-dependent R-loops formation, thus maintaining genome stability (36, 38, 53). In addition, chromatin dissociation and

loss of splicing factors leads to accumulation of R loops which leads to genome instability (39, 54, 61). Therefore, the interaction of TTDN1 with AQR and its chromatin dissociation in response to UV-induced DNA damage might indicate that TTDN1 itself also has a role in prevention or resolution of R-loops and thereby in promoting genome stability.

Although further analysis is needed to understand the precise function of TTDN1 in splicing and how this relates to its function in response to DNA damage and possibly R loop processing, we are confident that the link we have uncovered between TTDN1, DDR and splicing is an important step forward to understanding the precise molecular defects that underlie the NPS-TTD phenotypes observed in patients.

Acknowledgements

We are thankful to the Erasmus MC Optical Imaging Center for support with microscopes. This work was supported by the Marie Curie Initial Training Network 'aDDRess' funded by the European Commission 7th Framework Programme [316390], a European Research Council Advanced Grant [340988-ERC-ID]. This work is part of the Oncode Institute which is partly financed by the Dutch Cancer Society and was funded by the gravitation program CancerGenomiCs.nl from the Netherlands Organization for Scientific Research (NWO).

References

1. Faghri S, Tamura D, Kraemer KH, DiGiovanna JJ (2008) Trichothiodystrophy: A systematic review of 112 published cases characterises a wide spectrum of clinical manifestations. *J Med Genet* 45(10):609–621.
2. Stefanini M, et al. (1986) Xeroderma pigmentosum (complementation group D) mutation is present in patients affected by trichothiodystrophy with photosensitivity. *Hum Genet* 74(2):107–112.
3. Weeda G, et al. (1997) A mutation in the XPB/ERCC3 DNA repair transcription gene, associated with trichothiodystrophy. *Am J Hum Genet* 60(2):320–9.
4. Giglia-Mari G, et al. (2004) A new, tenth subunit TFIIH is responsible for the DNA repair syndrome trichothiodystrophy group A. *Nat Genet* 36(7):714–719.
5. Compe E, Egly JM (2012) TFIIH: When transcription met DNA repair. *Nat Rev Mol Cell Biol* 13(6):343–354.
6. Stefanini M, Botta E, Lanzafame M, Orioli D (2010) Trichothiodystrophy: From basic mechanisms to clinical implications. *DNA Repair (Amst)* 9(1):2–10.
7. Theil AF, Hoeijmakers JHJ, Vermeulen W (2014) TTDA: Big impact of a small protein. *Exp Cell Res* 329(1):61–68.
8. De Boer J, et al. (1998) A mouse model for the basal transcription/DNA repair syndrome trichothiodystrophy. *Mol Cell* 1(7):981–990.
9. Theil AF, et al. (2013) Disruption of TTDA Results in Complete Nucleotide Excision Repair Deficiency and Embryonic Lethality. *PLoS Genet* 9(4):e1003431.
10. Vermeulen W, et al. (1994) Three unusual repair deficiencies associated with transcription factor BTF2(TFIIH): Evidence for the existence of a transcription syndrome. *Cold Spring Harbor Symposia on Quantitative Biology*, pp 317–329.
11. Kuschal C, et al. (2016) GTF2E2 Mutations Destabilize the General Transcription Factor Complex TFIIE in Individuals with DNA Repair-Proficient Trichothiodystrophy. *Am J Hum Genet* 98(4):627–642.
12. Theil AF, et al. (2017) Trichothiodystrophy causative TFIIEβ mutation affects transcription in highly differentiated tissue. *Hum Mol Genet* 26(23):4689–4698.
13. Corbett MA, et al. (2015) A novel X-linked trichothiodystrophy associated with a nonsense mutation in RNF113A. *J Med Genet* 52(4):269–274.
14. Heller ER, et al. (2015) Mutations in the TTDN1 gene are associated with a distinct trichothiodystrophy phenotype. *J Invest Dermatol* 135(3):734–741.
15. Bessonov S, et al. (2010) Characterization of purified human Bact spliceosomal complexes reveals compositional and morphological changes during spliceosome activation and first step catalysis. *RNA* 16(12):2384–2403.
16. Hegele A, et al. (2012) Dynamic Protein-Protein Interaction Wiring of the Human Spliceosome. *Mol Cell* 45(4):567–580.
17. Nakabayashi K, et al. (2005) Identification of C7orf11 (TTDN1) gene mutations and genetic heterogeneity in nonphotosensitive trichothiodystrophy. *Am J Hum Genet* 76(3):510–516.
18. Zhang Y, et al. (2007) TTDN1 is a Plk1-interacting protein involved in maintenance of cell cycle integrity. *Cell Mol Life Sci* 64(5):632–640.
19. Ribeiro-Silva C, et al. (2018) DNA damage sensitivity of SWI/SNF-deficient cells depends on TFIIH subunit p62/GTF2H1. *Nat Commun* 9(1):4067.
20. Campeau E, et al. (2009) A versatile viral system for expression and depletion of proteins in mammalian cells. *PLoS One* 4(8):e6529.
21. Pines A, et al. (2018) TRiC controls transcription resumption after UV damage by regulating Cockayne syndrome protein A. *Nat Commun* 9(1):1040.
22. Aydin ÖZ, et al. (2014) Human ISWI complexes are targeted by SMARCA5 ATPase and SLIDE domains to help resolve lesion-stalled transcription. *Nucleic Acids Res* 42(13):8473–85.
23. Lachaud C, et al. (2014) Distinct functional roles for the two SLX4 ubiquitin-binding UBZ domains mutated in Fanconi anemia. *J Cell Sci* 127(13):2811–2817.

24. Slyskova J, et al. (2018) Base and nucleotide excision repair facilitate resolution of platinum drugs-induced transcription blockage. *Nucleic Acids Res* 46(18):9537–9549.
25. Botta E, et al. (1998) Analysis of mutations in the XPD gene in Italian patients with trichothiodystrophy: site of mutation correlates with repair deficiency, but gene dosage appears to determine clinical severity. *Am J Hum Genet* 63(4):1036–1048.
26. Botta E, et al. (2007) Mutations in the C7orf11 (TTDN1) gene in six nonphotosensitive trichothiodystrophy patients: No obvious genotype-phenotype relationships. *Hum Mutat* 28(1):92–96.
27. Chapman KB, Boeke JD (1991) Isolation and characterization of the gene encoding yeast debranching enzyme. *Cell* 65(3):483–492.
28. Montemayor EJ, et al. (2014) Structural basis of lariat RNA recognition by the intron debranching enzyme Dbr1. *Nucleic Acids Res* 42(16):10845–55.
29. Garrey SM, et al. (2014) A homolog of lariat-debranching enzyme modulates turnover of branched RNA. *RNA* 20(8):1337–1348.
30. Kuraoka I, et al. (2008) Isolation of XAB2 complex involved in pre-mRNA splicing, transcription, and transcription-coupled repair. *J Biol Chem* 283(2):940–950.
31. Chanarat S, Sträßer K (2013) Splicing and beyond: The many faces of the Prp19 complex. *Biochim Biophys Acta - Mol Cell Res* 1833(10):2126–2134.
32. Makarova O V, et al. (2004) A subset of human 35S U5 proteins, including Prp19, function prior to catalytic step 1 of splicing. *EMBO J* 23(12):2381–2391.
33. Nakatsu Y, et al. (2000) XAB2, a novel tetratricopeptide repeat protein involved in transcription-coupled DNA repair and transcription. *J Biol Chem* 275(45):34931–34937.
34. Ideue T, Sasaki YTF, Hagiwara M, Hirose T (2007) Introns play an essential role in splicing-dependent formation of the exon junction complex. *Genes Dev* 21(16):1993–1998.
35. De I, et al. (2015) The RNA helicase Aquarius exhibits structural adaptations mediating its recruitment to spliceosomes. *Nat Struct Mol Biol* 22(2):138–144.
36. Paulsen RD, et al. (2009) A Genome-wide siRNA Screen Reveals Diverse Cellular Processes and Pathways that Mediate Genome Stability. *Mol Cell* 35(2):228–239.
37. Fairman-Williams ME, Guenther UP, Jankowsky E (2010) SF1 and SF2 helicases: Family matters. *Curr Opin Struct Biol* 20(3):313–324.
38. Sollier J, et al. (2014) Transcription-Coupled Nucleotide Excision Repair Factors Promote R-Loop-Induced Genome Instability. *Mol Cell* 56(6):777–785.
39. Tresini M, et al. (2015) The core spliceosome as target and effector of non-canonical ATM signalling. *Nature* 523(7558):53–58.
40. Hoogstraten D, et al. (2008) Versatile DNA damage detection by the global genome nucleotide excision repair protein XPC. *J Cell Sci* 121(23):3991–3991.
41. Vermeulen W (2011) Dynamics of mammalian NER proteins. *DNA Repair (Amst)* 10(7):760–771.
42. Reynolds P, Botchway SW, Parker AW, O'Neill P (2013) Spatiotemporal dynamics of DNA repair proteins following laser microbeam induced DNA damage - When is a DSB not a DSB? *Mutat Res - Genet Toxicol Environ Mutagen* 756(1–2):14–20.
43. Duquette ML, et al. (2012) CtIP Is Required to Initiate Replication-Dependent Interstrand Crosslink Repair. *PLoS Genet* 8(11):e1003050.
44. Dinant C, et al. (2007) Activation of multiple DNA repair pathways by sub-nuclear damage induction methods. *J Cell Sci* 120(15):2731–2740.
45. Meldrum RA, Botchway SW (2003) Nanoscale spatial induction of ultraviolet photoproducts in cellular DNA by three-photon near-infrared absorption. *EMBO Rep* 4(12):1144–1149.
46. Godon C, et al. (2008) PARP inhibition versus PARP-1 silencing: Different outcomes in terms of single-strand break repair and radiation susceptibility. *Nucleic Acids Res* 36(13):4454–4464.
47. Pines A, Mullenders LH, van Attikum H, Luijsterburg MS (2013) Touching base with PARPs: Moonlighting in the repair of UV lesions and double-strand breaks. *Trends Biochem Sci* 38(6):321–330.
48. Muñoz IM, et al. (2009) Coordination of Structure-Specific Nucleases by Human SLX4/BTBD12 Is Required for DNA Repair. *Mol Cell* 35(1):116–127.

49. Yamamoto KN, et al. (2011) Involvement of SLX4 in interstrand cross-link repair is regulated by the Fanconi anemia pathway. *Proc Natl Acad Sci* 108(16):6492–6496.
50. Kim Y, et al. (2013) Regulation of multiple DNA repair pathways by the Fanconi anemia protein SLX4. *Blood* 121(1):54–63.
51. Klein Douwel D, et al. (2014) XPF-ERCC1 Acts in Unhooking DNA Interstrand Crosslinks in Cooperation with FANCD2 and FANCP/SLX4. *Mol Cell* 54(3):460–471.
52. Sognier MA, Hittelman WN (1986) Mitomycin-induced Chromatid Breaks in HeLa Cells: A Consequence of Incomplete DNA Replication. *Cancer Res* 46(8):4032–4040.
53. Sakasai R, et al. (2017) Aquarius is required for proper CtIP expression and homologous recombination repair. *Sci Rep* 7(1):13808.
54. Tanikawa M, Sanjiv K, Helleday T, Herr P, Mortusewicz O (2016) The spliceosome U2 snRNP factors promote genome stability through distinct mechanisms; transcription of repair factors and R-loop processing. *Oncogenesis* 5(12):e280.
55. Onyango DO, Howard SM, Neherin K, Yanez DA, Stark JM (2016) Tetratricopeptide repeat factor XAB2 mediates the end resection step of homologous recombination. *Nucleic Acids Res* 44(12):5702–5716.
56. Schwertman P, et al. (2012) UV-sensitive syndrome protein UVSSA recruits USP7 to regulate transcription-coupled repair. *Nat Genet* 44(5):598–602.
57. Dinant C, et al. (2013) Enhanced chromatin dynamics by fact promotes transcriptional restart after UV-induced DNA damage. *Mol Cell* 51(4):469–479.
58. Alzu A, et al. (2012) Senataxin associates with replication forks to protect fork integrity across RNA-polymerase-II-transcribed genes. *Cell* 151(4):835–846.
59. Mischo HE, et al. (2011) Yeast Sen1 helicase protects the genome from transcription-associated instability. *Mol Cell* 41(1):21–32.
60. Skourti-Stathaki K, Proudfoot NJ, Gromak N (2011) Human Senataxin Resolves RNA/DNA Hybrids Formed at Transcriptional Pause Sites to Promote Xrn2-Dependent Termination. *Mol Cell* 42(6):794–805.
61. Aguilera A, García-Muse T (2012) R Loops: From Transcription Byproducts to Threats to Genome Stability. *Mol Cell* 46(2):115–124.

CHAPTER 6

Future perspectives

The DNA damage response (DDR) is an intricate network of interconnected and collaborating DNA repair, signaling and damage tolerance pathways that provide cells with the potential to repair different types of DNA lesions or prevent further damage when required. Defects in the DDR have severe consequences to human health, such as the development of cancer and age-related diseases. This is why it is urgent to uncover the molecular mechanisms that drive and regulate the DDR and understand how its impairment causes cell dysfunction leading to the development of disease. In this thesis, different aspects of the DNA repair endonuclease ERCC1-XPF related to the DDR and disease have been investigated. Also, novel functions of the trichothiodystrophy (TTD)-causative gene TTDN1 have been uncovered. In this final chapter, I shortly recapitulate the intriguing results of each research chapter and discuss which directions future research based on these results could take.

Single allele functional analysis of ERCC1-XPF

It is commonly accepted that symptoms associated with xeroderma pigmentosum (XP), such as pigmentation changes and skin cancer, are caused by increased mutagenesis due to defects in global genome-nucleotide excision repair (GG-NER) (1). However, it is more difficult to envision how defects in transcription-coupled NER (TC-NER) cause symptoms observed in Cockayne syndrome (CS), such as growth retardation and neuronal degeneration specifically characterized by demyelination. Alternative models have therefore been put forward to explain (parts of) the etiology of CS, proposing for instance that besides impairment of TC-NER, specific defects in transcriptional programs or in mitochondrial function cause CS features (2–5). However, these models cannot explain why different mutations in ERCC1-XPF, which functions in multiple DNA repair pathways, can give rise to either XP or XP combined with CS features or even other diseases such as FA.

Because many XPF mutations have been found in patients as compound heterozygous, it is difficult to disentangle the pathogenic contribution of each allele to the phenotype. Therefore, we expressed individual *XPF* alleles in complete XPF-deficient cells to analyze their impact on XPF function (6, chapter 2). In this way, we revealed that XPF with XP-causative mutations partially retains repair capacity but is inefficiently recruited to DNA damage. Therefore, these mutations do not fully abolish but only slow down the NER reaction and still allow almost

complete transcription recovery after UV irradiation (7, 8, chapter 2). We therefore hypothesize that, as a consequence, mutations will accumulate in the genome, explaining the increased cancer incidence typically observed in XP patients (1), but transcription will not be strongly impaired, explaining the absence of CS features. Conversely, a xeroderma pigmentosum-Cockayne syndrome complex (XPCS)-causative mutation in XPF confers an extremely low repair capacity and induced persistent recruitment of the mutant XPF, as well as of the upstream core NER machinery, to DNA damage. We hypothesize that because of this, DNA lesions may be less accessible to other repair mechanisms and that other DNA-transacting processes, such as transcription and replication, will be impaired as well. As a consequence, persistent DDR-signaling, senescence and cell death may be induced, contributing to the more severe phenotypes and reduced cancer incidence observed in XPCS as compared to XP (2, 9).

Strikingly, we found one allele associated with both XP and XPCS that rendered XPF completely inactive, indicating that in patients carrying this allele the other compound *XPF* allele determines the phenotype. Together, these results clearly illustrate the utility of our approach to individually study the functionality of each allele in cells. Therefore, we propose to use this approach also to further verify our hypothesis by investigating NER in the presence of other known XPF mutations, such as: R153P, associated with even more severe progeria than XPCS (10); or R799W, associated with XP with late-onset neurological disease (11). Furthermore, it would be helpful to use our approach to functionally analyze XP- and XPCS-causative mutations that have been found in other repair factors, because mutations in XPB, XPD and XPG can also lead to either XP or XPCS (9) and because core NER factors are persistently recruited to DNA damage in XPCS patient fibroblasts with mutations in these other NER factors as well (chapter 2).

One important aspect of our hypotheses that needs to be addressed is whether and how XPCS-causative mutations affect the function of RNA polymerase II and/or transcription. Recently, an elegant cellular system was developed in our host institute, making use of a CRISPR/Cas9-mediated knock-in of GFP-tagged RNA polymerase II, to study the initiation, promoter-proximal pausing and elongation steps of the RNA polymerase II transcription cycle by confocal imaging (12). This RNA polymerase II knock-in system could be implemented in cells expressing XPF with patient mutations to investigate how XPCS-causative mutations impact

transcription. Nowadays, gene editing using the CRISPR/Cas9 technology is continuously being perfected and becoming more common, which is why it would furthermore be advantageous to implement this technique as part of our approach to study the impact of individual alleles in cells. Firstly, the study of fluorescently tagged mutant proteins generated by knock-in of a fluorescent tag would avoid possible artefacts due to overexpression of the proteins upon cDNA transfection and therefore make the analysis even more reliable. Secondly, the technology can be used to introduce point mutations in the endogenous locus of a gene to study the impact of individual alleles in an isogenic background instead of comparing different (often compound heterozygous) patient fibroblasts. Moreover, using CRISPR/Cas9 gene editing would allow us to study the impact of mutations in NER factors in a cellular context that is more relevant to the patient's phenotype. For instance, by using CRISPR/Cas9 technology to introduce fluorescently tagged NER mutant proteins in induced pluripotent stem (iPS) cells, followed by *in vitro* differentiation to e.g. neuronal cell cultures, it would be possible to study the link between NER mutations and neurodegeneration in a more defined and specific context.

Interestingly, our findings could potentially be used for diagnostics purposes. Typically, an XP diagnosis can be confirmed by reduced unscheduled DNA synthesis levels (UDS) and CS by reduced RNA recovery synthesis (RRS) (1, 4). Evaluation of whether there is persistent recruitment of the core NER machinery to DNA damage in patient-derived fibroblasts or in engineered cells carrying patients mutations could be coupled to UDS and RRS assays to further confirm the diagnosis and particularly to distinguish an XPCS (or a De Sanctis Cacchione syndrome) case from XP. Use of this approach would be especially valuable for a prompt diagnosis in young patients that do not show clear signs of neuronal degeneration or progeria yet, avoiding a false negative diagnosis if these features are not evident at early stages of the diseases (9). As persistent recruitment of NER factors to DNA damage might prospect neurological abnormalities that are only manifested at later stages of life, this will in the future possibly give patients the chance of pharmacological intervention to at least delay these symptoms.

Imaging of interstrand crosslink

In the past years, the continuing identification of new factors causative for FA, which function in interstrand crosslink repair (ICLR), and the development of a versatile *in vitro* ICLR assay using *Xenopus* egg extracts have made it possible to

gain a better mechanistic understanding of this complicated DNA repair pathway (13). Still, many questions about the specific functions of ICLR proteins and the consecutive ICLR steps remain unanswered. For instance, although it is now widely accepted that ERCC1-XPF is essential for ICLs unhooking, it is unclear whether the activity of this endonuclease is sufficient or whether the activity of one or more additional nucleases is needed for unhooking. Also, ICLR consists of the joint activity of multiple DNA repair pathways and utilizes proteins that often have other (DNA repair) functions as well. It is still not fully understood how these collaborative activities between different DNA repair pathways are organized. Considering the important role that ERCC1-XPF plays in both NER and ICLR, it is of particular interest to understand how the activity of this complex is regulated in both pathways. Although the importance of XPA in regulating ERCC1-XPF recruitment to UV damage is well known (14, 15, chapter 2), not much is known about how the complex is recruited to ICLs in human cells, except that this is mediated by its interaction with SLX4 (18–20).

A technical difficulty when studying recruitment of DNA repair factors to ICLs by microscopy is that common ICL-inducing agents such as cisplatin and psoralens not only create ICLs but also monoadducts and intrastrand crosslinks, which are NER substrates. To circumvent this problem, we took advantage of the CRISPR/Cas9 technology to knock out (KO) XPA to specifically investigate how ERCC1-XPF is recruited to psoralen-DNA crosslinks independently of XPA and thus independently of NER (chapter 3). Additionally, we set up a new imaging approach in the lab, making use of local UVA laser irradiation in nuclei of cells exposed to 8-methoxypsoralen, to measure recruitment of proteins to psoralen-DNA crosslinks. We used cell lines stably expressing either ERCC1-GFP or XPF-GFP (wild-type or with specific disease-causing mutations) in combination with this newly developed ICLs imaging procedure. This approach allowed us to show in human cells that recruitment of ERCC1-XPF to ICLs is regulated by the ICLR key factor FANCD2 and that XPF ICLR-defective mutants do not associate efficiently with ICLs. These results are in line with experiments in *Xenopus* egg extracts showing dependence of ERCC1-XPF on FANCD2 (19; chapter 3), suggesting that our XPA KO cells are a well-suited tool to study which regulatory factors facilitate recruitment of ERCC1-XPF to ICLs in human cells, besides the already known FANCD2 and SLX4 (18–20). Also, as it has been suggested that ERCC1-XPF incises DNA around the ICL in collaboration with other nucleases such as

SNM1A (21, 22) or FAN1 (23, 24), our approach could be used to test recruitment of these nucleases, and possibly others, to ICLs as well.

The combination of stably expressed GFP-tagged ERCC1 or XPF with the KO of XPA makes these cell lines also very suitable for mass spectrometry based identification of novel factors involved in the specific recruitment of ERCC1-XPF to ICLs. To this aim, immunoprecipitation using the GFP-tag as bait in extracts from cells pretreated with ICL-inducing agents, followed by mass spectrometry analysis, could be used, similarly as we have done after UV irradiation (chapter 3). In addition, the same GFP-ERCC1/XPF expressing cells can be used to investigate how these novel interactors regulate recruitment of the complex to ICLs, by knocking down the expression of these new factors by e.g. RNA-interference. Although it is clear that ICLR differs per cell phase, the exact difference between replication-dependent and replication-independent ICLR is still not understood. To address this question and specifically study recruitment of ERCC1-XPF in non-replicating cells, our approach of studying ICLR in XPA KO cells could be combined with a live cell cycle marker, such as Fucci (25), that allows to distinguish between cells in G1 phase or S-G2-M, or with a synchronizing agent, such as Lovastatin that synchronizes cells in G1 phase (26). Finally, the PALM dissection microscope that was used for UVA laser irradiation, to induce local psoralen-DNA crosslinks, did not allow simultaneous high resolution real-time imaging of fluorescent proteins, because of which we imaged the ICL recruitment of ERCC1-XPF in fixed cells. Therefore, to be able to measure involvement of proteins in ICLR in real-time, our system could be improved by coupling the 355 nm UVA laser to a confocal microscope that allows live cell imaging and time lapse investigations.

C. elegans as tool to study tissue-specific NER activity *in vivo*

The way DDR deals with DNA lesions depends on their type, genomic location and cell cycle phase (27). However, it is becoming increasingly clear that this is also influenced by the cell type and its developmental and differentiation state (28). This is also suggested by the observation that in many DNA repair diseases not all tissues are equally affected (29). For instance, in case of hereditary ERCC1-XPF deficiency, in particular neuronal cells - in severe XP and CS - and the hematopoietic system - in FA - are affected (9, 30–32). As it is not fully understood to which extent this variety in symptoms reflects a tissue-specific activity of the complex or of the respective NER and ICLR pathways, it is extremely important to

elucidate how DDR is organized *in vivo*. Using imaging of GFP-tagged ERCC1-XPF in germ cells, neurons and muscles of the nematode *C. elegans,* we demonstrated that NER functions in a tissue specific manner (chapter 4). Our results suggest that in oocytes, the *C. elegans* XPF ortholog XPF-1 ensures extremely rapid removal of UV-induced DNA lesions throughout the genome as part of GG-NER. In post-mitotic neurons, instead, XPF-1 appears to act as part of TC-NER to remove lesions from transcribed genes only. Remarkably, no XPF-1 activity was observed in muscles cells.

The rapid CPD repair in oocytes contrasts the much slower global genome CPD repair that is observed in yeast and human cells in culture and in other *C. elegans* cell types (6, 33–36), suggesting that it may be oocyte-specific. However, it is unclear which mechanisms facilitate this extremely rapid repair reaction. GG-NER is initiated by damage detection by the key factor XPC-1 (ortholog of human XPC). Therefore, the same live imaging procedure that we applied to visualize the spatio-temporal dynamics of XPF-1 could be used to measure the spatio-temporal dynamics of XPC-1, to confirm and further investigate this fascinating and rapid CPD repair in *C. elegans* oocytes. Strikingly, in mammals, CPDs are poorly recognized by XPC and therefore CPD binding by the UV-DDB complex, consisting of DDB1 and DDB2, is first required to enable XPC to detect CPDs (37). However, DDB2 does not have a clear ortholog in *C. elegans*. It is therefore at this moment unclear how *C. elegans* XPC-1 is able to detect CPDs without an obvious DDB2 candidate and initiate rapid GG-NER. To study this further, *C. elegans* XPC-1 could be expressed in XPC-deficient human cells in order to verify and compare any differences in CPD recognition and in the speed of the repair reaction with human XPC. Also, to further explore the mechanisms that might be responsible for the rapid repair reaction in oocytes and other tissues of *C. elegans*, it would be interesting to investigate the XPC-1 interactome. To this aim, endogenous XPC-1 tagged by knock-in of an Avi tag in combination with tissue-specific expression of a biotin ligase could be used to perform tissue-specific immunoprecipitation and mass spectrometry analysis (38) to identify interactors that might speed up the repair reaction in oocytes.

We showed that GG-NER is the main pathway that preserves genomic integrity in germ cells and early embryos, whereas TC-NER only becomes essential for cellular function in post-mitotic somatic cells such as neurons (39; chapter 4). Therefore, it

would also be interesting to further investigate DNA repair in *C. elegans* by looking in a similar manner more specifically at the TC-NER key factor CSB-1 (human CSB ortholog). Our *in vivo* imaging approach, together with tissue-specific immunoprecipitation and mass spectrometry analysis, of a GFP- or Avi-tagged CSB knock-in could help to elucidate the mechanisms that regulate TC-NER in post-mitotic neurons. Moreover, comparing the XPC-1 and CSB-1 interactomes in different tissues might also help to clarify why the two NER subpathways are differently regulated in tissues and how GG-NER activity might be confined to transcribed genes only in differentiated tissues. It was previously observed that as animals develop, the repair rate is highest in actively transcribed genomic regions (35, 36) and similarly, that upon *in vitro* differentiation, mammalian cells lose GG-NER capacity but retain repair in active genes (40, 41). It was suggested that this developmental-stage-specific change in repair activity depends on differentiation-driven switch from GG-NER to TC-NER, but the mechanisms underlying this switch are not completely understood. Therefore, the combination of *in vivo* imaging and proteomics of XPC-1 and CSB-1 could be a valuable strategy to further explore the regulation of these mechanisms. Strikingly, we did not observe any measurable NER activity in muscles cells, suggesting that differences may exist in NER regulation even between post-mitotic tissues (i.e. muscles and neurons). Therefore, studying the repair activity and interactome of XPC-1 and CSB-1 in different tissues of *C. elegans* might also help explain why differences between post-mitotic tissues exist and shed light on whether NER is active or not in muscle cells. Moreover, the regulators identified with this approach could be further studied in *in vitro* differentiated human iPS cells to evaluate to what extent these mechanisms are conserved.

Finally, *C. elegans* could be used to closely evaluate the progression of specific phenotypes associated with NER disorders. For instance, *C. elegans* is commonly used to study development and functionality of the nervous system, which is why this model organism may also be well suited to study the induction and progression of neurodegeneration after e.g. ERCC-1/XPF-1 deficiency. The neural cell lineage of *C. elegans* is completely mapped (42) and imaging of any change in neuronal development or the onset and progression of neurodegeneration in time in ERCC-1/XPF-1-deficient worms in unperturbed conditions or exposed to UV irradiation would possibly provide insight into the development of similar symptoms observed in patients. In particular, considering the fact that TC-

NER is the main NER pathway functioning in neurons, we hypothesize that neurological symptoms arise from transcription defects due to the accumulation of DNA damage produced by endogenous metabolism (27). To investigate this, the impact of DNA damage on transcription in these cells could be monitored by visualizing the incorporation of 5-ethynyluridine into nascent RNA (as in chapter 2), which could then possibly be correlated to any changes or defects in neuronal development or function observed after DNA damage induction.

Further investigation of TTDN1 functions

Trichothiodystrophy (TTD) is a rare recessive disorder characterized by a heterogeneous and broad spectrum of clinical features and thought to be caused by impairment of transcription and/or gene expression. Eighteen patients with non-photosensitive TTD carry mutations in *TTDN1*, whose function is unknown (43). To better understand TTDN1 function, we performed mass spectrometry analysis of GFP-tagged TTDN1 overexpressed in TTDN1-deficient fibroblasts (chapter 5). Our analysis revealed that TTDN1 interacts with splicing factors and an RNA/DNA helicase, suggesting a role of the protein in RNA processing. This finding is in line with the idea that TTD is caused by gene expression impairment and opens up a new intriguing research line to follow up in the near future. Firstly, generation of an affinity tagged TTDN1 knock-in would represent a more physiological platform to validate the interactome of the protein, by performing quantitative mass spectrometry analysis in unperturbed conditions but also after transcription inhibition and DNA damage induction. Next, a deeper understanding of the TTDN1 functions in splicing could be obtained by performing RNA-Seq in wild type and TTDN1-depleted or knockout fibroblasts to detect putative differences in the splicing and expression of genes when TTDN1 is not functional. Moreover, RNA-Seq analysis should be performed after DNA damage induction, to test whether any changes in splicing occur, depending on TTDN1.

Our study also showed that TTDN1-deficient cells are hypersensitive to the ICL-inducing agent mitomycin C (MMC) and that TTDN1 itself is recruited to psoralen-DNA crosslinks and DNA damage induced by multiphoton (MP) laser in a PARP-dependent manner. These results suggest a role of the protein in the DDR to ICLs or double strand breaks (DSB). To analyze this further, it would be interesting to investigate the spatio-temporal response of fluorescently tagged TTDN1 and sensitivity of TTDN1-deficient cells to different types of ICLs as

well, i.e. also those induced by cisplatin or oxaliplatin. Furthermore, similar as for ERCC1-XPF in chapter 4, it could be investigated if recruitment of TTDN1 to psoralen-DNA crosslinks is dependent on any known FA protein or if, vice versa, TTDN1 is needed for recruitment of FA proteins to ICLs. Furthermore, it could be investigated if the PARP-dependent TTDN1 recruitment to MP damage reflects a specific role of the protein in DSB repair. First of all, the sensitivity of TTDN1-deficient cells to DSB-inducing agents, such as ionizing radiation, bleomycin and/or etoposide, could be tested to validate a role in DSB repair. Also, fluorescent reporter assays specific for determining non-homologous end-joining or homologous recombination efficiency (44) could be used to assess a possible role of TTDN1 in one of these DBS repair pathways.

Finally, it would be interesting to investigate if a putative role of TTDN1 in ICLR and/or DSB repair is linked to its role in splicing. Therefore, analysis of its DDR function could also be performed after treatment with transcription and/or splicing inhibitors. In addition, as suggested above, it would be worth investigating the TTDN1-dependent spliceosome after the induction of DNA damage. However, even if any involvement of TTDN1 in the DDR to ICLs or DSBs is confirmed, the biggest question that would need to be addressed is whether and how this unexpected role of TTDN1 is connected to any symptoms displayed by TTD patients.

References

1. Lehmann AR, McGibbon D SM (2011) Xeroderma pigmentosum. *Orphanet J Rare Dis* 6(70):1–6.
2. Marteijn JA, Lans H, Vermeulen W, Hoeijmakers JHJ (2014) Understanding nucleotide excision repair and its roles in cancer and ageing. *Nat Rev Mol Cell Biol* 15(7):465–481.
3. Vélez-Cruz R, Egly JM (2013) Cockayne syndrome group B (CSB) protein: At the crossroads of transcriptional networks. *Mech Ageing Dev* 134(5–6):234–242.
4. Karikkineth AC, Scheibye-Knudsen M, Fivenson E, Croteau DL, Bohr VA (2017) Cockayne syndrome: Clinical features, model systems and pathways. *Ageing Res Rev* 33:3–17.
5. Wang Y, et al. (2014) Dysregulation of gene expression as a cause of Cockayne syndrome neurological disease. *Proc Natl Acad Sci* 111(40):14454–14459.
6. Sabatella M, et al. (2018) Repair protein persistence at DNA lesions characterizes XPF defect with Cockayne syndrome features. *Nucleic Acids Res* 46(18):9563–9577.
7. Ahmad A, et al. (2010) Mislocalization of XPF-ERCC1 nuclease contributes to reduced DNA repair in XP-F patients. *PLoS Genet* 6(3):e1000871.
8. Fassihi H, et al. (2016) Deep phenotyping of 89 xeroderma pigmentosum patients reveals unexpected heterogeneity dependent on the precise molecular defect. *Proc Natl Acad Sci* 113(9):E1236–E1245.
9. Natale V, Raquer H (2017) Xeroderma pigmentosum-Cockayne syndrome complex. *Orphanet J Rare Dis* 12(1):65.
10. Niedernhofer LJ, et al. (2006) A new progeroid syndrome reveals that genotoxic stress suppresses the somatotroph axis. *Nature* 444(7122):1038–1043.
11. Sijbers AM, et al. (1998) Homozygous R788W point mutation in the XPF gene of a patient with xeroderma pigmentosum and late-onset neurologic disease. *J Invest Dermatol* 110(5):832–836.
12. Steurer B, et al. (2018) Live-cell analysis of endogenous GFP-RPB1 uncovers rapid turnover of initiating and promoter-paused RNA Polymerase II. *Proc Natl Acad Sci*:201717920.
13. Ceccaldi R, Sarangi P, D'Andrea AD (2016) The Fanconi anaemia pathway: new players and new functions. *Nat Rev Mol Cell Biol* 17(6):337–349.
14. Li L, Elledge SJ, Peterson CA, Bales ES, Legerski RJ (1994) Specific association between the human DNA repair proteins XPA and ERCC1. *Proc Natl Acad Sci U S A* 91(11):5012–6.
15. Sugitani N, Sivley RM, Perry KE, Capra JA, Chazin WJ (2016) XPA: A key scaffold for human nucleotide excision repair. *DNA Repair (Amst)* 44:123–135.
16. Houtsmuller AB, et al. (1999) Action of DNA repair endonuclease ERCC1/XPF in living cells. *Science* 284(5416):958–61.
17. Volker M, et al. (2001) Sequential assembly of the nucleotide excision repair factors in vivo. *Mol Cell* 8(1):213–224.
18. Muñoz IM, et al. (2009) Coordination of Structure-Specific Nucleases by Human SLX4/BTBD12 Is Required for DNA Repair. *Mol Cell* 35(1):116–127.
19. Klein Douwel D, et al. (2014) XPF-ERCC1 Acts in Unhooking DNA Interstrand Crosslinks in Cooperation with FANCD2 and FANCP/SLX4. *Mol Cell* 54(3):460–471.
20. Hodskinson MRG, et al. (2014) Mouse SLX4 Is a Tumor Suppressor that Stimulates the Activity of the Nuclease XPF-ERCC1 in DNA Crosslink Repair. *Mol Cell* 54(3):472–484.
21. Wang AT, et al. (2011) Human SNM1a and XPF-ERCC1 collaborate to initiate DNA interstrand cross-link repair. *Genes Dev* 25(17):1859–1870.
22. Abdullah UB, et al. (2017) RPA activates the XPF-ERCC1 endonuclease to initiate processing of DNA interstrand crosslinks. *EMBO J* 36(14):2047–2060.
23. Wang R, et al. (2014) Mechanism of DNA interstrand cross-link processing by repair nuclease FAN1. *Science (80-)* 346(6213):1127–1130.
24. Pizzolato J, Mukherjee S, Schärer OD, Jiricny J (2015) FANCD2-associated nuclease 1, but not exonuclease 1 or flap endonuclease 1, is able to unhook DNA interstrand cross-links in vitro. *J Biol Chem* 290(37):22602–22611.
25. Newman RH, Zhang J (2008) Fucci: Street Lights on the Road to Mitosis. *Chem Biol* 15(2):97–98.

26. Moghadam-Kamrani SJ, Keyomarsi K (2008) Synchronization of the cell cycle using lovastatin. *Cell Cycle* 7(15):2434–2440.
27. Hoeijmakers JHJ (2009) DNA Damage, Aging, and Cancer. *N Engl J Med* 361(15):1475–1485.
28. Lans H, Vermeulen W (2015) Tissue specific response to DNA damage: C. elegans as role model. *DNA Repair (Amst)* 32:141–148.
29. Niedernhofer LJ (2008) Tissue-specific accelerated aging in nucleotide excision repair deficiency. *Mech Ageing Dev* 129(7–8):408–15.
30. Digiovanna JJ, Kraemer KH (2012) Shining a light on xeroderma pigmentosum. *J Invest Dermatol* 132(3 PART 2):785–796.
31. Dufour C (2017) How I manage patients with Fanconi anaemia. *Br J Haematol* 178(1):32–47.
32. Nalepa G, Clapp DW (2018) Fanconi anaemia and cancer: An intricate relationship. *Nat Rev Cancer* 18(3):168–185.
33. Mitchell DL, Haipek CA, Clarkson JM (1985) (6–4)Photoproducts are removed from the DNA of UV-irradiated mammalian cells more efficiently than cyclobutane pyrimidine dimers. *Mutat Res - Mutat Res Lett* 143(3):109–112.
34. Teng Y, Li S, Waters R, Reed SH (1997) Excision repair at the level of the nucleotide in the Saccharomyces cerevisiae MFA2 gene: Mapping of where enhanced repair in the transcribed strand begins or ends and identification of only a partial Rad16 requisite for repairing upstream control sequenc. *J Mol Biol* 267(2):324–337.
35. Hartman PS, Hevelone J, Dwarakanath V, Mitchell DL (1989) Excision repair of UV radiation-induced DNA damage in Caenorhabditis elegans. *Genetics* 122(2):379–385.
36. Meyer JN, et al. (2007) Decline of nucleotide excision repair capacity in aging Caenorhabditis elegans. *Genome Biol* 8(5):R70.
37. Sugasawa K (2016) Molecular mechanisms of DNA damage recognition for mammalian nucleotide excision repair. *DNA Repair (Amst)* 44:110–117.
38. Waaijers S, et al. (2016) A tissue-specific protein purification approach in Caenorhabditis elegans identifies novel interaction partners of DLG-1/Discs large. *BMC Biol* 14(1):66.
39. Lans H, et al. (2010) Involvement of global genome repair, transcription coupled repair, and chromatin remodeling in UV DNA damage response changes during developm. *PLoS Genet* 6(5):e1000941.
40. Nouspikel T, Hanawalt PC (2002) DNA repair in terminally differentiated cells. *Thierry Nouspikel, Philip C Hanawalt 2002 DNA repair Termin Differ cells DNA Repair 1 59-75* 1(1):59–75.
41. van der Wees C, et al. (2007) Nucleotide excision repair in differentiated cells. *Mutat Res Mol Mech Mutagen* 614(1–2):16–23.
42. Chalfie M (1984) Neuronal development in Caenorhabditis elegans. *Trends Neurosci* 7(6):197–202.
43. Zhou YK, et al. (2018) A homozygous G insertion in MPLKIP leads to TTDN1 with the hypergonadotropic hypogonadism symptom. *BMC Med Genet* 19(S1):214.
44. Weinstock DM, Nakanishi K, Helgadottir HR, Jasin M (2006) Assaying Double-Strand Break Repair Pathway Choice in Mammalian Cells Using a Targeted Endonuclease or the RAG Recombinase. *Methods Enzymol* 409:524–540.

Summary

Cells are equipped with an intricate network of DNA repair and signaling pathways, called the DNA damage response (DDR). The DDR maintains genome integrity by coping with DNA lesions that are continuously induced by endogenous and exogenous agents. Two major DNA repair pathways are investigated in this thesis: the first is nucleotide excision repair (NER), which removes DNA-helix distorting lesions such as those induced by UV light. The second is interstrand crosslink repair (ICLR), which removes covalent linkages between bases on opposing DNA strands induced by DNA crosslinking chemicals and antitumor agents, such as cisplatin, psoralens and mitomycin C. The structure specific endonuclease ERCC1-XPF is essential to incise DNA next to lesions during both NER and ICLR. In humans, mutations in this complex give rise to hereditary DNA repair syndromes such as xeroderma pigmentosum (XP), Cockayne syndrome (CS), xeroderma pigmentosum-Cockayne syndrome complex (XPCS), and Fanconi anemia (FA). In **chapter 1**, current knowledge of the multistep mechanisms of NER and ICLR, of the ERCC1-XPF function in these pathways and the clinical features associated with these DNA repair syndromes are described. Intriguingly, ERCC1-XPF deficiency in the model organism *C. elegans* gives rise to similar pleiotropic features as those observed in humans. An overview of the biology of *C. elegans* and its use to study DDR *in vivo* is also presented in the first chapter.

In **chapter 2**, we investigated XPF mutations that are carried as heterozygous compound by XP and XPCS patients, which makes it difficult to dissect the pathogenic impact of each individual *XPF* allele. To better understand how each mutation may influence XPF function, we expressed fluorescently tagged XPF proteins carrying a single patient-derived mutation in XPF-deficient cells and analyzed their spatio-temporal response to UV damage. We show that XPF proteins carrying XP-causative mutations are inefficiently recruited to DNA damage, but retain repair capacity, albeit less efficient. In contrast, XPF with an XPCS mutation shows completely impaired repair capacity, and is associated with persistent binding or continuous recruitment of XPF and the core NER machinery to UV-induced DNA damage. As the same remarkable continuous recruitment was observed in XPCS cells with mutations in other NER proteins, we hypothesize that CS features are in part due to this persistent, futile targeting of the NER machinery to DNA damage. Moreover, we found that an XPF mutation reported as heterozygous compound in mild and severe XP and in XPCS induces mislocalization and impaired activity of XPF. This observation suggests that the

different patient phenotypes associated with this mutation are dependent on the ability of the other compound XPF allele to function in NER. These results clearly illustrate the importance of analyzing the functionality of individual alleles to better understand the different pathogenesis of NER diseases.

While it is well known that engagement of ERCC1-XPF in NER is facilitated by binding to the key factor XPA, how its recruitment in ICLR is regulated is less clear. It is therefore difficult to understand why certain XPF mutations cause hypersensitivity to interstrand crosslinks (ICLs) and not to the DNA lesions repaired by NER. In **chapter 3**, we investigated recruitment of fluorescently tagged ERCC1 and XPF to different types of psoralen-DNA crosslinks, repaired by NER or ICLR. Our results confirm that ERCC1-XPF recruitment as part of the NER machinery is XPA-dependent and furthermore show that engagement in ICLR is dependent on the ICLR factor FANCD2. We also investigated the impact of two XPF mutations causing ICLR defects, of which one is found in an FA patient, and observed that they impair recruitment of the protein to psoralen-DNA ICLs. These studies open up the possibility to further study the determining factors that govern ERCC1/XPF function in ICLR.

DDR deficiency affects tissues differently, suggesting that cells deal differently with DNA damage. However, knowledge about DDR is mostly derived from *in vitro* and cell culture studies with which it is difficult to investigate whether the DDR differs *in vivo,* depending on the cell type and developmental stage of cells. Therefore, we utilized the multicellular *C. elegans* as *in vivo* model organism to study DDR. Because of the many functions of ERCC1-XPF in DDR and the pleiotropic symptoms displayed by ERCC1-XPF patients, we focused on this complex to investigate the existence of tissue-specific DNA repair. In **chapter 4**, we used UV survival assays and *in vivo* imaging of fluorescently tagged XPF-1 in *C. elegans* to demonstrate that in oocytes, representing an immortal cell lineage, XPF-1 ensures rapid removal of DNA-helix distorting lesions throughout the genome as part of the global genome sub-pathway of NER. In contrast, in terminally differentiated neurons, XPF-1 is involved in repair of transcribed genes only while no activity of the protein was observed in muscle cells. These results show that NER indeed displays differences depending on the cell type and suggest the existence of a tissue-specific organization of DDR.

Trichothiodystrophy (TTD) is an autosomal recessive disorder characterized by brittle hair and nails, neurological problems and a broad spectrum of additional clinical features. Interestingly, half of the patients is sensitive to UV light (photosensitive), which is due to disease-causing mutations in genes involved in both NER and transcription. The other half of the patients is non-photosensitive and carries mutations in *TFIIEβ*, involved in regulating transcription, *RNF113*, involved in activating the spliceosome, or *MPLKIP/TTDN1,* whose function is unknown. In **chapter 5**, we combined mass spectrometry analysis, DNA damage sensitivity assays and live cell imaging approaches to investigate the unknown function of TTDN1. Interestingly, we found that TTDN1 function is likely linked to mRNA splicing and/or maturation, suggesting that transcriptional defects are also at the base of TTD caused by mutations in TTDN1. Moreover, our data surprisingly suggests an involvement of TTDN1 in the DDR to ICLs and/or DNA strand breaks.

In **chapter 6**, we shortly discuss the results presented in chapter 2, 3, 4 and 5 and describe which future research approaches could be undertaken to deepen our knowledge of DDR mechanisms and their relation to health and disease.

Samenvatting

De integriteit van het genoom wordt in elke cel gewaarborgd door een veelomvattend en complex netwerk van mechanismen die samen voor herkenning, signalering en reparatie van DNA-schade zorgen. Dit netwerk, dat de DNA-schade respons wordt genoemd, verwijdert veel verschillende soorten DNA-schade, die continu worden veroorzaakt door blootstelling van DNA aan verschillende endogene en exogene genotoxische agentia. In dit proefschrift worden twee DNA-reparatie mechanismen bestudeerd. De eerste is 'nucleotide excisie reparatie' (NER), dat schades verwijdert die de DNA-helix verstoren, zoals bijvoorbeeld veroorzaakt door UV-licht. De tweede is 'interstreng crosslink reparatie' (ICLR), dat covalente verbindingen tussen basen op tegenoverstelde DNA-strengen verwijdert. Deze covalente verbindingen, die 'interstreng crosslinks' worden genoemd, worden veroorzaakt door blootstelling aan crosslinkers en antikanker medicijnen, zoals cisplatine, psoraleen en mitomycine C. Het endonuclease eiwitcomplex ERCC1-XPF is essentieel voor het inknippen van DNA vlak naast DNA-schade tijdens NER en ICLR. Mutaties in dit eiwitcomplex kunnen leiden tot specifieke erfelijke DNA-reparatie syndromen in mensen, zoals xeroderma pigmentosum (XP), Cockayne syndroom (CS), xeroderma pigmentosum-Cockayne syndroom complex (XPCS) en Fanconi anemie (FA). In **hoofdstuk 1** van dit proefschrift wordt achtereenvolgens beschreven wat bekend is over het werkingsmechanisme van NER en ICLR, hoe ERCC1-XPF functioneert in beide DNA-reparatie processen en wat de klinische symptomen van bovengenoemde DNA-reparatie syndromen zijn. In het model organisme *C. elegans* leidt ERCC1-XPF deficiëntie interessant genoeg tot fenotypische kenmerken die vergelijkbaar zijn met die in patiënten. In het eerste hoofdstuk wordt ook een overzicht van de biologie van *C. elegans* gegeven en wordt besproken hoe dit modelorganisme in de wetenschap wordt gebruikt om de DNA-schade respons te bestuderen.

In **hoofdstuk 2** hebben we mutaties in XPF bestudeerd die XP of XPCS veroorzaken. In patiënten komen deze mutaties vaak als samengesteld heterozygoot voor, waardoor het lastig is om de impact van elk individueel *XPF*-allel op de ziekte te bestuderen. Om de invloed van iedere individuele mutatie op XPF beter te begrijpen, hebben we fluorescent-gelabelde XPF-eiwitten met individuele patiëntenmutaties in XPF-deficiënte cellen tot expressie gebracht en hun spatio-temporele activiteit gemeten na het induceren van DNA-schade door UV-licht. Ons onderzoek laat zien dat XPF-eiwitten met XP-veroorzakende mutaties minder efficiënt naar DNA-schade worden gebracht, terwijl ze wel DNA-reparatie kunnen uitvoeren, zij het

met verminderde efficiëntie. Daarentegen vertonen XPF-eiwitten met een XPCS-patiëntenmutatie een defect in DNA-reparatie waardoor zowel XPF- als andere essentiële NER-eiwitten steeds opnieuw naar DNA-schade worden toegebracht. Aangezien ditzelfde ook in cellen van XPCS-patiënten met mutaties in andere NER genen wordt gemeten, stellen we in dit hoofdstuk voor dat CS-symptomen voor een deel worden veroorzaakt door deze continue maar zinloze ophoping van NER-eiwitten bij DNA-schade. Verder ontdekten we dat een XPF-mutatie die als samengesteld heterozygoot wordt gevonden in milde en ernstige XP- en in XPCS-patiënten ervoor zorgt dat XPF niet goed wordt gedistribueerd in de cel en inactief is. Dit suggereert dat het fenotype van de patiënten met deze mutatie afhangt van hoe goed het andere samengestelde allel kan functioneren in NER. Deze resultaten tonen aan dat het zeer nuttig is om de invloed van individuele mutaties op de functionaliteit van een eiwit te bestuderen om de pathogenese van NER-ziekten goed te begrijpen.

De betrokkenheid van ERCC1-XPF in NER wordt gereguleerd door aan het NER-eiwit XPA te binden. Het is echter nog onduidelijk hoe de betrokkenheid van ERCC1-XPF in ICLR wordt gereguleerd, waardoor het moeilijk is om te begrijpen waarom sommige mutaties in XPF specifiek leiden tot overgevoeligheid voor chemicaliën die interstreng crosslinks veroorzaken. In **hoofdstuk 3** hebben we daarom onderzocht hoe fluorescent-gemarkeerde ERCC1- en XPF-eiwitten naar verschillende, door psoraleen-geïnduceerde, DNA crosslinks gebracht worden, die door NER of door ICLR worden gerepareerd. Onze resultaten bevestigen dat XPA nodig is voor de betrokkenheid van ERCC1-XPF in NER. Bovendien laten we zien dat de betrokkenheid in ICLR afhankelijk is van het FANCD2-eiwit. Verder onderzoek naar de pathogene impact van twee XPF-mutaties die tot ICLR-defecten leiden, waarvan er één is gevonden in een FA-patiënt, laat zien dat deze mutaties ervoor zorgen dat XPF niet efficiënt naar psoraleen-DNA interstreng crosslinks wordt gebracht. Door deze studie kan nu verder onderzoek worden verricht naar de factoren die de functie van ERCC1-XPF in ICLR reguleren.

Defecten in de DNA-schade respons hebben een verschillende impact op weefsels. Dit suggereert dat cellen op verschillende manieren omgaan met DNA-schade. Kennis van de DNA-schade response is echter vooral gebaseerd op resultaten verkregen met *in vitro* experimenten en met gekweekte cellen. Met deze model systemen kan de mogelijke celtype-, en ontwikkelingsstadium-afhankelijke DNA-

schade respons niet worden bestudeerd. Om die reden hebben we gebruik gemaakt van het meercellige organisme *C. elegans* als *in vivo* model voor de DNA-schade respons. Om weefselspecifieke DNA-reparatie te bestuderen, hebben we de functie van ERCC1-XPF bestudeerd, omdat dit eiwitcomplex meerdere functies heeft en patiënten met mutaties hierin een grote verscheidenheid aan symptomen laat zien. In **hoofdstuk 4** hebben we door middel van UV-gevoeligheidsassays en *in vivo* microscopie van fluorescent-gemarkeerde XPF-1 in *C. elegans* aangetoond dat in oöcyten, dat wil zeggen in een onsterfelijke cellijn, XPF-1 helpt om DNA-schade snel te repareren in het gehele genoom, via het 'globale-genoom' mechanisme van NER. In terminaal gedifferentieerde neuronen is XPF-1 echter alleen betrokken bij het verwijderen van DNA-schade in getranscribeerde genen. Daarnaast kon in spiercellen geen activiteit van XPF-1 worden gemeten. Deze resultaten laten zien dat NER anders werkt afhankelijk van het celtype en suggereren daarom dat de DNA-schade response op een weefselspecifieke manier georganiseerd is.

Trichothiodystrophy (TTD) is een autosomale recessieve ziekte die gekarakteriseerd wordt door broze haren en nagels, neurologische problemen en een breed spectrum aan andere klinische verschijnselen. De helft van de patiënten met deze ziekte is overgevoelig voor UV-licht, doordat zij drager zijn van ziekte-veroorzakende mutaties in genen die zowel voor NER als voor transcriptie belangrijk zijn. De andere helft van patiënten is niet overgevoelig voor UV-licht en draagt mutaties in het *TFIIEβ* gen, dat betrokken is bij transcriptie, in *RNF113*, dat betrokken is bij transcriptie-geassocieerde spliceosome activatie, of in *MPLKIP/ TTDN1,* waarvan de functie onbekend is. In **hoofdstuk 5** hebben we door middel van massaspectrometrie, DNA-schade gevoeligheidsassays en levende-cel-microscopie de functie van het TTDN1 eiwit bestudeerd. Onze resultaten laten interessant genoeg zien dat TTDN1 waarschijnlijk betrokken is bij mRNA-splicing en/of -maturatie. Dit suggereert dat transcriptiedefecten ook aan de basis liggen van TTD veroorzaakt door mutaties in TTDN1. Ons onderzoek laat, tot onze verrassing, zien dat TTDN1 mogelijk betrokken is bij de DNA-schade response tegen DNA-dubbelstrengsbreuken en/of interstreng crosslinks.

In **hoofdstuk 6** worden tenslotte de resultaten uit de hoofdstukken 2 tot en met 5 kort bediscussieerd en worden mogelijkheden voor verder onderzoek besproken, om tot een beter begrip van de DNA-schade respons en de relatie met ziekte en gezondheid te komen.

Riassunto

Le cellule sono fornite di un intricato sistema molecolare di meccanismi di segnalazione e riparazione del DNA denominato risposta al danno al DNA (DDR). La DDR mantiene l'integrità del genoma facendo fronte alle lesioni del DNA che vengono costantemente indotte da agenti endogeni ed esogeni. In questa tesi vengono analizzati due dei più importanti meccanismi di riparazione del DNA: il primo è noto come riparazione per escissione di nucleotidi (NER) e rimuove lesioni che creano distorsioni nella doppia elica del DNA come quelle indotte dai raggi UV. Il secondo è noto come riparazione di interstrand crosslink (ICLR) e rimuove legami crociati (crosslinks) che si formano tra le basi di due eliche opposte (interstrand) del DNA in seguito ad esposizione ad agenti chimici ed antitumorali quali cisplatino, psoraleni e mitomicina-C. L'endonucleasi ERCC1-XPF è un complesso proteico che incide il DNA nei pressi della lesione ed è essenziale sia nel NER che nel ICLR. Mutazioni in questo complesso proteico portano allo sviluppo di sindromi ereditarie associate a difetti di riparazione del DNA, per esempio: xeroderma pigmentosum (XP), Sindrome di Cockayne (CS), complesso xeroderma pigmentosum - sindrome di Cockayne (XPCS) e anemia di Fanconi (FA). Nel **capitolo 1** viene descritto ciò che al momento è noto riguardo ai vari processi del NER e del ICLR, alle funzioni svolte da ERCC1-XPF in entrambi i meccanismi e alle sindromi ereditarie associate a difetti del NER e del ICLR. È interessante notare che anche nell'organismo modello *C. elegans* alterazioni in ERCC1-XPF portano allo sviluppo di effetti pleiotropici simili a quelli osservati nell'uomo. Nel capitolo 1 viene fornita una breve descrizione della biologia di *C. elegans* e di come esso venga utilizzato per studiare la DDR *in vivo*.

Nel **capitolo 2**, sono state esaminate specifiche mutazioni del gene *XPF* identificate in pazienti affetti da XP o XPCS. Questi pazienti sono spesso eterozigoti compositi di queste mutazioni per cui è complicato studiare l'impatto patologico del singolo allele. Per poter meglio comprendere come ogni singola mutazione possa influenzare le funzioni di XPF, abbiamo coniugato un *reporter* fluorescente a XPF contenente una singola mutazione precedentemente descritta nei pazienti. Le proteine così marcate sono state espresse in cellule deficienti per XPF al fine di poter studiare la loro risposta spazio-temporale al danno al DNA provocato da raggi UV. I nostri risultati hanno rivelato che quando XPF presenta mutazioni che causano XP, la proteina viene reclutata in modo inefficiente presso il sito della lesione al DNA ma ritiene la sua capacità di riparazione, sebbene questa sia meno efficace. Al contrario, quando XPF presenta mutazioni che causano XPCS, la proteina non è in

grado di riparare il DNA e resta persistentemente associata o viene continuamente reclutata, insieme a tutti i componenti principali del NER, presso il sito della lesione al DNA provocato da raggi UV. Poiché lo stesso fenomeno è stato osservato in cellule derivate da pazienti affetti da XPCS ma con mutazioni in altre proteine coinvolte nel NER, abbiamo ipotizzato che i sintomi associati alla CS siano in parte dovuti a questo continuo e vano accumulo del macchinario di riparazione del DNA al sito della lesione. Inoltre, abbiamo osservato che una specifica mutazione eterozigote composita in XPF, precendentemente riportata in pazienti affetti da forme di XP lieve e severo e da XPCS, causa mislocalizzazione e deficit del funzionamento di XPF. Questa osservazione suggerisce che i vari fenotipi riportati nei patienti e associati a questa mutazione sono dovuti alla capacità di riparo del DNA dell'allele composito. I nostri risultati mostrano chiaramente l'importanza di analizzare la funzionalità di ogni singolo allele per poter comprendere i vari aspetti clinici delle patologie dovute a difetti del NER.

Mentre è ben noto che il reclutamento di ERCC1-XPF nel macchinario del NER sia dovuto all'interazione con XPA, fattore chiave di questo meccanismo, non è del tutto chiaro come il complesso proteico venga reclutato nel ICLR. Di conseguenza, non è semplice capire come mai alcune mutazioni in XPF causino ipersensibilità ad agenti che inducono interstrand crosslink ma non ad agenti quali i raggi UV che causano lesioni riparate dal NER. Nel **capitolo 3**, abbiamo analizzato come ERCC1 e XPF, coniugate ad un *reporter* fluorescente, vengano reclutate presso interstrand crosslink psoraleni-DNA che sono riparati da NER ed ICLR. I nostri risultati hanno confermato che il reclutamento di ERCC1-XPF nel macchinario del NER dipende da XPA ed hanno dimostrato che il reclutamento nel macchinario del ICLR dipende da FANCD2, altro componente del ICLR. In questo capitolo abbiamo anche studiato l'impatto di due mutazioni in XPF che inducono difetti nel ICLR, una delle quali identificata in un paziente affetto da anemia di Falconi. Abbiamo così rivelato che queste due mutazioni riducono il reclutamento della proteina presso interstrand crosslink psoraleni-DNA. Questi studi aprono le porte alla possibilità di investigare in modo più dettagliato quali fattori regolano e supportano le funzioni di ERCC1-XPF nel ICLR.

Difetti nella DDR compromettono i tessuti in modo diverso, suggerendo che le cellule reagiscano differentemente al danno al DNA. Al momento, le conoscenze che riguardano la DDR derivano maggiormente da studi fatti *in vitro* o su cellule

in coltura, tuttavia questi studi non permettono di investigare se la DDR funzioni diversamente *in vivo* e se le eventuali differenze siano dovute al tipo cellulare o allo stadio di sviluppo delle cellule. A questo scopo, abbiamo utilizzato l'organismo multicellulare *C. elegans* come modello per studiare la DDR *in vivo*. Considerando le multiple funzioni di ERCC1-XPF nella DDR e dei sintomi pleiotropici mostrati dai pazienti che presentano mutazioni in ERCC1-XPF, abbiamo focalizzato la nostra attenzione su questo complesso proteico per poter verificare la possibilità che i processi di riparazione del DNA funzionino in modo tessuto-specifico. Per poter verificare questa ipotesi abbiamo utilizzato saggi di sopravvivenza ai raggi UV e microscopia *in vivo* di *C. elegans* che esprimono XPF-1 coniugato ad un *reporter* fluorescente. Nel **capitolo 4**, questi mezzi ci hanno permesso di dimostrate che negli ovociti, che rappresentano una linea cellulare immortale, XPF-1 assicura una rapida rimozione da tutto il genoma delle lesioni che creano distorsioni nella doppia elica del DNA tramite il meccanismo di `riparazione globale del genoma` che è parte del NER. Al contrario, in cellule neuronali terminalmente differenziate, XPF-1 è coinvolto solo nella riparazione di geni che vengono attivamente trascritti. Nelle cellule muscolari, invece, non è stata osservata nessuna attività della proteina. Questi risultati rivelano che il NER funziona diversamente a seconda del tipo cellulare e suggerisce l´esistenza di una organizzazione tessuto-specifica della DDR.

La tricotiodistrofia (TTD) è una malattia autosomica recessiva caratterizzata da capelli ed unghie fragili, problemi neurologici e un ampio spettro di altre caratteristiche cliniche. È interessante notare che la metà dei pazienti affetti da questa malattia è sensibile ai raggi UV (fotosensibile) a causa di mutazioni in geni che funzionano sia nel NER che nei meccanismi di trascrizione. L´altra metà dei pazienti è non-fotosensibile ed ha mutazioni in *TFIIEβ*, coinvolto nella regolazione della trascrizione, in *RNF113*, coinvolto nell´attivazione dello spliceosoma, o in *MPLKIP/TTDN1,* le cui funzioni sono sconosciute. Nel **capitolo 5**, abbiamo utilizzato spettrometria di massa, saggi di sensibilitá ad agenti che inducono danni al DNA e microscopia di cellule viventi per investigare le possibili funzioni di TTDN1. Abbiamo cosí osservato che TTDN1 potrebbe essere coinvolta nella maturazione e/o nello splicing del mRNA. Ciò suggerisce che alterazioni nei processi di trascrizione siano anche all´origine della TTD causata da mutazioni in TTDN1. Inoltre, i nostri risultati suggeriscono che TTDN1 potrebbe essere coinvolta anche nella DDR nel interstrand crosslink e/o nelle rotture a doppio filamento.

Nel **capitolo 6**, vengono ulteriormente discussi i risultati presentati nei capitoli 2, 3, 4, e 5 insieme a spunti per ricerche future che potrebbero favorire una più profonda conoscenza dei meccanismi di DDR e la loro relazione con salute e malattia.

Curriculum vitae

Name: Mariangela Sabatella
Date of birth: 5 October 1987
Place of birth: Potenza (Italy)

Education

2010 - 2012: MSc in Medical Biotechnologies
Final grade: 110/110 cum laude
University of Naples "Federico II", Faculty of Biotechnological Science (Naples, Italy)

2007 - 2010: BSc in Biotechnologies for Health - medical curriculum
Final grade: 106/110
University of Naples "Federico II", Faculty of Biotechnological Science (Naples, Italy)

Work experience

2018 - present: Postdoctoral researcher
Princess Maxima Center for pediatric oncology (Utrecht, The Netherlands)

2013 - 2017: PhD student in Biomedical Science_
Fellowship: Marie-Curie ITN aDDRess
Molecular Genetics Department, Erasmus MC (Rotterdam, The Netherlands)

2011 - 2013: Internship
CEINGE Biotecnologie avanzate, University of Naples "Federico II" (Naples, Italy)

2010 - 2011: Internship
CNR, Institute of Genetics and Biophysics (IGB) (Naples, Italy)

International activities

2014: Lab visit as ESR trainee under the Marie-Curie ITN aDDRess
Prof. John Rouse, MRC, University of Dundee (Dundee, United Kingdom)

Awards

2017:	GSA poster award at the 21st International *C. elegans* Meeting (Los Angeles, USA)
2017:	Travel grant: The Simons Foundation Fund (Rotterdam, The Netherlands)
2015:	Travel grant: Vereniging Trustfonds Erasmus Universiteit (Rotterdam, The Netherlands)

List of publications

Ribeiro-Silva C., **Sabatella M.**, Helfricht A., Theil A.F., Vermeulen W., Lans H. DDB2 comes and goes to promote nucleotide excision repair progression. *(Manuscript in preparation)*

Sabatella M., Thijssen K., Vermeulen W., Lans H. Tissue-specific DNA repair activity of ERCC-1/XPF-1 in *C. elegans*. *(Submitted)*

Sabatella M., Pines A., Slyskova J., Vermeulen W., Lans H. ERCC1-XPF targeting to psoralen-DNA crosslinks depends on XPA and FANCD2. *Cellular and Molecular Life Sciences 2019*

Doshi S., Price E., Landis J., Barot U., **Sabatella M.**, Lans H., Kalb R.G. Neuropeptide signaling regulates the susceptibility of developing *C. elegans* to anoxia. *Free Radic Biol Med. 2019*

Sabatella M., Theil A.F., Ribeiro-Silva C., Slyskova J., Thijssen K., Voskamp C., Lans H., Vermeulen W. Repair protein persistence at DNA lesions characterizes XPF defect with Cockayne syndrome features. *Nucleic Acids Res. 2018*

Slyskova J., **Sabatella M.**, Ribeiro-Silva C., Stok C., Theil A.F., Vermeulen W., Lans H. Base and nucleotide excision repair facilitate resolution of platinum drugs-induced transcription blockage. *Nucleic Acids Res. 2018*

Jablonski A., Lamitina T., Liachko N., **Sabatella M.**, Liu J., Ostrow L., Gupta P., Chia-Yen Wu, Doshi S., Mojsilovic-Petrovic J., Lans H., Wang J., Kraemer B., Kalb R.G. Loss of RAD-23 Protects Against Models of Motor Neuron Disease by Enhancing Mutant Protein Clearance. *J Neurosci. 2015*

van Cuijk L., van Belle G.J., Turkyilmaz Y., Poulsen S.L., Janssens R.C., Theil A.F., **Sabatella M.**, Lans H., Mailand N., Houtsmuller A.B., Vermeulen W., Marteijn J.A. (2015) SUMO and ubiquitin-dependent XPC exchange drives nucleotide excision repair *Nat Commun. 2015*

Sasso E., Vitale M., Monteleone F., Boffo F.L., Santoriello M., Sarnataro D., Garbi C., **Sabatella M.**, Crifò B., Paolella L.A., Minopoli G., Winum J.Y., Zambrano N. (2015) Binding of Carbonic Anhydrase IX to 45S rDNA Genes Is Prevented by Exportin-1 in Hypoxic Cells. *Biomed Res Int. 2015*

PhD portfolio

Name:	Mariangela Sabatella
PhD period:	May 2013 - November 2017
Erasmus MC department:	Molecular Genetics
Research School:	MGC
Promotor:	Prof. dr. Wim Vermeulen
Supervisor:	Dr. Hannes Lans

Courses

2016: Biomedical English writing and communication
2014: Research Integrity
2014: Genetics_
2014: MGC Epigenetic Regulation in Health and Disease
2014: MGC Genome Maintenance and Cancer
2014: MGC Technology Facilities: Proteomics
2014: The Microscopic Image Analysis: from theory to practice
2014: Cell and Developmental Biology
2013: Safe Laboratory Techniques
2013: Functional Imaging and Super Resolution
2013: Biochemistry and Biophysics
2013: Biostatistical methods I: basic principles part A
2013: ML-I (work permit for GMOs)
2013: ML-II (work permit for Adenovirus and Lentivirus)

Workshops

2014: Photoshop and Illustrator CS6
2014: Indesign CS6
2014: aDDRess/CodeAge Joint Summer School and Mid Term Review (Crete, Greece)
2013: 1st aDDRess/CodeAge 1st Training Workshop and Annual Meeting (Milan, Italy)

Teaching and Supervising

2017: Biomolecular Dynamics (Biochemistry and Molecular Biology) course (Bsc Nanobiology of the Erasmus MC and TU Delft, The Netherlands)
2016: Biomolecular Dynamics (Biochemistry and Molecular Biology) course (Bsc Nanobiology of the Erasmus MC and TU Delft, The Netherlands)
2016: Bachelor student internship supervisor
2015: Genetics course (Bsc Nanobiology of the Erasmus MC and TU Delft, The Netherlands)
2015: Master student internship supervisor
2015: Biomolecular Dynamics (Biochemistry and Molecular Biology) course (Bsc Nanobiology of the Erasmus MC and TU Delft, The Netherlands)
2014: Genetics course (Bsc Nanobiology of the Erasmus MC and TU Delft, The Netherlands)
2013: Genetics course (Bsc Nanobiology of the Erasmus MC and TU Delft, The Netherlands)

Oral presentations

2017: MGC DNA Repair Meeting (Leiden, The Netherlands)
2016: MGC DNA Repair Meeting (Rotterdam, The Netherlands)
2016: The Final aDDRess & CodeAge ITN Conference (Crete, Greece)
2016: 23rd MGC PhD Workshop (Dortmund, Germany)
2015: 3rd aDDress Annual Meeting (Cologne, Germany)
2015: Dutch Worm Meeting 2015 (Wageningen, The Netherlands)
2014: aDDRess/CodeAge Joint Summer School and Mid Term Review (Crete, Greece)
2014: Dutch Worm Meeting 2014 (Groningen, The Netherlands)
2013: 1st aDDRess/CodeAge Training Workshop and Annual Meeting (Milan, Italy)

Poster presentations

2017: 21th International *C. elegans* Meeting (Los Angeles, USA)
2016: 10th Quinquennial Conference on Responses to DNA damage: from molecule to disease (Egmond aan Zee, The Netherlands)
2015: 20th International *C. elegans* Meeting (Los Angeles, USA)
2015: 22nd MGC PhD Workshop (Maastricht, The Netherlands)

Other conferences

Monthly: MGC DNA Repair Meeting (Rotterdam/Leiden, The Netherlands)

2015: The promise of PARP inhibitors for personalized cancer treatment (Amsterdam, The Netherlands)

2014: 24rd MGC Symposium (Rotterdam, The Netherlands)

2014: Annual Cancer Genomics NL Meeting 2014 (Utrecht, The Netherlands)

2013: Dutch Chromatin Meeting (Rotterdam, The Netherlands)

2013: 23rd MGC Symposium (Rotterdam, The Netherlands)

Acknowledgements
Dankwoord
Ringraziamenti

It is almost hard to believe, this amazing experience is at its end. Although it feels like the last years flied, I realize it has been a long and hard journey made of big changes, lots of fun and some sad and frustrating moments but all of this contributed to make my PhD unforgettable. It is difficult to express in words how thankful I am for all I have learned and the amazing people I got to know during these years. You all helped me grow and improve my scientific skills, my English and my Dutch.

I want to acknowledge especially all those that have been not only my colleagues but became quite like a family. First of all, Wim and Hannes who gave me the opportunity to join the lab and understood and supported me in all the situations I had to go through.

Hannes, samengevat in vijf woorden: Je bent een geweldige supervisor (Ja, dat dacht ik zelfs ten tijde van het aandachtig corrigeren van dit proefschrift of al die keren dat je een mening had over mijn 'Disney-kleuren'). Jouw benadering van de wetenschap is inspirerend en leerzaam en hopelijk behoud ik eenzelfde enthousiasme bij het krijgen en uittesten van nieuwe ideeën. Dank voor het lachen mét me (en niet om me) wanneer ik weer eens rondhuppelde door het lab met coole resultaten of mijn vreugdesprong toen ik mee kon naar de *C. elegans* meeting en bij het winnen van de posterprijs. Nog meer dank voor het vertrouwen dat je me gaf in mezelf, mijn ideeën en het werk wat ik deed/doe. Ook voor het geduld en de ondersteuning toen ik niet zo efficiënt was als normaal. Jouw 'MEIMITYEFO' advies zal ik nimmer vergeten, ik krijg het nog niet altijd toegepast, maar daar wordt aan gewerkt.

Wim, je was er altijd op het juiste moment; om mijn twijfels weg te nemen en om mij verstandige adviezen te geven. Je bent ons NER-geschiedenisboek. Je hebt me altijd gesteund, gemotiveerd gehouden en geholpen met op een positieve manier naar de dingen te blijven kijken. Vaak dacht ik dat mijn inbreng aan de technieken die ik probeerde te optimaliseren vanzelfsprekend was. Juist op dié momenten bracht je me altijd in herinnering dat ik iets belangrijks deed om proberen bij te dragen aan de wetenschap. Dank daarvoor!

Jan en **Koos**, jullie zijn rolmodellen door jullie onbegrensde kennis en vriendelijkheid. Fijn dat jullie altijd tijd kunnen vrijmaken voor advies en hulp

aan ons jonge en leergierige wetenschappers in-de-dop. Blij dat we van gedachten konden wisselen over de meest uiteenlopende onderwerpen, het was een eer en geluk jullie te mogen ontmoeten.

Ik kan niet in woorden vangen hoe gelukkig ik me voel dat ik jou heb mogen leren kennen en met jou heb mogen samenwerken **Karen**. Vanaf het eerste moment hadden we een klik en waren we een echt team; het *C. elegans*-team. Ik ben dankbaar dat ik van jouw ervaring gebruik kon maken en zoveel van je kon leren. Jouw aanstekelijke enthousiasme over werken met *C. elegans* veranderde me nog meer in 'the worm-girl'. Uiteindelijk was je niet enkel een gewone collega, maar meer een hartsvriendin. We konden altijd met elkaar praten over alles en je was nabij en ondersteunend wanneer ik dat nodig had. Onze mini-vakantie en etentjes waren altijd echt gezellig, zó gezellig dat we ze niet willen missen, dus die houden we in ere.

Cristina, you are the person with whom I shared the most: office, Marie Curie fellowship, trips and meetings, nights and weekends in the lab or behind the microscope. They all felt fine with you. I will always remember our quick 'hamburger break' during one of our looong working nights and all our trips together, always productive, funny and full of chit-chats. I am happy I found a friend like you and that we could share so much together.

Jullie bijnaam is vanzelfsprekend, **Gezellige Meisjes**. Genieten waren onze uitstapjes en etentjes. Nachos smaken niet hetzelfde zonder jullie. Fijn waren de pauzes waarin we tijd hadden voor een praatje, onbedaarlijk lachen en vele knuffels. Jullie zijn écht lief! **Imke** en **Serena**, helaas zien we elkaar nu minder en hierdoor mis ik jullie gezelligheid. Hopelijk kunnen we snel weer afspreken. **Marjolein**… als ik jouw naam uitsprak stond je altijd meteen paraat met advies, hulp en om te knuffelen. Inderdaad, we hebben nog een lange gezamenlijke 'to-do-lijst' op ons wachten, dus… aan de slag!

Arjan, de grote man waar ik in eerste instantie een beetje bang voor was, maar je bleek een aardige en leuke vent. Het was fijn om samen te werken aan een deel van je project. **Alex**, grazie per le chiacchierate, i tuoi preziosi consigli e per i "labtricks" che mi hai insegnato. **Bert-Jaap**, bedankt voor je hulp met microscopie en statistiek. **Jurgen**, blij dat je onder de indruk was van mijn roze geschilderde

muur op de achtergrond bij ons eerste Skype-interview. Jouw commentaren waren altijd nuttig en bruikbaar en gelukkig blijft iemand anders je weer bezighouden met presentaties over *C. elegans*. **Roel**, dank voor je vriendelijkheid en eindeloze geduld (als enige man in het kantoor). **Özge** (my first friend in the lab) and **Yasemin**, I had a lot of fun during our Mediterranean moments, hope in the future we can have more moments like those together. **Barbara**, **Franzi**, **Jana**, **Marit**, **Angela**, **Maria**, **Masaki**, **Akos**, **Kishan**, **Di**, **Marvin**, I feel lucky I could share a lot of fun with you in the lab as well as outside. Each one of you contributed to make this experience even more enjoyable. **Chantal** en **Ciske**, thanks for your contribution to this work. It was a pleasure to have you as students.

I also want to thank all the other colleagues of the departments, for feedback, questions, suggestions and nice chit-chats and the **OIC people** for helping me and giving me introduction to almost all microscopes available at the EMC. Zonder de kennis en inzet van de mensen die achter de schermen werken zou alles nog ingewikkelder zijn geweest. Dank aan: **Jasperina**, **Sonja**, **Marike**, **Fatima**, **Joke**, **Koos**, **Leo**, en **de mannen van de IT-service**.

Of course a special place of this section is reserved to my family and my friends outside the lab.

Sei contento Papi? Ce l'abbiamo fatta anche questa volta, come promesso. 'A capa è tosta ma non sarei arrivata fin qui senza la mia **mamma** e il mio **papà**. Non vi ringrazierò mai abbastanza per tutto l'amore, la forza e l'esempio che mi avete dato e per avermi sempre supportato e sopportato. Siamo 'una squadra fortissimi' e questo non cambierà mai.

Grazie anche al resto della famiglia e soprattutto ad una parte speciale di essa: **Rocco** e **Ninetta**, i nostri 'angeli custodi', **Giuseppe**, **Nicola**, **Lidia** e **Lucia**, i fratelli che non ho mai avuto. Grazie per esserci sempre e comunque, quando possiamo condividere i nostri sorrisi e quando motivi per sorridere proprio non ce ne sono.

Tijdens dit avontuur heb ik ook geleerd wat voor bijzondere vriendschappen kunnen voortkomen uit geloof: zorgzaam, lief, betrouwbaar en beschermend. De laatste tijd zou het nog moeilijker zijn geweest zonder dit alles. Grazie **Ramon**! Dank aan al mijn lieve **'WJD vrienden'**, de **Blauwe Zusters**, die mij me altijd thuis

hebben laten voelen, en aan alle mensen die ons begeleid hebben tijdens onze katholieke activiteiten.

Grazie a **Tania** (per l'affetto e anche per i rimproveri :p), **Angela**, **Don Nicola**, **Elisa** e **Fabio** per essere vicini anche da lontano.